TÉCNICO LISBOA

Path-following and Cooperative Path-following for Underwater Snake Robots

Gonçalo Diogo Francisco Filipe de Carvalho

Thesis to obtain the Master of Science Degree in

Electrical and Computer Engineering

Supervisors: Prof. João Fernando Cardoso Silva Sequeira
Prof. António Manuel dos Santos Pascoal

Examination Committee

Chairperson: Prof. Pedro Manuel Urbano de Almeida Lima
Supervisor: Prof. João Fernando Cardoso Silva Sequeira
Member of the Committee: Prof. António Pedro Rodrigues Aguiar

January 2021

Declaration

I declare that this document is an original work of my own authorship and that it fulfills all the requirements of the Code of Conduct and Good Practices of Universidade de Lisboa.

Acknowledgments

Throughout the writing of this dissertation I have received a great deal of support and assistance.

I would first like to thank my supervisor at NTNU, Professor Kristin Y. Pettersen, who received me with open arms and whose expertise was invaluable in formulating the research questions and methodology. Her insightful feedback pushed me to sharpen my thinking and she has always found time for me and my problems.

I would like to acknowledge my supervisors at IST, Professor João Sequeira and Professor Antonio Pascoal for their wonderful help and guidance in the last months, and for the patient support and orientation.

Last but not least my sincerest thanks go to my family and friends. To my parents Sandra and Reinaldo, for their unconditional support, who have raised me to be who I am today. For my aunts, Bé and Sónia, for always believing in me and being proud of all my accomplishments. To my best-friends back home, Ruka, Mariana and Carolina, that I miss endlessly. To my friend Sophie for not letting me go down. To my friend Lisa, that made Trondheim a bit more special. To my friend and room-mate João for pushing each others through the pandemic. To Charlotte, Eline and Malene, for their entire love with my move to Oslo.

Finally, to my grandmother, Mimi, for not seeing her biggest wish come true.

Abstract

Small, flexible, and maneuverable robots that can perform light tasks, inspection, maintenance, and access small places at low cost are a growing need for the thriving market of subsea exploration. Underwater Snake Robots have the ability and efficiency to overcome what once was, a costly operation when using Remotely Operated Vehicles (ROVs), or Autonomous Underwater Vehicles (AUVs). Path-following is an essential problem within pipe/cable inspection as it might be required for the robot to inspect a considerable length of pipes and cables without moving away from them in the presence of external disturbances. By resorting to cooperative path-following, the inspection of the can be sped up with Underwater Snake Robots (USRs) working together and synchronized. This thesis presents two models for underwater snake robots, where the influence of constant and irrotational ocean currents is considered. An analysis of different controllers for path following is addressed. Moreover, a solution to the CPF problem concerning this type of robot will be divided into two steps. Having as the main goal the coordination of the robots along a path, CPF can be decoupling into two sub-problems: i) The problem of the path-following mentioned above for a single vehicle and ii) multi-agent system (MAS) coordination. Simulations will support the work.

Keywords

Underwater Snake Robot, Cooperative Path-following, Path-following, Multi agent System

Resumo

Robôs pequenos, flexíveis e manobráveis que podem realizar tarefas leves, inspeção, manutenção e aceder a estreitos locais a baixo custo são uma necessidade crescente para o próspero mercado de exploração submarina. Os robôs cobra subaquáticos têm a capacidade e a eficiência de superar o que antes era uma operação cara ao usar veículos operados remotamente (ROVs) ou veículos subaquáticos autônomos (AUVs). Seguir o caminho é um problema essencial na inspeção de tubos / cabos, pois pode ser necessário para o robô inspecionar um comprimento considerável dos mesmos sem se afastar deles na presença de perturbações externas, como correntes maritimas. Recorrendo ao path-following cooperativo, a inspeção do pode ser acelerada com USRs fazedo-os trabalhar em conjunto e de forma sincronizada. Esta tese apresenta dois modelos para robôs cobra subaquáticos, onde é considerada a influência de correntes oceânicas constantes e irrotacionais. Uma análise de diferentes controladores para seguir o caminho é abordada. Além disso, uma solução para o problema do CPF referente a este tipo de robô será dividida em duas etapas. Tendo como objetivo principal a coordenação dos robôs ao longo de um percurso, o CPF pode ser desacoplado em dois subproblemas: i) O problema do seguimento do percurso mencionado acima para um único veículo e ii) coordenação do sistema multiagente (MAS). Simulações darão o suporte necessario ao trabalho.

Palavras Chave

Robô cobra submarino; Seguimento de Caminho; Seguimento de Caminho Cooperativo; Sistema Multiagente;

Contents

List of Figures

List of Tables

Acronyms

AUV	Autonomous Underwater Vehicle
ROV	Remotely Operated Vehicle
IMR	Inspection, Maintenance, and Repair
USR	Underwater Snake Robot
UUV	Unmanned Underwater Vehicle
UV	Uninhabited Vehicle
DP	Dynamic Positioning
GNC	Guidance, Navigation, and Control
GNSS	Global Navigation Satellite System
INS	Inertial Navigation System
CPG	Central Pattern Generator
CM	Center of mass
LOS	Line-of-Sight
ILOS	Integral Line-of-Sight
CB	Constant Bearing
PP	Pure Pursuit
PF	Path-Following
VHC	Virtual Holonomic Constraints
CLF	Control-Lyapunov Function
CPF	Cooperative Path-Following

1

Introduction

Contents

1.1 Motivation

From the air we breathe to the water we drink, the weather, and climate patterns, the oceans play a role in virtually everything, but despite this fact, we know very little about our ocean. Through its exploration, we can acquire information needed to understand environmental changes better, reducing unknowns in the deep-ocean and providing high-value environmental expertise needed to address both current and emerging science and management needs. This information can reveal new sources for medical drugs, food, and energy resources that otherwise would remain unknown. Information acquired during deep-ocean exploration missions can help predict earthquakes and tsunamis, for example, using underwater fiber-optic cables [2]. In recent years, there has been a substantial increase in the number of subsea companies. As the offshore industry's carbon footprints continue to grow, these companies are looking at ways to cut costs and reduce environmental impacts. The growth in the number of subsea production installation has created a demand for subsea Inspection, Maintenance, and Repair (IMR) operations, making it a field of technology with enormous potential for autonomous marine robotics to thrive. Their use will, therefore, give environmentally friendly and safer solutions and reduced operational costs. Nowadays, these types of subsea operations are employed using ROVs endowed with at least one manipulator arm. Remotely Operated Vehicles (ROVs) are, as the name implies, remotely controlled by an operator, often connected to a ship by umbilical cables, which allows a human-being to command them from above the surface, usually on-board a surface ship. Being controlled directly, they can serve many different uses, whether it is hull inspection or collecting evidence from the seafloor. ROVs often substitute the work of human divers in cases where it is not safe for a diver to operate. Autonomous Underwater Vehicles (AUVs) can conduct their survey missions without operator intervention. Once completed their tasks, they will return to a pre-programmed location where data can be downloaded and processed. Their survey missions cover a wide range of possibilities, such as detecting and mapping shipwrecks, seabeds, and places that can be a hazard to navigation for commercial and recreational vessels. For AUVs, energy is a limitation, and therefore their hydrodynamics are adapted to reduce this problem. Contrary to ROVs, AUVs do not have an external power source, so an efficient propulsion system is essential. As a result of these limitations, the industry is starting to see the need for a new generation of Unmanned Underwater Vehicle (UUV) that are more versatile, robust, and cost-efficient, providing the ability to solve the progressively more complicated tasks that may arise.

Biomimetics has been used for centuries to seek solutions for technical problems with inspiration from the natural world. In nature, snakes are one of the creatures that exhibit excellent mobility in various terrains and environments. This ability appears as a result of millions of years of evolution. Sea snakes move efficiently through the water and in between rocks and corals using their long and slender bodies. Inspited by the robustness and stability of biological fishes and snake locomotion,Underwater Snake Robots (USRs) afford the potential to overcome the challenges mentioned for AUVs/ROVs and to

extend the capabilities of traditional UUV. They further hold promise to meet the growing need for IMR operations in challenging and unknown environments and to improve the efficiency and maneuverability of modern-day underwater vehicles. The fact that a USR has the shape of a biological snake makes it ideal for moving in high viscosity environments such as water. USR is an articulated structure consisting of serially connected joint modules. Although it can mimic the eel-like motion of biological snakes, this solution has its limitations. It becomes challenging to navigate in tight areas as the entire body must move to generate propulsive forces. Moving the whole body has a direct impact on tasks such as Dynamic Positioning (DP), becoming much harder to maintain its position. Adding thruster modules will open up a full new range of applications as it can achieve forward, backward, and sideways motion without performing undulatory movements. This class of robots is promising and is a potential solution to replace both ROVs and AUVs in light interventions, covering vast distances and access narrow and challenging locations but also provide a range of new applications. Thus, many problems of theoretical and practical nature must be solved first to realize operational snake robots for such underwater applications. This thesis addresses some of these problems, with particular emphasis on control design challenges, where a critical control problem concerns the ability to follow a given reference path under the influence of ocean currents. This problem will be approached and tackled according to the maneuvering control problem [3] that is, by solving the one of the two separated tasks that entail. On the one hand, we have a Geometric task, which entails convergence to the desired path and, on the other hand, a Dynamic one, which entails convergence to an assigned speed. The geometric task can be seen as a path-following control problem whilst the Dynamic task is a velocity control problem. We will be focused on guarantee the fulfilment of the geometric task. Furthermore, a cooperative path-following concerning this class of robots will also be of particular importance.

1.2 Main Objectives

The aim of the work presented in this thesis is to design systems for motion control of underwater snake robots entailing system modeling and design of algorithms for path-following and cooperative path-following in the presence of unknown currents. This study will thereby be evaluated based on system performance analysis and numerical simulations. The work will include the presentation of two models for underwater snake robots. Line-of-Sight approaches will be used in USR for path following in order to make them follow a straight line as this approach is motivated by the effective application of LOS guidance laws for path following control of underactuated (they have fewer control inputs than degrees of freedom) marine surface vessels, a characteristic that both share. An approach to Virtual Holonomic Constraitns will be carried out to make it possible to solve the maneuvering problem and later. The cooperative Path Following in Underwater Snake Robots will be solved and evaluated based on system

performance analysis.

1.3 Organization of the chapter

This thesis is is organized as follows:

Chapter 2 presents a review of the background knowledge and state of the art of the addressed subjects such as guidance and control for marine robots, path-following of both marine robots and underwater snake robots and an overview of the work done on the subject of cooperative path-following in Autonomous Marine Vehicles

win **Chapter 3** the mathematical model of the kinematics and dynamics of underwater snake robots swimming in virtual horizontal plane is presented. The hydrodynamic model presented in 3.3, considers both resistive fluid forces and reactive fluid forces, fluid moments and the effect of constant and irrotational ocean currents.

Chapter 4, a simplified model based on prismatic joints instead of revolute joints is derived, under the assumptions of ocean currents as chapter in 3. This chapter also includes preliminary results, demonstrating that using a sinusoidal gait pattern is possible to achieve propulsion on an USR.

Chapter 5 presents a review of the control system that allows the underwater snake robot to converge for a path and progress along without any velocity constraint and under the presence of ocean currents as done in [4, 5]. In addition new simulation analysis, with new insights are performed using the control oriented model of the underwater snake robot moving in 2D as it lacks in [4, 5].

Chapter 6 makes the bridge needed, from the Maneuvering Problem using Virtual Holonomic Constraints to the Underwater Snake Robot Formation. Here the Maneuvering Problem using Virtual Holonomic Constraints that was developed for terrestrial snake robots in [6] is extended to the Maneuvering Problem using VHC for Underwater Snake Robots with the respective stability proofs.

Chapter 7 presents the derivation of a control method for coordination control of multiple underwater snake robots. Here are considered relative forward velocities due to the ocean currents. The works of [6, 7] for terrestrial snake robots lack on diversity of formations and number of robots working to achieve a desired formation. As a result, a simulation analysis focusing in increasing the number of robots and the type of formations is presented in latter.

2

State of The Art

Contents

2.1 Literature Review of Snake and Underwater Snake Robots

This section contains a fast paced survey of the state of the art of snake robots. Over the last years, attempts to mimic animal motion have resulted in many technological advances. Besides these advances, scientists and engineers have yet not replicated the fluidity of animal movement. Biological snakes can traverse a wide range of challenging and complex environments. Snake robots have been successful in mimicking real snakes, but there is still a big gap between both. J. Gray studied the mechanisms of locomotion on snakes [8] and fishes, where eels [9] were his focus. His studies were the basis for the development of both land and underwater snake robots.

A Snake Robot is a robotic mechanism designed to move like a biological snake. These mechanisms usually consist of a set of connected joint modules capable of bending into one or more planes. They can be classified as Uninhabited Vehicle (UV). Uninhabited Vehicles are mobile systems without the need to have an operator on board to control it [10]. They can either be remotely controlled or remotely guided vehicles and also be autonomous vehicles that are able to sense their environment and navigate on their own. Based on the operational environment, UVs can be defined as: Unmanned Underwater Vehicles (UUVs), often known as underwater drone; Unmanned Surface Vehicles (USVs) such as Autonomous Surface Vehicles, used to operate at the surface of the water; Unmanned Aerial Vehicles (UAVs) (e.g., drones); Unmanned ground vehicles (UGVs, e.g., autonomous cars); Unmanned Spacecraft can be remote controlled (e.g., unmanned space mission) and autonomous (e.g., space probe). The potential ability of snake robots to perform a wide variety of tasks, places this class of robots as a highly adaptable UV system.

Figure 2.1: ROV

Shigeo Hirose was the pioneer researcher on snake robots whose work culminated with the construction of prototypes of snake robots [11]. He provides an excellent overview of several snake robots, as well as some discussion on snake kinematics [12]. In addition to his research, new work has emerged (see [13] and references within). Some of the most significant systems can locomote on flat or slightly

rough surfaces, such as the toroidal skin drive (TSD) snake robot [14]. Others can climb slopes, pipes or even trees, such as the Creeping snake Robot, PIKo, and Uncle Sam [15–17], respectively. Some can also locomote in the presence of obstacles such as the Aiko snake robot [18] or the Kulko snake robot [19]. And, most importantly, for this thesis, there is widespread interest in the development of amphibious and underwater snake robots [20, 21]. The referred work is not a complete list of all the significant work done. As a matter of fact and for a more comprehensive insight, some reviews of snake robots should be taken into account [12, 22].

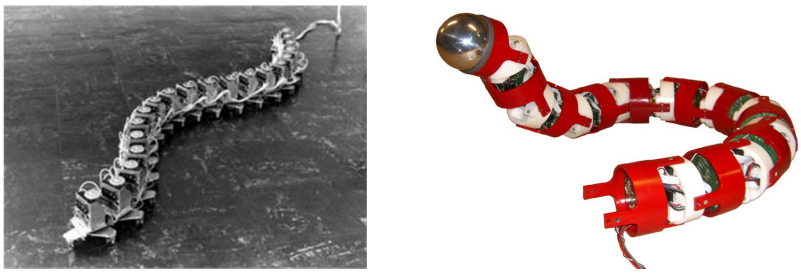

(a) The snake robot ACM III, world's first snake robot

(b) Aiko Robot

Figure 2.2: Some examples of snake robots

In comparison to conventional snake robots, amphibious snake robots (also referred to as eel-like robots) can locomote in aquatic environments. The research on amphibious snake robots has resulted in fewer prototypes than their land counterparts [20, 23, 24]. As underwater snake robots, they are both inspired by biological systems. Biological snakes demonstrate different gaits such as serpentine, concertina, crotaline or side-winding, and rectilinear movement [9]. In water-based environments, biological fish present different gaits such as carangiform, in which a higher proportion of the body undulates. Other types of locomotion include thunniform, in which the tail moves mostly independently of the body and anguilliform (i.e., eel-like), in which the entire extent of the body moves in a series of curved waves passing from head to tail [25].

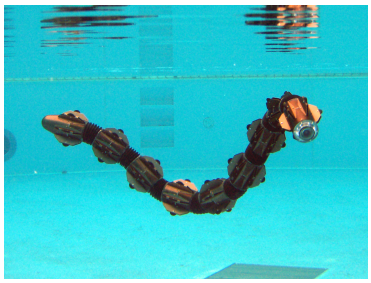

Figure 2.3: ACM-R5 amphibious snake robot

One of the principal interests of the bio-inspired snake robots is to increase motion efficiency by

improving their method of locomotion. To do so, researchers have been studying aquatic biological systems and their ways of movement [26–29]. Nonetheless, agility and maneuverability can likewise be improved by improving the methods of locomotion. Both agility and maneuverability are associated with a general decrease in the size of the robot, as well as the flexibility of its internal shape.

2.2 Guidance and control

2.2.1 Marine robots

Guidance, Navigation, and Control (GNC) systems represent three independent, interconnected subsystems that are at the core of any autonomous mobile robot. Each subsystem performs different tasks that are classified according to guidance, navigation, and control [1].

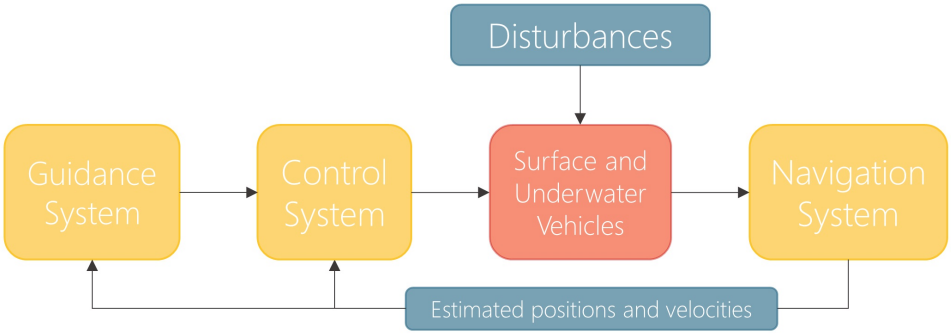

Figure 2.4: GNC [1]

Guidance has the responsibility to continuously compute the desired (reference) position, velocity, and acceleration based on data acquired by the necessary components of the guidance system, such as motion sensors, weather data, and a computer. The computer processes the information obtained, and the results are fed to the motion control system.

Navigation is responsible for determining the position and attitude, course; distance traveled by the velocity and also the acceleration of a vehicle using Global Navigation Satellite System (GNSS) combined with Inertial Navigation System (INS).

Control, also known as motion control, is the procedure of determining control outputs based on control inputs, so that they satisfy a desired control objective(e.g., setpoint regulation, trajectory-tracking, path-following), usually seen in conjunction with the guidance system. Concerning figure 2.4, environmental disturbances should be taken into account when designing a motion control system. For Surfaces Vehicles such as Marine crafts, wind, waves, and ocean currents must play an important role when designing such systems.

For the sole purpose of underwater vehicles and under the assumption that they are moving at

a reasonable depth, we can disregard the influence of both wind and waves and consider only the influence of ocean currents. The navigation subsystem presents different challenges for both surface and underwater vehicles. These challenges lie in the technology and navigation techniques used by surface vessels that are mostly not used by underwater vehicles. GPS is an example of technology used by surface vehicles that are not applied to UVs due to the impossibility to transmit electromagnetic information at specific frequencies [30].

2.2.2 Path-following control of Marine Robots

Marine vehicle control is a challenging and exciting problem since, besides the vehicle dynamics, the external disturbances such as ocean currents must be taken into account. Furthermore, usually, vehicles are under-actuated; This means that the vehicle cannot control precisely its motion because the number of actuators is less than the number degrees of freedom.

The path-following problem refers to a control objective in which either a surface or underwater vehicle should converge to and follow a desired predefined path and progress along with non-zero velocity, without any explicit temporal constraints [1]. There are multiple approaches to this problem, being the most commonly used the ones pervasive in the missile community, such as Line-of-Sight (LOS) guidance, Pure Pursuit (PP) guidance, and the Constant Bearing (CB) guidance (see [31] for a detailed study of the methodologies mentioned).

LOS is designated as a three-point guidance scheme. This scheme involves a reference point, a target point, and the interceptor that can be either the surface or the underwater vehicle. The vehicle points to the target point, which is at a certain distance ahead of the vehicle, in order to approach the path smoothly [1]. LOS can also be used to track a moving target but is disregarded from this point on as it is of no interest in this thesis. Multiple studies in the literature address the problem of the path-following. It was initially developed for straight-lines but was also achieved for curved paths [32] .

One of the biggest problems that marine vehicles face when dealing with path-following is the existence of disturbances (e.g., wind, ocean currents, and waves). The presence of constant ocean currents will push the vehicle of its path. If that is the case and the current is transverse to the movement of the vehicle, a constant offset will arise. There are ways to tackle this problem, being the most common one using the Integral Line-of-Sight (ILOS). It can be proved in [33] that, once a robot converges to a straight-line path its stays in that path if not disturbed. The difference between both guidance laws is that the ILOS compensates for the steady-state offset, which occurs as a consequence of the constant transverse current, making use of integral action. This guidance law is proved to be working for a surface vessel [34] and for underwater vehicles moving in 3D [35]. A general approach to compensate for the disturbances caused by unknown ocean currents when both position and relative velocity is known precisely, is the introduction of observers and adaptative techniques, allowing to achieve path-

following of marine and underwater vehicles [36]. In [37], an observer is used as a control strategy for the path-following of a straight path, to estimate the oceans' current magnitude and direction.

2.2.3 Path-following control of USR

While the research of path-following for Marine and underwater vehicles is extensive, in what concerns underwater snake robots and fish-like robots, the studies are limited. USRs can propel their body by propagating a wave through it from head to tail using different types of gaits. Biological snakes and eel-like fishes inspire these movements. Recently studies for a robotic fish [38] show that a nonlinear model predictive control (NMPC) approach can make the system converge and stay on the desired path. Also, in [39], the guidance control law for the fish-like robot with a Carangiform gait makes the system converge to the desired trajectory.

Figure 2.5: Underwater Snake Robot Mamba

[40] introduces LOS guidance to fish robots in order to head them towards the predefined waypoints. Nonetheless, and regarding the path-following of both straight and curved trajectories, the works of [27], [41] and [42] propose controllers to that matter and also synthesize gaits for rotational and translational motion of various fish-like robots. The problem of tracking trajectory is addressed in [43], wherein the presence of constant currents fish-like robots showed that two flow sensors and a Braitenberg controller [44] are sufficient to keep the fish swimming towards the flow. The LOS guidance strategy studied for snake robots moving on land in [22], can also be applied to swimming robots, as relative velocity is the same as absolute velocity under the condition of absence of ocean currents [45], both models become identical by replacing the ground-friction coefficients by hydrodynamic drag parameters. In an environment where ocean currents are presented, this guidance law will not enable the convergence of the robot to the desired path. LOS guidance has been extended to work around these disturbances.

A USR, besides being able to propel its body by following a gait pattern, can as well turn towards the path by adding an offset to the joint references. For the problem of path following problem, the offset is calculated so that the robot converges to the desired path, and it stays there. In a real-world case scenario, there is no ocean current-free environment. As mentioned previously in Path-following control of Marine Robots for a constant ocean current that is transverse to the movement of the vehicle, a steady-state offset will arise, and the general LOS guidance law is not able to make the vehicle to converge to the desired path. These conclusions can be applied to USR that as well will drift from the desired path under constant currents.

An extend from the LOS guidance law that uses the integral effect is used in [4] to tackle this problem.

2.2.4 Cooperative Path-Following for Autonomous Marine Vehicles

Cooperative Path-Following (CPF) follows the same principle as regular path following, but with the addition of the number of vehicles that to maintain a desired inter-vehicle formation pattern and path are obliged to rely on inter-vehicle-communication. CPF is, in itself, a challenging and exciting problem able to improve the efficiency, performance significantly and create a wide range of new capabilities beyond the ones of individual vehicles.

CPF is divided into two main tasks - a motion controller task responsible for following the desired path, tracking a virtual target (which is made in [46] using two different approaches), and a dynamic assignment task accountable for adjusting the speed of the virtual goals as a means to maintain the desired formation between the vehicles. As to Path-Following (PF) in USR, the research on CPF for Autonomous Marine Vehicles is scarce. In [46], both stability and convergence of the overall system are formally proved to this problem.

In [47], LOS curved path-following for AUVs worked in unknown currents. Also, in [48], the approach using ILOS control for path-following guarantees global asymptotic path following of straight-line path in the presence of unknown and irrotational ocean currents. The most significant overhead for CPF is still the communication between vehicles. Underwater communication systems lack good bandwidth and require to exchange information at a discrete instant of time. In [49], different communication settings were tested to address the communication bandwidth constraints imposed by water environments. No studies on CPF were done and applied to USR to this day. In further chapters, this problem is addressed and supported by a solid background on USR and CPF as well as supported by simulations and, eventually, practical experiments.

3

Modeling of an Underwater Snake Robot

Contents

In this chapter the model of an underwater snake robot moving in 2D using the first principles is presented based on the work done in [5, 22], without any relevant changes. This chapter is organized as follows. First the model for underwater snake robots is derived from the work done in the aforementioned references, after which, a control-oriented model, where the robot is modelled as a set of prismatic joints instead of the revolute joints, is also derived based from [5]. This second model captures the essential behavior of the robot, when designing controllers for path-following and will be the model where we will focus our attention further on.

Contributions of the chapter This chapter serves as a review of the both models

3.1 Basic Notation

The following matrices and vectors are vastly used in the formulation of the model of underwater snake robots and they are defined as :

$$\boldsymbol{A} = \begin{bmatrix} 1 & 1 & & \\ & \ddots & \ddots & \\ & & 1 & 1 \end{bmatrix} \in \mathbb{R}^{(N-1)\times N}, \qquad \boldsymbol{D} = \begin{bmatrix} 1 & -1 & & \\ & \ddots & \ddots & \\ & & 1 & -1 \end{bmatrix} \in \mathbb{R}^{(N-1)\times N},$$

$$\boldsymbol{e} = \begin{bmatrix} 1 & \dots & 1 \end{bmatrix}^T \in \mathbb{R}^N, \qquad \boldsymbol{E} = \begin{bmatrix} e & 0_{N\times 1} \\ 0_{N\times 1} & e \end{bmatrix} \in \mathbb{R}^{N\times N},$$

$$I_n = \begin{bmatrix} 1 & & 0 \\ \vdots & \ddots & \\ 0 & \dots & 1 \end{bmatrix} \in \mathbb{R}^{2N\times 2} \qquad \boldsymbol{K} = \boldsymbol{A}^T \left(\boldsymbol{D}\boldsymbol{D}^T\right)^{-1} \boldsymbol{D} \in \mathbb{R}^{N\times N}$$

$$\boldsymbol{H} = \left(\boldsymbol{I}_n - \tfrac{1}{n}\boldsymbol{e}\boldsymbol{e}^T\right)^{-1} \boldsymbol{K}^T \in \mathbb{R}^{N\times N}, \qquad \boldsymbol{V} = \boldsymbol{A}^T \left(\boldsymbol{D}\boldsymbol{D}^T\right)^{-1} \boldsymbol{A} \in \mathbb{R}^{N\times N}$$

The matrix A and D represent the addition and difference matrix respectively. A is responsible for adding pair of adjacent elements of vectors while D is responsible for subtracting them. The matrix I_N is an identity matrix of size $N \times N$ and e represents the summation vector responsible for summing all the elements from a n-dimensional vector. The diagonal operator, $diag(\cdot)$, produces a matrix where the diagonal has the argument of the operator. Also some other operators are of special importance as they are defined for the vector of link angles $\boldsymbol{\theta} = [\theta_1 \dots \theta_N]$ as follows:

$$sin(\boldsymbol{\theta}) = \begin{bmatrix} sin(\theta_1) & \dots & sin(\theta_N) \end{bmatrix}^T \in \mathbb{R}^N, \qquad \boldsymbol{S_\theta} = diag(sin(\boldsymbol{\theta})) \in \mathbb{R}^{N\times N},$$

$$cos(\boldsymbol{\theta}) = \begin{bmatrix} cos(\theta_1) & \dots & cos(\theta_N) \end{bmatrix}^T \in \mathbb{R}^N, \qquad \boldsymbol{C_\theta} = diag(cos(\boldsymbol{\theta})) \in \mathbb{R}^{N\times N},$$

$$sgn(\boldsymbol{\theta}) = \begin{bmatrix} sgn(\theta_1) & \dots & sgn(\theta_N) \end{bmatrix}^T \in \mathbb{R}^N, \qquad \dot{\boldsymbol{\theta}}^2 = \begin{bmatrix} \dot{\theta_1}^2 & \dots & \dot{\theta_N}^2 \end{bmatrix}^T \in \mathbb{R}^N.$$

3.2 Kinematic modelling

The snake robot consists of a rigid body with mass, m_i, uniformly distributed so that the Center of mass (CM) of each link is located at the mid-point of each link. Every link has length $2l_i$ and therefore

the moment of inertia, J_i, for each link is given by:

$$J = \frac{1}{3} m_i l_i^2 \tag{3.1}$$

N-1 motorized joint do the connection between each of the N links and change the joint angle between link i and i+1. The total mass of the robot is given by the general formula:

$$m = \sum_{i=1}^{N} m_i \tag{3.2}$$

However for this thesis it is assumed that all the links have the same mass, m, and thus the total mass of the robot is defined as Nm.

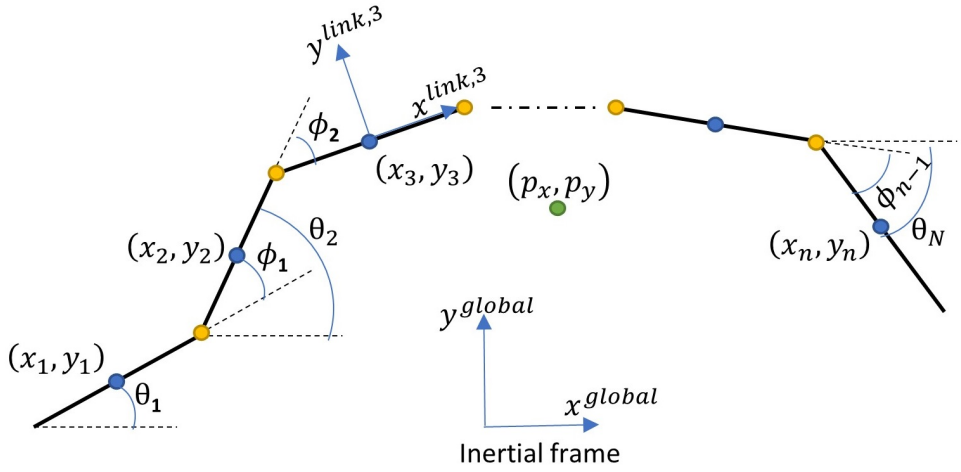

Figure 3.1: Kinematics of USR

Both underwater snake robots and snake robots move in a 2D virtual horizontal and flat planes and have $N + 2$ degrees of freedom composed by N link angles and two degrees of freedom related to the x-y position of the robot. The angles θ and ϕ come into play in the model, so an explanation to avoid ambiguity between both is considered.

***Definition* 3.2.1.** The link angles θ_i (orientation of the link i) is defined as the angle formed between the global x-axis and the link i , $i \in \{1, \ldots, N\}$. The positive direction is counter-clockwise.

The link angles can be assembled in a vector $\boldsymbol{\theta} = [\theta_1, \ldots, \theta_N] \in \mathbb{R}^N$

***Definition* 3.2.2.** The joint angle Φ_i is the relative angle between two links and are defined as:

$$\Phi_i = \theta_i - \theta_{i+1}, i \in \{1, \ldots, N\} \tag{3.3}$$

This angle can be assembled into a vector $\mathbf{\Phi} = [\Phi_1, \ldots, \Phi_{N-1}] \in \mathbb{R}^{N-1}$ In the literature, different conventions for Φ are considered. For this thesis, the aforementioned convention is considered as opposite to the one used in [22]. Both conventions consider the positive direction as being counter-clockwise.
The heading and orientation of the robot is not unique and should be chosen accordingly to control purposes. In [50] and an approach based on segmented kinematics is proposed for this problem. Throughout this thesis the heading or orientation of the snake is defined as the average of all link angles, that is,

$$\bar{\theta} = \frac{1}{N} \sum_{i=1}^{N} \theta_i \tag{3.4}$$

There are other ways of defining the orientation, such as considering the angle of the head link θ_N as the orientation of the robot. In $\bar{\theta}$, we are considering the system as a whole, based on the average of all links, whereas the heading given only by θ_N makes the control design easier for purposes where the head of the robot is needed to be used with precision.

***Definition* 3.2.3.** The center of mass of each link is given by (x_i, y_i) and can be assembled into a vector $\boldsymbol{X} = [x_1, \ldots, x_N]^T$ and $\boldsymbol{Y} = [y_1, \ldots, y_N]^T$. The CM of the robot in the global frame is given by:

$$\boldsymbol{P}_{CM} = \begin{bmatrix} p_x \\ p_y \end{bmatrix} = \frac{1}{N} \begin{bmatrix} \boldsymbol{e}^T \mathsf{X} \\ \boldsymbol{e}^T \mathsf{Y} \end{bmatrix} \tag{3.5}$$

Furthermore, the local frame of each link is placed at the CM of each link with x-axis tangential to the link and the y-axis normal to it. If the link angle, θ_i, is zero the local frame and the global frame will be aligned and we can derive the rotation matrix from the global frame to the link i frame as

$$R_{link_i}^{global} = \begin{bmatrix} \cos\theta_i & -\sin\theta_i \\ \sin\theta_i & \cos\theta_i \end{bmatrix} \tag{3.6}$$

The velocity of the components of the center of mass are given with respect to the heading of the robot as:

$$\bar{v} = \begin{cases} \bar{v_t} = \dot{p}_x \cos\bar{\theta} + \dot{p}_y \sin\bar{\theta} \\ \bar{v_n} = \dot{p}_x \sin\bar{\theta} - \dot{p}_y \cos\bar{\theta} \end{cases} \tag{3.7}$$

where $\dot{p}_x$ and $\dot{p}_y$ are the velocity of the center of mass in the inertial frame of the robot given by:

$$\dot{\boldsymbol{p}}_{CM} = \begin{bmatrix} \dot{p}_x \\ \dot{p}_y \end{bmatrix} \tag{3.8}$$

A general equation for the components of the CM velocity (3.10) can be derived from 3.6 and 3.8:

$$\begin{bmatrix} \bar{v}_t \\ \bar{v}_n \end{bmatrix} = R_{\bar{\theta}}^T \dot{\boldsymbol{p}}_{CM}, \tag{3.9}$$

where $R_{\bar{\theta}}$ is the Rotation Matrix where the argument $\bar{\theta}$ is dependent of the convention choose to represent the heading of the robot.

***Definition* 3.2.4.** The position of each link *i* is given by:

$$\begin{cases} \mathsf{X}_{\boldsymbol{i}} = -l\boldsymbol{K_i}^T \cos\boldsymbol{\theta} + p_x \\ \mathsf{Y}_{\boldsymbol{i}} = -l\boldsymbol{K_i}^T \sin\boldsymbol{\theta} + p_y \end{cases} \tag{3.10}$$

where $\boldsymbol{K}_i$ denotes the row *i* in the matrix $\boldsymbol{K}$ defined in section 3.1 and $\boldsymbol{\theta}$ is the joint angles of all links. Therefore, the velocity of the individual links are given by differentiating the position of each link with respect to time, yielding

$$\begin{cases} \dot{\mathsf{X}}_i = -l\boldsymbol{K_i}^T \boldsymbol{S}_\theta \dot{\boldsymbol{\theta}} + \dot{p}_x \\ \dot{\mathsf{Y}}_i = -l\boldsymbol{K_i}^T \boldsymbol{C}_\theta \dot{\boldsymbol{\theta}} + \dot{p}_y \end{cases} \tag{3.11}$$

Nonetheless and as the linear accelerations are necessary to express the fluid forces in the hydrodynamic model, differentiating the velocity of the individual links (3.11) and using the second derivative of equation (3.5) with respect to time yields

$$\begin{cases} \ddot{\mathsf{X}} = l\boldsymbol{H}^T \left(\boldsymbol{C}_\theta \dot{\boldsymbol{\theta}}^2 + \boldsymbol{S}_\theta \ddot{\boldsymbol{\theta}} \right) \\ \ddot{\mathsf{Y}} = l\boldsymbol{H}^T \left(\boldsymbol{S}_\theta \dot{\boldsymbol{\theta}}^2 - \boldsymbol{C}_\theta \ddot{\boldsymbol{\theta}} \right) \end{cases}, \tag{3.12}$$

where $\boldsymbol{H}$ is defined in section 3.1.

3.3 Hydrodynamic Modeling

The fluid forces induced by the motion of a rigid body in an underwater environment are highly non-linear and some of the effects are often not taken into account. The modeling approach considered in this thesis consider linear and non-linear drag forces, added mass effects, fluid moments, current effects and also resistive torques and inertial torques. The fluid moments provide a more accurate model from an energy efficiency standpoint, however, they are mainly discarded as they have little influence on underwater snake robot motion. Generally, on the one hand for slow swimming objects, viscous forces are dominant, on the other hand, for larger swimming objects it is the added mass effect that is dominant. Both the drag forces (resistive forces) and added mass effects as they are of critical importance to make USR go forward. The drag forces are dependent on the relative velocity of the center of mass and on the drag coefficients. Moreover for high velocities, non-linear drag forces $f_D^{''}$ in 3.19 are dominant, while linear drag forces $f_D^{'}$ in 3.18 are dominant for slow velocities. For the hydrodynamic model, three important assumptions underlying the fluid effects are considered [21]:

***Assumption* 1.** In the inertial frame, the fluid is viscid, irrotational and incompressible.

***Assumption* 2.** The robot is neutrally boyant, which means that the gravity and boyancy cancel each other and the robot remains at the same depth and working in the 2D plane.

***Assumption* 3.** The current $\boldsymbol{v_c} = [V_x, V_y]^T$ is constant and irrotational in the inertial frame

The expression for the global frame fluid forces on the links can be assembled in a matrix form as:

$$\mathsf{f} = \mathsf{f}_{\boldsymbol{A}} + \mathsf{f}_{\boldsymbol{D}}, \tag{3.13}$$

where f_A is the added mass effect forces that depend on the relative link acceleration in the body frame:

$$\begin{bmatrix} \boldsymbol{V_{r_x}} \\ \boldsymbol{V_{r_y}} \end{bmatrix} = \begin{bmatrix} \mathsf{C}_\theta & \mathsf{S}_\theta \\ -\mathsf{S}_\theta & \mathsf{C}_\theta \end{bmatrix} \begin{bmatrix} \dot{\mathsf{X}} - \boldsymbol{V}_x \\ \dot{\mathsf{Y}} - \boldsymbol{V}_y \end{bmatrix} \tag{3.14}$$

$$\begin{bmatrix} \dot{\boldsymbol{V}}_{\boldsymbol{r_x}} \\ \dot{\boldsymbol{V}}_{\boldsymbol{r_y}} \end{bmatrix} = \begin{bmatrix} \mathsf{C}_\theta & \mathsf{S}_\theta \\ -\mathsf{S}_\theta & \mathsf{C}_\theta \end{bmatrix} \begin{bmatrix} \ddot{\mathsf{X}} \\ \ddot{\mathsf{Y}} \end{bmatrix} + \begin{bmatrix} -\mathsf{S}_\theta & \mathsf{C}_\theta \\ -\mathsf{C}_\theta & -\mathsf{S}_\theta \end{bmatrix} \begin{bmatrix} diag(\dot{\boldsymbol{\theta}}) & 0 \\ 0 & diag(\dot{\boldsymbol{\theta}}) \end{bmatrix} \begin{bmatrix} \dot{\mathsf{X}} - \boldsymbol{V}_x \\ \dot{\mathsf{Y}} - \boldsymbol{V}_y \end{bmatrix}, \tag{3.15}$$

with the formulas for the relative link acceleration we derive f_A as :

$$\mathsf{f}_A = \begin{bmatrix} \mathsf{f}_{\boldsymbol{A}}, \boldsymbol{x} \\ \mathsf{f}_{\boldsymbol{A}}, \boldsymbol{y} \end{bmatrix} = - \begin{bmatrix} 0 & -\mu_n \mathsf{S}_{\boldsymbol{\theta}} \\ 0 & \mu_n \mathsf{C}_{\boldsymbol{\theta}} \end{bmatrix} \begin{bmatrix} \dot{\boldsymbol{V}}_{\boldsymbol{r_x}} \\ \dot{\boldsymbol{V}}_{\boldsymbol{r_y}} \end{bmatrix} \tag{3.16}$$

The parameter μ_t is set to zero as the added mass if a slender body in the longitudinal direction can be neglected compared to its body mass [51] and so it is not contemplated in 3.16 . The global frame drag forces f_D on the links can be written as:

$$\mathsf{f}_{\boldsymbol{D}} = \mathsf{f}_{\boldsymbol{D}}^{\boldsymbol{I}} + \mathsf{f}_{\boldsymbol{D}}^{\boldsymbol{II}}, \tag{3.17}$$

the linear drag forces are given by:

$$\mathsf{f}_{\boldsymbol{D}}^{\boldsymbol{I}} = -\begin{bmatrix} c_t \boldsymbol{C_\theta} & -c_n \boldsymbol{S_\theta} \\ c_t \boldsymbol{S_\theta} & c_n \boldsymbol{C_\theta} \end{bmatrix} \begin{bmatrix} \boldsymbol{V_{r_x}} \\ \boldsymbol{V_{r_y}} \end{bmatrix}, \tag{3.18}$$

whereas the non-linear drag forces f_D^{II} are:

$$\mathsf{f}_{\boldsymbol{D}}^{\boldsymbol{II}} = -\begin{bmatrix} c_t \boldsymbol{C_\theta} & -c_n \boldsymbol{S_\theta} \\ c_t \boldsymbol{S_\theta} & c_n \boldsymbol{C_\theta} \end{bmatrix} sgn\left(\begin{bmatrix} \boldsymbol{V_{r_x}} \\ \boldsymbol{V_{r_y}} \end{bmatrix}\right) \begin{bmatrix} \boldsymbol{V_{r_x}}^2 \\ \boldsymbol{V_{r_y}}^2 \end{bmatrix}. \tag{3.19}$$

The fluid torques acting on all the links are given by [21]:

$$\tau = -\lambda_1 \boldsymbol{I}_n \ddot{\boldsymbol{\theta}} - \lambda_2 \boldsymbol{I}_n \dot{\boldsymbol{\theta}} - \lambda_3 diag\left(sgn(\dot{\boldsymbol{\theta}})\dot{\boldsymbol{\theta}}^2\right), \tag{3.20}$$

the parameters λ_1 represents the added mass parameter, and the coefficients λ_2 and λ_3 the drag torques parameters. we can split equation 3.20 into both components as:

$$\begin{cases} \tau_A = -\lambda_1 \boldsymbol{I}_n \ddot{\boldsymbol{\theta}} \\ \tau_D = -\lambda_2 \boldsymbol{I}_n \dot{\boldsymbol{\theta}} - \lambda_3 diag\left(sgn(\dot{\boldsymbol{\theta}})\dot{\boldsymbol{\theta}}^2\right) \end{cases}, \tag{3.21}$$

the parameters λ_1,λ_2 and λ_3 are dependent on the shape of the body and fluid characteristics. One still needs to find a value for them. For the derivation of those parameters, the reader is referred to [21]. An important property for USR locomotion is to have an higher resistive force normal to the links than tangential to them so that the propel can be achieved by sideway motion of link *i* given by the undulatory gain pattern [52], that is,

$$c_n > c_t$$

3.4 Dynamic model

The equations of motion for the underwater snake robot are formulated in terms of the acceleration of the position of the center of mass $\ddot{\boldsymbol{P}}_{CM}$ and the acceleration of the link angles $\ddot{\boldsymbol{\theta}}$. They can be obtained using the previously obtained formulas and formulating both force and torque balance equations for each

link. The equations of motion are given by the following expressions:

$$\boldsymbol{M}_\theta \ddot{\boldsymbol{\theta}} + \boldsymbol{W}_\theta \dot{\boldsymbol{\theta}}^2 + \boldsymbol{V}_\theta \dot{\boldsymbol{\theta}} - \tau - l\boldsymbol{S}_{\boldsymbol{\theta}} \boldsymbol{K} \mathbf{f}_{\boldsymbol{D},\boldsymbol{x}} + l\boldsymbol{C}_{\boldsymbol{\theta}} \boldsymbol{K} \mathbf{f}_{\boldsymbol{D},\boldsymbol{y}} = -\boldsymbol{D}^T \mathbf{u} \tag{3.22a}$$

$$Nm\ddot{\boldsymbol{P}}_{CM} = \boldsymbol{E}^T \mathbf{f}, \tag{3.22b}$$

where $\boldsymbol{M}_\theta, \boldsymbol{W}_\theta, \boldsymbol{V}_\theta$are given in [21], $\mathbf{f}_{D,x}$ and $\mathbf{f}_{D,y}$ given by equation 3.18 and $\mathbf{u} \in \mathbb{R}^(N-1)$ is a vector that contains the motor torques of single joints. The disregard of the added mass effect is a frequent assumption for bio-inspired robots [53] and for slowly moving underwater vehicles [1]. In the disregard of this effects, $\mathbf{f}_A$ and τ_A, the effect of the fluid on the robots is described only by the linear and non-linear drag forces and the resistive fluid torque. With these assumptions, we can write the equations of motion as:

$$\boldsymbol{M}_\theta \ddot{\boldsymbol{\theta}} + \boldsymbol{W}_\theta \dot{\boldsymbol{\theta}}^2 + \boldsymbol{V}_\theta \dot{\boldsymbol{\theta}} + \tau_D - l\boldsymbol{S}_{\boldsymbol{\theta}} \boldsymbol{K} \mathbf{f}_{\boldsymbol{D},\boldsymbol{x}} - l\boldsymbol{C}_{\boldsymbol{\theta}} \boldsymbol{K} \mathbf{f}_{\boldsymbol{D},\boldsymbol{y}} = \boldsymbol{D}^T \mathbf{u} \tag{3.23a}$$

$$Nm\ddot{\boldsymbol{P}}_{CM} = \boldsymbol{E}^T \mathbf{f}_D, \tag{3.23b}$$

These equations are identical to the ones obtained in [22] for snake robots moving on land, where instead of fluid drag forces, ground friction forces are employed and the resistive fluid torques are negleted. The model for USR can so be simplified to the one used in terrestrial snake robots making use of the aforementioned changes but also assuming ocean currents being zero, drag parameters c_n and c_t, replaced by viscious friction coefficients and negleting non-linear drag forces.

4

Control-Oriented model USR

Contents

4.1 Control-oriented model

In this section, a simplified model of the one obtained in the previous sections is derived for Underwater Snake Robots moving on a 2D horizontal plane with a planar sinusoidal gait with small amplitudes. The deduction of this model was first implied in [22] for snake robots moving on land and for underwater snake robots in the absence of unknown ocean currents in [54]. In this model, transversal links displacements are modeled instead of rotational joint motion corresponding on replacing the revolute joints by a set of prismatic joints. Using this methodology, it is possible to capture the propulsion of the robot when designing controllers for path following, a subject of great importance for this thesis. This model employs constant ocean currents in its equations in addition of what was done in [54]. In the following sections a basic notation is presented, both kinematics and hydrodynamic models are derived as well as the equations of motion. Finally, a simulation study and discussion is presented.

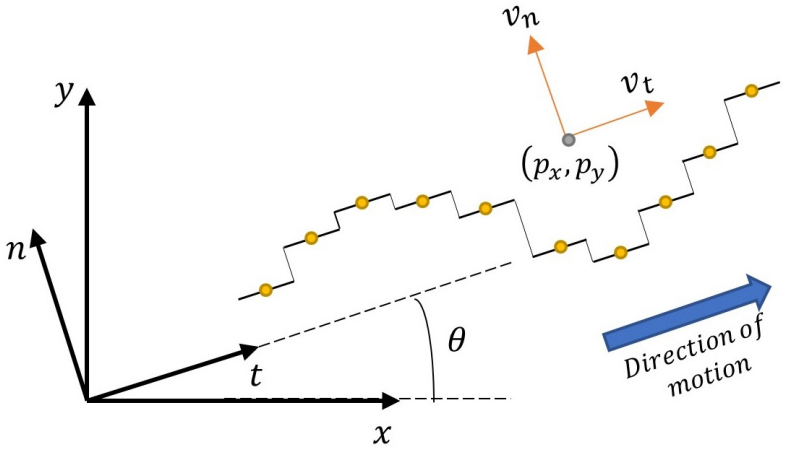

Figure 4.1: Control Oriented Model

4.1.1 Basic Notation

As for the model derived in the previous sections, the simplified model also consists of N links of length 2l with mass uniformly distributed in each link so as the CM is at the midpoint of each link. To derive the control-oriented model the revolute joints are modelled as prismatic joints that move transversal to the direction of movement (figure 4.1). This approximation is valid for sinusoidal gaits that follow the following properties [55]:

***Property* 1.** Forward propulsion, under the assumption that $c_n > c_t$, is achieved through transversal motion of the links

***Property* 2.** The motion of the links, under sinusoidal gait pattern, consists mainly of a normal displacement of the CM of the links

The motion of the robot is defined with respect to the global fixed x-y and t-n frame where the origin of both coincide. The t-n frame is always aligned with the direction of the robot as it is seen in figure 4.1. The t-axis will represent the forward direction while the n-axis the normal direction. From the t-n frame the velocity components of the robot are written as forward velocity, v_t and sideways velocity, v_n. The angle θ is expressed with respect to the global axis with counter-clockwise positive direction. As the links of the USR doesn't rotate w.r.t each other they all have the same orientation, that is coincident with the t-n frame, θ can be defined as:

***Definition* 4.1.1.** The orientation of the robot is given by $\theta \in \mathbb{R}$ with counter-clockwise positive direction.

The robot has $N+2$ degrees of freedom corresponding respectively to N-1 joint coordinates of the prismatic joints, a position (p_x, p_y) of the robot in the plane and the orientation of the robot, θ. In addition to what was introduced in 3.1 the following vectors are defined:

$$\bar{\boldsymbol{e}} = [1 \dots 1]^T \in \mathbb{R}^{N-1} \qquad \bar{\boldsymbol{D}} = \boldsymbol{D}^T \left(\boldsymbol{D}\boldsymbol{D}^T\right)^{-1} \in \mathbb{R}^{(N \times N-1)}, \qquad \boldsymbol{\phi} = [\phi_1 \dots \phi_{N-1}]^T \in \mathbb{R}^{N-1}$$

where $\bar{e}$ is the summation vector with dimensions $N-1$ and $\bar{\boldsymbol{D}}$ is the pseudo-inverse.

The position of the center of mass of each link in the t-n frame are given in vector form as [55]:

$$\mathbf{t} = [t_1 \dots t_{N-1}] = p_t \boldsymbol{e} - l\bar{\boldsymbol{D}}\bar{\boldsymbol{e}} \tag{4.1a}$$

$$\mathbf{n} = [n_1 \dots n_{N-1}] = p_n \boldsymbol{e} - \bar{\boldsymbol{D}}\boldsymbol{\phi} \tag{4.1b}$$

where p_t and p_n are the position of the robot in the t-n frame. Differentiating 4.1a the velocity of each CM link is given by:

$$\dot{\mathbf{t}} = \left(v_t + p_n\dot{\theta}\right)\boldsymbol{e} \tag{4.2a}$$

$$\dot{\mathbf{n}} = \left(v_n + p_t\dot{\theta}\right)\boldsymbol{e} - \bar{\boldsymbol{D}}\boldsymbol{\phi} \tag{4.2b}$$

Also the velocities in the x-y frame are derived in [22] as:

$$\dot{\mathbf{p}}_x = v_t \cos\theta - v_n \sin\theta \tag{4.3a}$$

$$\dot{\mathbf{p}}_y = v_t \sin\theta + v_n \cos\theta \tag{4.3b}$$

4.1.2 Hydrodynamic model

In order to derive the fluid forces two assumptions made in [22] and [55] are of special importance:

***Assumption* 4.** For small link angles θ_i the following approximations are valid:
$\sin(\theta_i)^2 \approx 0, \cos(\theta_i)^2 \approx 1$ and $\sin(\theta_i)\cos(\theta_i) \approx \theta_i$

This approximations are valid and a good approximation if $|\theta_i| < 20°$.

***Assumption* 5.** The angular velocity $\dot{\theta}_i$ is neglected in the control oriented model.

This assumption is valid since the dynamics of the angular motion will be much slower than the body shape dynamics.

***Assumption* 6.** The non-linear drag forces (3.19) are negligible during undulatory locomotion

The velocity of the robot is relatively during undulatory locomotion, special for small link angles,θ_i, and so, as mentioned in section 3.3 for slow moving robots the linear drag forces dominate over the non-linear ones. In addition, as discussed in section 3.4, the added mass effect can be neglected for slow moving robots and the following assumption is therefore made:

***Assumption* 7.** The added mass effect are negligible during undulatory movement.

From these previous assumptions and equation 3.18 the fluid forces at each link in x-y frame is written as :

$$\begin{bmatrix} f_{r_{x,i}} \\ f_{r_{y,i}} \end{bmatrix} = -\begin{bmatrix} c_t & (c_t - c_n)\,\theta_i \\ (c_t - c_n)\,\theta_i & c_n \end{bmatrix} \begin{bmatrix} \dot{x}_i - V_x \\ \dot{y}_i - V_y \end{bmatrix}, \tag{4.4}$$

where $\dot{x}_i$ and $\dot{y}_i$ are the velocities of link i in x-y frame. Since this model uses joint coordinates instead of link angles, it is necessary to express (4.4) in terms of joint coordinates. From [22] the link angle can be approximated as :

$$\theta_i \approx \sin\theta_i \approx \frac{y_{i+1} - y_{i-1}}{2l} = \frac{\phi_{i-1} + \phi_i}{2l}. \tag{4.5}$$

For the case considered, where the robots' orientation is aligned with the global x-axis and under the assumption 5, as shown in [22], the following holds: $\dot{x}_i = \dot{t}_i, \dot{y}_i = \dot{n}_i, f_{r_{x,i}} = f_{t,i}$, and $f_{r_{y,i}} = f_{n,i}$. Substituting them and equation (4.5) in equation (4.4), the fluid forces in t-n frame are given by:

$$\begin{bmatrix} f_{t_i} \\ f_{n_i} \end{bmatrix} = \begin{bmatrix} -c_t & c_p\,(\phi_{i-1} + \phi_i) \\ c_p\,(\phi_{i-1} + \phi_i) & -c_t \end{bmatrix} \begin{bmatrix} \dot{t}_i - V_t \\ \dot{n}_i - V_n \end{bmatrix}, \tag{4.6}$$

where V_t and V_n are the ocean current components in the t-n frame. The propulsion coefficient is given by:

$$c_p = \frac{c_n - c_t}{2l} \tag{4.7}$$

4.1.3 Dynamic model

4.1.3.A Translational dynamics

From the deductions in [22], the translational dynamics are given by:

$$\begin{aligned} \ddot{\boldsymbol{\phi}} &= -\frac{1}{m}\boldsymbol{D}\boldsymbol{f}_n + \frac{1}{m}\boldsymbol{D}\boldsymbol{D}^T\boldsymbol{u} \\ \dot{v}_t &= \frac{1}{Nm}\boldsymbol{e}^T\boldsymbol{f}_t \\ \dot{v}_n &= \frac{1}{Nm}\boldsymbol{e}^T\boldsymbol{f}_n \end{aligned} \tag{4.8}$$

And substituting the matrix form of (4.6) in (4.8) the closed-form for the dynamic equations is found and given by:

$$\ddot{\boldsymbol{\phi}} = -\frac{c_n}{m}\dot{\boldsymbol{\phi}} + \frac{c_p}{m}v_{t,rel}\boldsymbol{A}\boldsymbol{D}^T\boldsymbol{\phi} + \frac{1}{m}\boldsymbol{D}\boldsymbol{D}^T\mathbf{u} \tag{4.9}$$

$$\dot{v}_t = -\frac{c_n}{m}v_{t,rel} + \frac{2c_p}{Nm}v_{n,rel}\bar{\boldsymbol{e}}^T\boldsymbol{\phi} - \frac{c_p}{Nm}\boldsymbol{\phi}^T\boldsymbol{A}\bar{\boldsymbol{D}}\dot{\boldsymbol{\phi}} \tag{4.10}$$

$$\dot{v}_n = -\frac{c_n}{m}v_{n,rel} + \frac{2c_p}{Nm}v_{n,rel}\bar{\boldsymbol{e}}^T\boldsymbol{\phi} \tag{4.11}$$

$v_{t,rel}$ and $v_{n,rel}$ are the relative velocities in the body aligned frame:

$$\begin{bmatrix} v_{t,rel} \\ v_{n,rel} \end{bmatrix} = \begin{bmatrix} v_t \\ v_n \end{bmatrix} - R_\theta^T\boldsymbol{v_c} \tag{4.12}$$

with $\boldsymbol{v_c}$ given by assumption 3.

4.1.3.B Rotational dynamics

The translational dynamics of the links were derived in the previous subsection under the assumption that it is possible to approximate the motion of revolute joints as prismatic joints. This assumption, although valid, introduces a drawback in calculating the rotational dynamics of the USR with this model approach. A simplified model to obtain a expression for $\ddot{\theta}$ is obtained as a consequence of the geometry of the problem expressed by (3.4) and (3.10) that states that during lateral undulation the direction of motion changes when the average of its joint angles are non-zero. The average of all joint links are responsible for which direction the robot will turn (if positive, counter-clockwise, if negative, otherwise), but it is also responsible for the turning rate alongside with the forward velocity. Taking this in mind an equation for the overall torque that induces rotational motion can be derived based on the forward velocity and the average of the joint coordinates as:

$$\ddot{\theta}_{rotation} = \lambda_2 v_t \frac{\bar{\boldsymbol{e}}^T\boldsymbol{\phi}}{N-1} \tag{4.13}$$

The fluid forces are the added mass effects and the linear drag forces, the rotational fluid torques are obtained due to the added mass effects and linear drag forces. The torque due to the added mass effect is given by:

$$\ddot{\theta}_{add} = \lambda_3 \ddot{\theta} \tag{4.14}$$

In addition the linear drag forces are modeled as

$$\ddot{\theta}_{drag} = \lambda_1 \dot{\theta} \tag{4.15}$$

Putting together equations (4.13), (4.14), (4.15) and substituting v_t by the relative velocity due to the effect of constant ocean currents, the control-oriented model of the rotational dynamics is obtained:

$$\ddot{\theta} = -\frac{1}{\lambda_3 + 1}\left(\lambda_1 \dot{\theta} - \frac{\lambda_2}{N-1} v_{t,rel} \bar{\boldsymbol{e}}^T \boldsymbol{\phi}\right) \tag{4.16}$$

4.1.3.C Complete control-oriented model

The complete control-oriented model is given by the following equations:

$$\ddot{\boldsymbol{\phi}} = -\frac{c_n}{m}\dot{\boldsymbol{\phi}} + \frac{c_p}{m} v_{t,rel} \boldsymbol{A}\boldsymbol{D}^T \boldsymbol{\phi} + \frac{1}{m}\boldsymbol{D}\boldsymbol{D}^T \mathbf{u} \tag{4.17a}$$

$$\ddot{\theta} = -\frac{1}{\lambda_3 + 1}\left(\lambda_1 \dot{\theta} - \frac{\lambda_2}{N-1} v_{t,rel} \bar{\boldsymbol{e}}^T \boldsymbol{\phi}\right) \tag{4.17b}$$

$$\dot{v}_t = -\frac{c_n}{m} v_{t,rel} + \frac{2c_p}{Nm} v_{n,rel} \bar{\boldsymbol{e}}^T \boldsymbol{\phi} - \frac{c_p}{Nm} \boldsymbol{\phi}^T \boldsymbol{A}\bar{\boldsymbol{D}}\dot{\boldsymbol{\phi}} \tag{4.17c}$$

$$\dot{v}_n = -\frac{c_n}{m} v_{n,rel} + \frac{2c_p}{Nm} v_{t,rel} \bar{\boldsymbol{e}}^T \boldsymbol{\phi} \tag{4.17d}$$

$$\dot{p}_x = v_t \cos\theta - v_n \sin\theta \tag{4.17e}$$

$$\dot{p}_y = v_t \sin\theta + v_n \cos\theta \tag{4.17f}$$

The corresponding state-vector is $x = \left[\boldsymbol{\phi}^T, \theta, p_x, p_y, \dot{\boldsymbol{\phi}}, \dot{\theta}, v_t, v_n\right]^T \in \mathbb{R}^{2N+4}$.

4.1.4 Preliminary results

Some preliminary simulations were conducted to show that the underwater snake robot is able to achieve forward propulsion when moving with a undulatory gait pattern. The parameters were chosen based on experiments performed in a real USR, such as Mamba [56]. Two different motions are employed in the simulation being them, Eel-like motion and lateral undulation. Both are an undulatory gait pattern, and so is expected that with those motions, forward movement is achieved. Both motions are obtained by

controlling each joint of the snake robot according to the reference signal :

$$\phi_{i,ref} = \alpha g(i,N)\sin(\omega t + (i-1)\delta) + \phi_0 \tag{4.18}$$

The origin of this equation will be addressed in the next chapter. In order to obtained a eel-like motion, i.e., the robot moving with increasing amplitude from head to tail [53], the parameter $\alpha g(i,N) = \alpha\frac{N-i}{N+1}$ multiplying a $\sin()$ function is considered. For the lateral undulation, where the robot oscillates with the same amplitude from head to tail, the function g is set to one and the parameter α is responsible for the amplitude of the serpentine wave. ω is the angular frequency of the sinusoidal joint motion, δ responsible for the phase shift. The parameter ϕ_0 is a constant offset, introduced for being responsible to control the direction of locomotion of the USR as it induces turning. The following controller [55] is applied to (4.17a):

$$\boldsymbol{u} = m\left(\boldsymbol{D}\boldsymbol{D}^T\right)^{-1}\left[\bar{\boldsymbol{u}} + \frac{c_n}{m}\dot{\boldsymbol{\phi}} - \frac{c_p}{m}v_{t,rel}\boldsymbol{A}\boldsymbol{D}^T\boldsymbol{\phi}\right] \tag{4.19}$$

and (4.17a) becomes just $\ddot{\phi} = \bar{\boldsymbol{u}} \in \mathbb{R}^{(N-1)}$ where $\bar{\boldsymbol{u}}$ directly controls the joint coordinates and is given by:

$$\bar{\boldsymbol{u}} = \ddot{\phi}_{ref} - k_{v_\phi}(\dot{\phi} - \dot{\phi}_{ref}) - k_\phi(\phi - \phi_{ref}) \tag{4.20}$$

The following parameters were used to simulate the model: The number of links, N = 10, the length, 2l = 0.18 m, the mass, m = 1.56kg, the propulsion coefficient of the control oriented model, $cp = 35.7$, the normal drag parameter,$c_n = 17.3$, the rotational damping, $\lambda_1 = 6$ and the coupling, $\lambda_2 = 120$. Because of assumption 4 the value of $\alpha = 20°$, $\delta = 40°$ and $\omega = 120°$. For the value of the controller gains, $k_\phi = 20$ and $k_{v_\phi} = 5$

The presented results show that the robot using undulatory motion can propel its body and move forward. In both cases, the robot moves in an environment without ocean currents and its orientation is 0º(alongside the x-axis direction). From the results obtained it can be inferred that with this method of locomotion the robot moves forward while keeping the orientation needed. When using lateral undulation the robot displacement in the x direction is larger than that obtained with eel-like motions.

These preliminary results are important for the next phase of this thesis, showing that the robot indeed can move dense fluid environments.

Both figures 4.4 and 4.5 show the evolution of some joint coordinates of special importance (the head and tail, and one in-between used for comparison purposes) in eel-like and lateral undulation motion. From there we can infer and prove what was explained about both motion and how they evolve over time from head-to-tail.

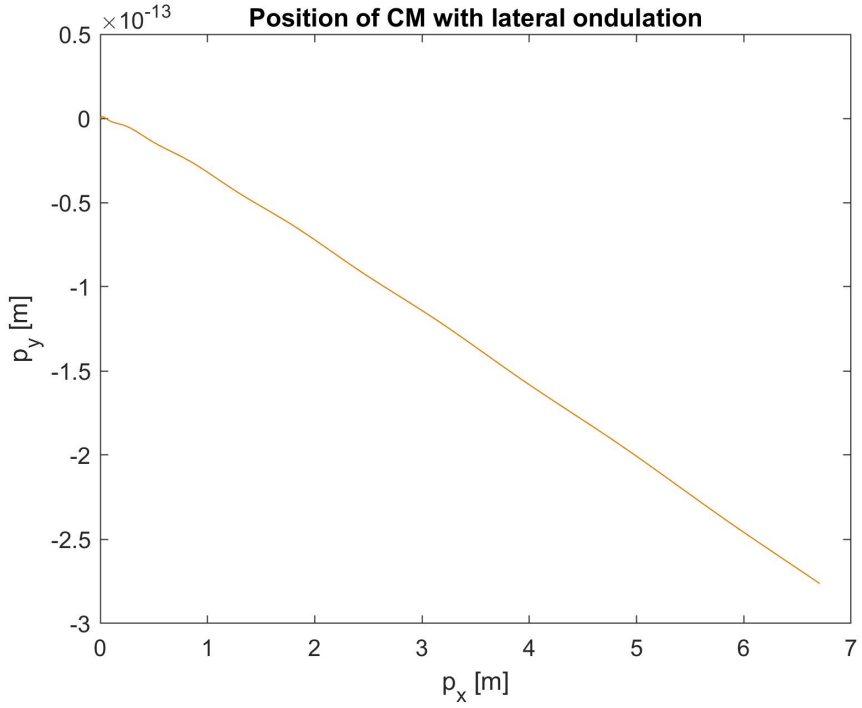

Figure 4.2: Position of CM using lateral undulation for control-oriented model

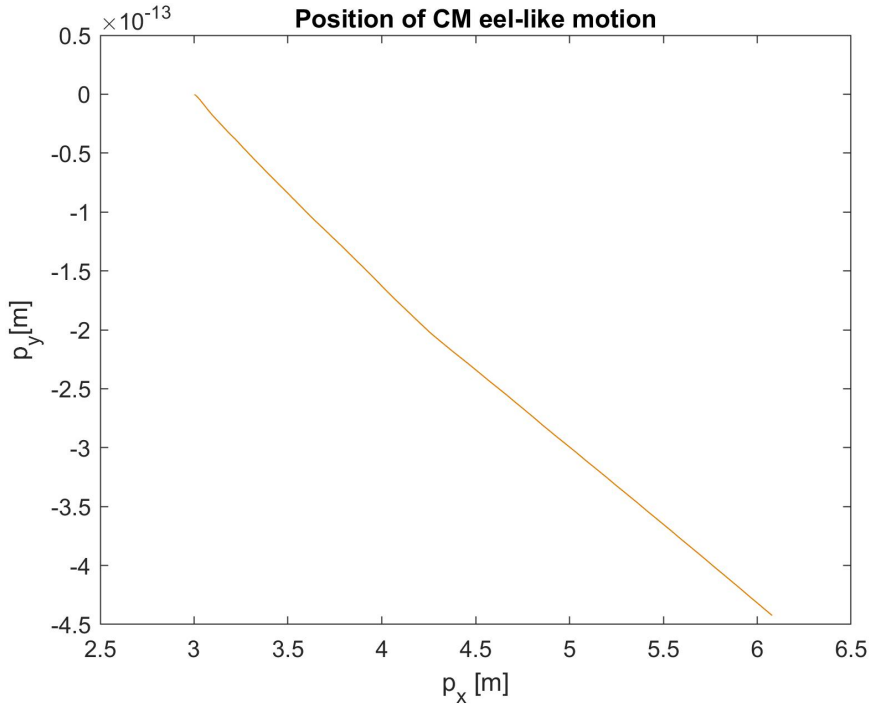

Figure 4.3: Position of CM using eel-like motion for control-oriented model

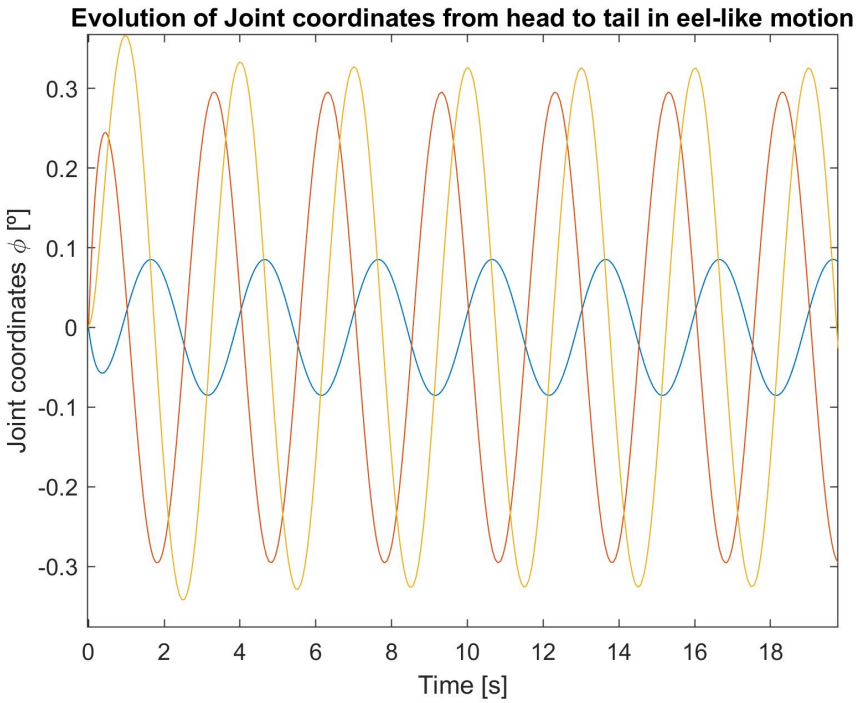

Figure 4.4: Evolution of Joint coordinates for eel-like motion. θ_9 - Blue (head), θ_3 - Red, θ_1 - Yellow (tail)

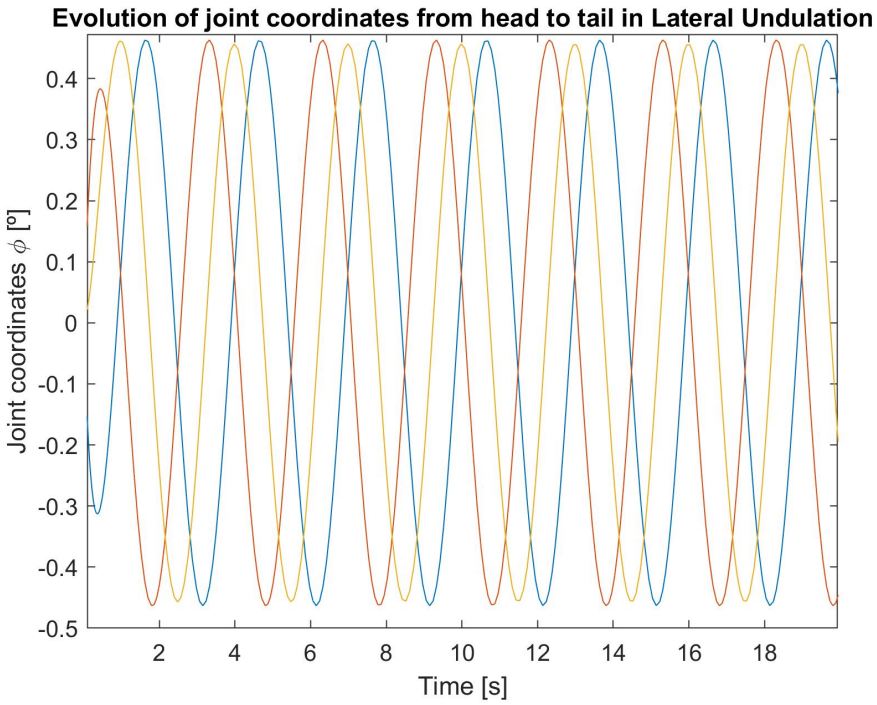

Figure 4.5: Evolution of Joint coordinates for lateral undulation motion. θ_9 - Blue (head), θ_3 - Red, θ_1 - Yellow (tail)

5

Integral Line-Of-Sight Guidance

Contents

In the following chapter the simplified dynamic model of a planar snake is widely used in order to address the path following problem. It is considered that the robot is neutrally buoyant and that it moves with planar sinusoidal gait in the presence of constant, irrational and unknown ocean currents. Furthermore we aim to make the USR converge to and follow a desired straight line path without velocity constraints Before the path following problem is addressed and despite the focus for this chapter be in *Time reference trajectory tracking*, an overview on other control strategies will be provided so as an overview about the implementation of snake locomotion gaits. Furthermore, the control system is based on a control cascade design following along the line of work in [57], where the Line Of Sight guidance law is employed in the outer control loop in order to provide an orientation for the robot. Looking for a more realistic approach to a world case scenario, ocean currents are considered and are accounted for in the guidance scheme. This is made by augmenting it with an integral action to compensate for the steady state error that arise from constant ocean currents. At the end, the path following problem is shown to be solved, under the influence of ocean currents, relying in simulation analysis.

Contributions of this chapter

The contribution of this chapter is a review of the control system that allows the underwater snake robot to converge for a path and progress along without any velocity constraint and under the presence of ocean currents done in [4, 5]. Despite of the control system had been used in the aforementioned studies, it is included here for completeness, as the path following in one of the key aspects of the maneuvering problem and therefore of the formation control. In addition some equations are included for a more clear understanding as they will be important for further stability proofs and deductions. New simulation analysis are performed using the control oriented model of the underwater snake robot moving in 2D as it lacks in [4, 5].

5.1 The Gait Patterns

As talked before, the underwater snake robot is able to achieve forward propulsion by moving its links according to the general equation 4.18, which generates continuous body waves that are propagated from head to tail, whose amplitude is affected by a scaling factor function, $g : \mathbb{Z} \rightarrow [0, 1]$. By defining $g(i) = 1$ it is obtained a mathematical representation for the most common form of locomotion in biological snakes, called lateral undulation. [11] presented a well known mathematical description of the snake body shape during lateral undulation, which has a close approximation with a planar curve whose curvature varies sinusoidally. This curve is most known as serpentoid curve. It can be described by the following mathematical equation [22]:

$$\begin{bmatrix} x(s) \\ y(s) \end{bmatrix} = \int_0^s \begin{bmatrix} \cos\left(a\cos\left(b\sigma\right) + c\sigma\right) \\ \sin\left(a\cos\left(b\sigma\right) + c\sigma\right) \end{bmatrix} d\sigma \tag{5.1}$$

where $a, b, c > 0$ are constants and s is an arc length along the snake body. Furthermore this mathematical representation of the serpenoid curve can be approximated by a discrete mathematical formula frequently used as a gait for snake robots that consists of rigid links [22, 58] and achieved by making the joints track the reference 4.18. From chapter 4, by choosing $g(i)$ accordingly, the generalized robot gait 4.18 is not limited to lateral undulation only. Therefore, defining $g(i) = 1$ we can achieve lateral undulation and with $g(i) = \frac{N-i}{N+1}$, eel-like motion is ensured. These are the most common forms of locomotion, however other gaits were proposed in [59].

5.2 Control Strategies

Different control strategies were employed over the years to control the gait of bio-inspired snakes. These strategies fall into open-loop strategies and closed-loop strategies. For the purposes of this thesis the focus must be on the closed-loop strategies, however to provide the reader a more complete overview, the open-loop strategies will be included.

Central Pattern Generators (CPGs) are neural biological circuits that can produce rhythm patterns of neural activity without receiving rhythmic inputs. Inspired by this, CPGs are a popular method used for locomotion of both snake robots [60, 61] and underwater snake robots [24]. In [62], the proof for asymptotic stability in quadruped locomotion is presented. Using feedforward Central Pattern Generators control laws the asymptotic stability of a system with rhythmic movements can be verified through application of Poincare map, while using feedback control laws provide global stability [63].

There are two closed loop strategies that will be considered, naming them, ***Time reference trajectory tracking*** and ***Virtual Holonomic Constraints***. Both control strategies allow the robot to move forward making use of a similar reference signal as the one in 4.18, however, while one is time dependent, VHC enforces time independent relations on the robots configuration. In the present chapter the main focus will be the closed loop strategy of time reference trajectory tracking. The VHC strategy will be addressed in the following chapters as a way to overcome the maneuvering problem and the CPF.

5.3 Assumptions and Control-Oriented Model transformations

In time reference trajectory tracking closed-loop strategy, feedback controllers are employed to make the joints of the snake track time dependent reference signals (4.18). This closed loop strategy is a common and successful choice for implementation in physical robots [58, 64, 65]. Considering 4.18 as

a time-varying reference signal complicates both the motion planning and the mathematical analysis. Regardless these complications, $\phi_{i,ref}$ is used in [57] for the motion planning algorithm.

As mentioned previously on this chapter, a simplified dynamic model of a planar snake is used to solve the path following problem. From the analysis made in Chapter 4 and from Property 1, a planar sinusoidal gait with small joint angles will create propulsive forces that allow the USR to move forward with certain speed. Assuming that the unknown ocean current v_c is considered, the following assumptions can be made, and the forward velocity is now considered as relative forward velocity due to ocean currents.

***Assumption* 8.** The snake robot moving by a sinusoidal gait with a constant relative forward velocity, is bounded by V_{max} and V_{min}, $v_{trel} \in [V_{max}, V_{min}]$, $V_{max} \geq V_{min} > 0$

Nevertheless, in order to move forward in the presence of ocean currents, the forward velocity generated by the planar sinusoidal gait has to be such that compensates for the ocean current, if not the problem of path following can't be achieved. A new assumption is made with regards to this and states the following:

***Assumption* 9.** Under the influence of ocean current, the relative forward velocity must be large enough to compensate for this disturbance, i.e, $v_{trel} > V_{min} > V_{c,max} \geq 0$.

From the control oriented equations 4.17, the joint coordinates, ϕ are present in the equations of both the dynamics of the angular velocity, $\dot{v}_\theta$ and side-ways velocity, $\dot{v}_n$. As long as the joint coordinates are considered in 4.17b and in 4.17d the design of the control system will complicate as the body shape changes will affect both heading and sideways motion of the robot [5]. To overcome this problem a change of coordinates is performed. It is suggested in [5] and motivated by [57, 66] that in order to get rid of the effect of ϕ in the sideways velocity one should move the point that defines the position of the snake by a distance ϵ from the CM of the robot along the tangential direction of the robot to a point where the joint offset ϕ_0 generates a pure rotational motion and no sideways forces. Based on these, the following change of coordinates is defined:

$$\bar{p}_x = p_x + \epsilon \cos\theta \tag{5.2a}$$

$$\bar{p}_y = p_y + \epsilon \sin\theta \tag{5.2b}$$

$$\bar{v}_n = v_n + \epsilon v_\theta \tag{5.2c}$$

$$\epsilon = -\frac{2(N-1)}{\lambda_2}\frac{c_p}{Nm} \tag{5.2d}$$

For the chosen approach, absolute velocities should be removed from the model by introducing the

following relations:

$$v_t = v_{t,rel} + V_t \tag{5.3a}$$

$$\bar{v}_n = \bar{v}_{n,rel} + V_n \tag{5.3b}$$

where $V_t = V_x \cos\theta + V_y \sin\theta$ and $V_n = -V_x \sin\theta + V_y \cos\theta$ are the ocean currents expressed in the body frame of the robot. Taking the derivative of (5.3a) and substituting (5.2c) and (4.17c) in it, $\dot{v}_{t,rel}$ is easy to obtain and is given by:

$$\dot{v}_{t,rel} = -X_t v_{t,rel} + Y_t \bar{v}_{n,rel} - Z_t v_\theta - \frac{c_p}{m} \boldsymbol{\phi}^T A \bar{D} v_\phi, \tag{5.4}$$

with X_t, Y_t and Z_t defined in the next section.

5.3.1 Transformed Control-Oriented Model

Making the respective changes in the control oriented model 4.17 based on the equations defined in subsection 5.3, the transformed Control-Oriented Model is given by:

$$\ddot{\boldsymbol{\phi}} = -\frac{c_n}{m}\dot{\boldsymbol{\phi}} + \frac{c_p}{m} v_{t,rel} \boldsymbol{A}\boldsymbol{D}^T \boldsymbol{\phi} + \frac{1}{m}\boldsymbol{D}\boldsymbol{D}^T \mathbf{u} \tag{5.5a}$$

$$\ddot{\theta} = -\lambda_1 \dot{\theta} + \frac{\lambda_2}{N-1} v_{t,rel} \bar{\boldsymbol{e}}^T \boldsymbol{\phi} \tag{5.5b}$$

$$\dot{\bar{p}}_y = v_{t,rel} \sin\theta + \bar{v}_{n,rel} \cos\theta + V_y \tag{5.5c}$$

$$\dot{\bar{v}}_{n,rel} = \left(\epsilon \left(\frac{c_n}{m} - \lambda_1\right) + V_x \cos\theta + V_y \sin\theta\right) v_\theta - \frac{c_n}{m} \bar{v}_{n,rel} \tag{5.5d}$$

$$\dot{v}_{t,rel} = -X_t v_{t,rel} + Y_t \bar{v}_{n,rel} - Z_t v_\theta - \frac{c_p}{m} \boldsymbol{\phi}^T A \bar{D} v_\phi, \tag{5.5e}$$

Where $X_t = \frac{c_t}{m}$, $Y_t = \frac{2c_p}{Nm} \boldsymbol{e}^T \boldsymbol{\phi}_{ref}$ and $Z_t = Y_t \epsilon - V_x \sin\theta + V_y \cos\theta$.

5.4 Control Design Objectives

The path following problem consists in making the robot converge to a desired straight line path and once it converges, stay there with positive and sufficiently large forward velocity. A snake robot moving underwater will be subject to unknown ocean currents. Assuming that those ocean currents are constant and irrotational, it will make the robot drift from the desired path with a steady cross-track error. If a pure LOS guidance law is employed to tackle this problem, it will not compensate for the ocean disturbances, thus a new guidance law must be seek. One common approach to solve this, is augmenting the LOS

guidance law with an integral action. The idea of an Integral Line-Of-Sight guidance law for USR was first proposed in [5], augmented from the pure LOS guidance law applied to snake robots that doesn't take into consideration environmental disturbances. Both guidance laws consist on making the robot target a point that lies at a certain distance in the path that the robot wants to follow. The distances is commonly referred to as Look-Ahead-Distance and is given by the parameter $\Delta > 0$. It needs to be sufficiently large, or otherwise the system becomes unstable. This section formalises the control problem considered in this chapter.

***Remark* 1.** The control objectives proposed next do not take into consideration the accurate control of the relative forward velocity once the robot converges to the path. That matter will be addressed in the next chapter along with the control strategy of virtual holonomic constraints.

***Remark* 2.** The inertial reference frame is placed in such a way that the generic desired straight line path $P \triangleq \{(x, y) \in \mathbb{R}^2 : y = y^{path}_{tofollow}\}$, with $y^{path}_{tofollow} \in \mathbb{R}$ and the global x-axis are aligned.

The cross track error, $\tilde{\bar{p}}_y$, must be written taking into account the generic straight-line path as:

$$\tilde{\bar{p}}_y = \bar{p}_y - y^{path}_{tofollow}, \tag{5.6}$$

and so the objectives to be pursued by the control system can be formalized as follows.

The first control objective concerns the cross-track error, were we aim to make the robot's position converge to zero:

$$\lim_{t\to\infty} \tilde{\bar{p}}_y(t) = 0 \tag{5.7}$$

Furthermore, we seek to control the orientation of the robot, defining the second control objective as one that will allow to stabilize the orientation to a desired orientation, θ^{eq}, constant and such that $\theta^{eq} \in \left(-\frac{\pi}{2}, \frac{\pi}{2}\right)$, which is mainly non-zero [4] and given by $\theta^{eq} = -arctan\left(\frac{V_y}{\sqrt{v^2_{trel} - V^2_y}}\right)$ [5].

Thus, **the second and final control objective** can be formally written as:

$$\lim_{t\to\infty} \theta(t) = \theta^{eq} \tag{5.8}$$

As long as these two control objectives are met, the path following problem is solved.

5.5 Control system design

To meet the control objectives, a control law motivated by [57] is presented. The control system consists of two loops. An inner loop and an outer loop. The inner loop is responsible for the joint controller while the outer loop entails both the gait controller, to make the robot propel forward, and the orientation

controller for path following. The guidance law can either be defined as a pure LOS or an Integral LOS. The ILOS guidance law, the body shape controller and the orientation controller are introduced next.

5.5.1 Body Shape Controller

In this section, a feedback control law for the body shape is proposed, taking into consideration the model in subsection5.5. It is well known [11] that the gait pattern lateral undulation for a snake robot is achieved if the robots moves accordingly to the reference joint trajectory given by :

$$\phi_{i,ref} = \alpha g(i) \sin(\omega t + (i-1)\delta) + \phi_0 \tag{5.9}$$

It is shown in [58] that the relative forward velocity, v_{trel}, for a robot that moves based on the lateral undulatory gait induced by 5.9, is directly affected by the gait parameters(α, ω, δ). The gait controller is the last block of the inner control loop of the cascade control system, closing it , and is responsible to enforce the joint coordinate reference 5.9 . Thus, the feedback-linearizing control law ca be defined as in [5],

$$\boldsymbol{u} = m\left(\boldsymbol{D}\boldsymbol{D}^T\right)^{-1}\left[\bar{\boldsymbol{u}} + \frac{c_n}{m}\dot{\boldsymbol{\phi}} - \frac{c_p}{m}v_{t,rel}\boldsymbol{A}\boldsymbol{D}^T\boldsymbol{\phi}\right] \tag{5.10}$$

The input $\bar{\boldsymbol{u}}$ is chosen as the same one used for snakes moving on land and given by

$$\bar{\boldsymbol{u}} = \ddot{\phi}_{ref} - k_{v_\phi}(\dot{\phi} - \dot{\phi}_{ref}) - k_\phi(\phi - \phi_{ref}) \tag{5.11}$$

where, k_{v_ϕ}, k_ϕ >0 are controller gains. Defining the error variable for the joint coordinates as $\tilde{\boldsymbol{\phi}} = \boldsymbol{\phi} - \boldsymbol{\phi_{ref}}$, the closed dynamics of the joint error can be written, from 5.10, 5.11 and 5.5a, as:

$$\ddot{\tilde{\boldsymbol{\phi}}} + k_{v_\phi}\dot{\tilde{\boldsymbol{\phi}}} + k_\phi\tilde{\boldsymbol{\phi}} = 0 \tag{5.12}$$

5.5.2 Orientation controller and Path following

The snake robot has to converge to and follow the x-axis of the inertial frame and move along in order to solve the path following problem. The pure LOS guidance law was first used for snake robots in [57] motivated by [67]. It proved to be working and the convergence was achieved in a free-disturbance environment. Analogue to the studies of [57] the reference heading for underwater snake robots in a free-current environment can be defined as:

$$\theta_{ref} = -\arctan\left(\frac{\tilde{\bar{p}}_y}{\Delta}\right), \tag{5.13}$$

with the design parameter $\Delta > 0$ and $\bar{p}_y$ is cross-track error of the robot. To solve the problem with ocean currents, an integral line-of-sight guidance law is used. The referred guidance law was first used for marine vessels in [68]. Adapting the ILOS guidance law from [68], by considering the change of coordinates performed in section 5.3, it is possible to write the reference orientation for the robot defined as follows:

$$\theta_{ref} = -\arctan\left(\frac{\tilde{\bar{p}}_y + \sigma y_{int}}{\Delta}\right), \tag{5.14}$$

$$\dot{y}_{int} = \frac{\Delta \tilde{\bar{p}}_y}{\left(\tilde{\bar{p}}_y + \sigma y_{int}\right)^2 + \Delta^2}, \tag{5.15}$$

in which both Δ and σ are design parameters and $\Delta, \sigma > 0$. The integral effect will allow the snake robot to side-slip while maintaining the desired straight line path since it gives a non-zero θ_{ref}. In addition, the integral effect becomes significantly important when the snake is pushed away from the path by ocean currents. It is important to note that 5.15 gives less integral action when the vehicle is far from the path ($\tilde{\bar{p}}_y$ is large) reducing the risk of wind-up effect.

Follow the line of work in [22] to make sure that the orientation θ tracks the reference θ_{ref} (6.19), the joint offset ϕ_0, is responsible to steer the robot to the path, such that $\lim_{t\to\infty} \tilde{\theta}(t) = 0$, $\tilde{\theta} = \theta - \theta_{ref}$. Making use of $\tilde{\phi}$ defined in 5.5.1 and $\tilde{\theta}$ and insert it in (5.5b), the joint offset can be chosen as [5]:

$$\phi_0 = \frac{1}{\lambda_2 v_{trel}}\left(\ddot{\theta}_{ref} + \lambda_1 \dot{\theta}_{ref} - k_\theta\left(\theta - \theta_{ref}\right)\right) - \frac{1}{N-1}\sum_{i=1}^{N-1} \phi_{i,ref} \tag{5.16}$$

which has a singularity when $v_{rel} = 0$. A way to circumvent the singularity is only considering the orientation controller when the relative forward velocity in accordance with assumption 9.

The stability analysis of the closed loop system is not included here but the reader is referred to the work done in [69]

5.6 Simulation analysis

This sections presents the simulation result of the proposed control system 5.5, taking into consideration that ocean currents are presented, and that they are constant and irrotational. It is considered for these simulations results that both control oriented model, presented in 5.3.1 and the path following controller presented in 5.5 are implemented in Matlab R2019b. The dynamics of the system were computed using the **ode15s** solver, with absolute tolerance and relative tolerance equals to 10^{-5}.

Symbol	Description	Value	Lateral Undulation	Value	Eel-like	Value
N	Number of Links	10	$g(i)$	1	$g(i)$	$\frac{N-i}{N+1}$
$L = 2l$	Length of the links	$0.18\ m$	α	$0.08\ cm$	α	$0.09\ cm$
m	Mass of each link	$1.56\ kg$	ω	$120°/s$	ω	$130°/s$
c_p	Propulsion coefficient	35.7	δ	$40°/s$	δ	$40°$
c_t	Tangential drag parameter	4.45	Guidance system parameters			
c_n	Normal drag parameter	17.3	Look-ahead-distance, Δ	$1.2\ m$	Look-ahead-distance, Δ	$0.9\ m$
λ_1	Rotational damping coefficient	6	Integral gain, σ	$0.02\ cm/s$	Integral gain, σ	$0.02\ cm/s$
λ_2	Rotational coupling coefficient	120				

Table 5.1: USR, Gait and Guidance System Parameters

The Underwater Snake parameters used are presented in Table 5.1 and follow the same values as the MAMBA robot and validated in [70]. The gait parameters for the simulations are also included in Table 5.1 Two experiences were performed, one for each gait. The gait function $g(i)$ in the reference joint 5.9 was set to $g(i) = 1$ to mimic the lateral undulation motion at first, and changed to $g(i) = \frac{N-i}{N+1}$ in order to mimic the eel-like motion, after .

The value ϵ was computed based on the equation 5.2d and has the value of $\epsilon = -34.3cm$ The gains of the controller were defined as follows : $k_\phi = 20$, $k_{v_\phi} = 5$ and $k_\theta = 0.5$.

The guidance system requires values for the integral gain, σ, and for the look-ahead-distance, Δ. The look-ahead-distance requires to be large enough for the system not to became unstable, and so the guidance system parameters were chosen as defined in Table 5.1.

The initial conditions were defined as follow $\bar{p}_x = 0$ and $\bar{p}_y = 0$. The joint coordinate were set to zero, meaning that $\boldsymbol{\phi} = 0$. The straight line path that the robot has to follow is placed parallel to the x-axis in $y^{path}_{tofollow} = 2$ The initial tangential velocity was set to $v_{t,rel} = 0.1m/s$ to comply with Assumption 9. For last the orientation of the robot is aligned with the path to follow which means that $\theta = 0°$. For last, the ocean current was defined for the lateral undulation motion as $\boldsymbol{v_c} = [-0.08, 0.05]^T\ cm/s$ and for the eel-like as $\boldsymbol{v_c} = [-0.04, 0.04]^T\ cm/s$.

For the derivatives of both θ_{ref} and ϕ_0 reference models based on the ones presented in [22] were used. And so the parameters of the reference models were defined as: $\zeta = 1$ and $\omega_n = \frac{\pi}{2}$.

5.6.1 Simulation Results

Path following with lateral undulation motion

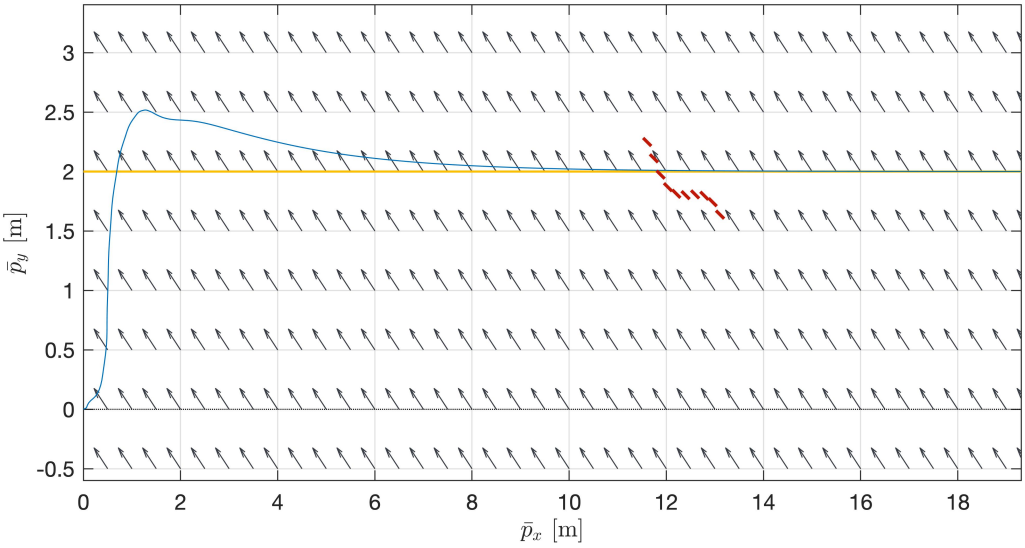

Figure 5.1: Path of the robot to $y = 2$ with lateral undulation motion

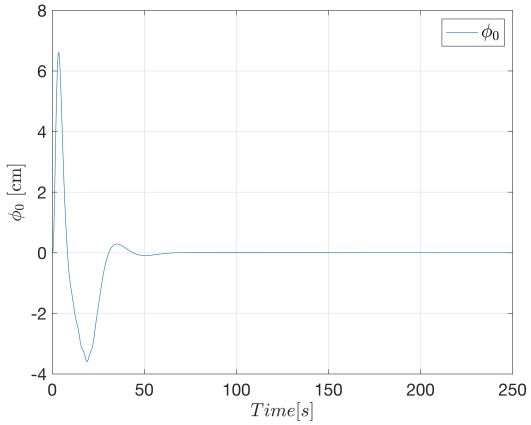

(a) Reference Joint Offset, ϕ_0

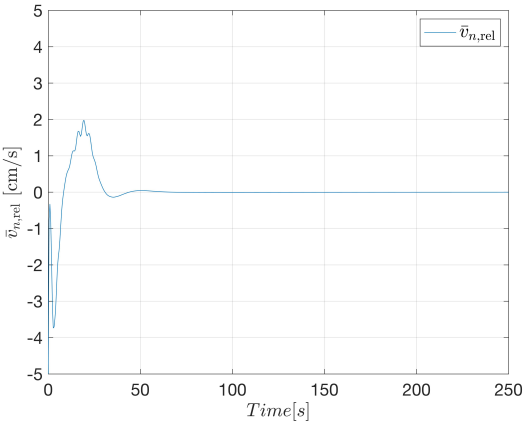

(b) Relative Normal Velocity, $\bar{v}_{n,rel}$

Figure 5.2: ϕ_0 and $\bar{v}_{n,rel}$ for lateral undulation motion

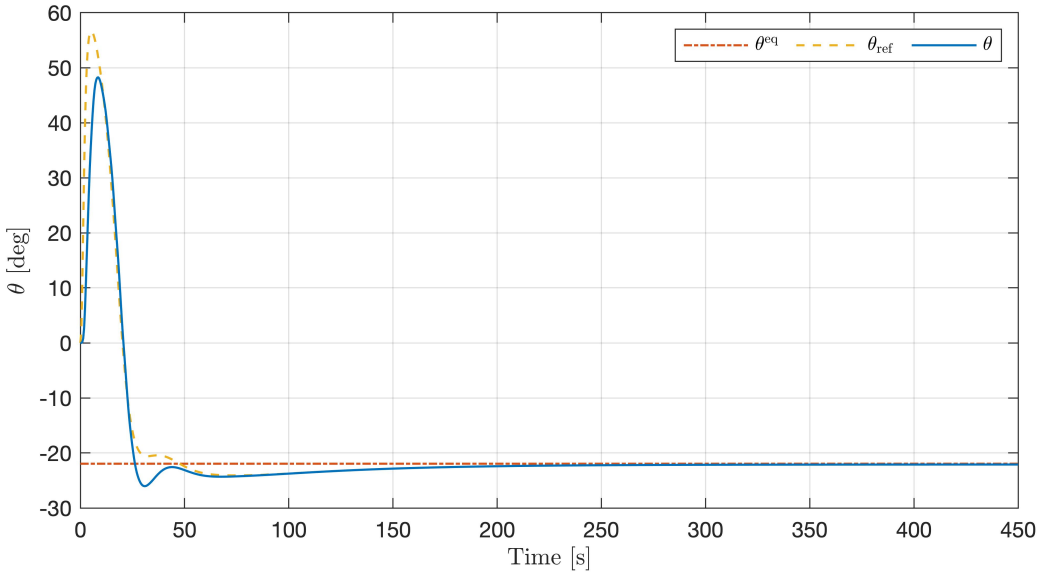

Figure 5.3: Orientation of the robot with lateral undulation motion

Path-Following with Eel-like motion

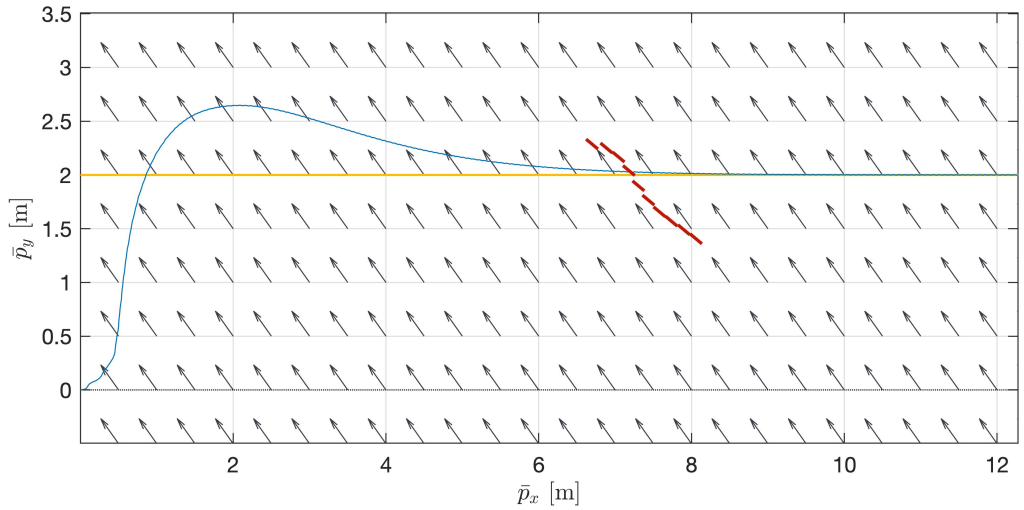

Figure 5.4: Path of the robot to $y = 2$ with eel-like motion

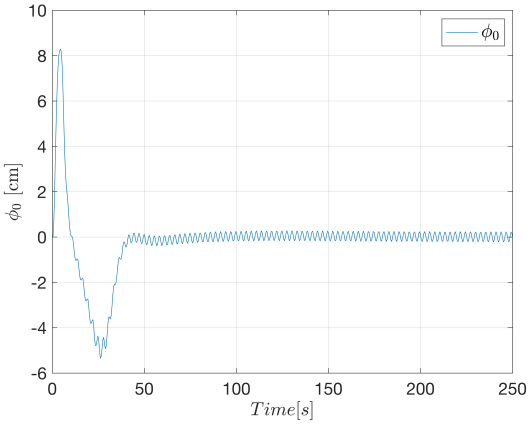

(a) Reference Joint Offset, ϕ_0

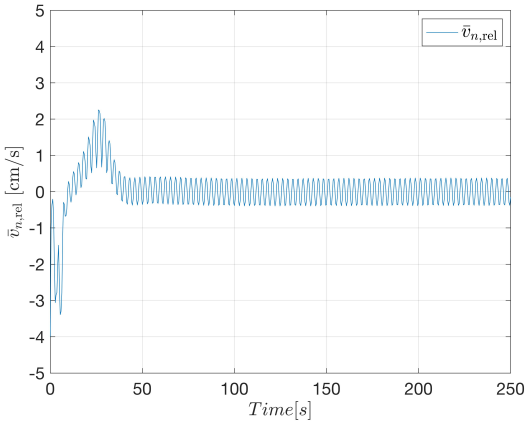

(b) Relative Normal Velocity, $\bar{v}_{n,rel}$

Figure 5.5: ϕ_0 and $\bar{v}_{n,rel}$ for eel-like motion

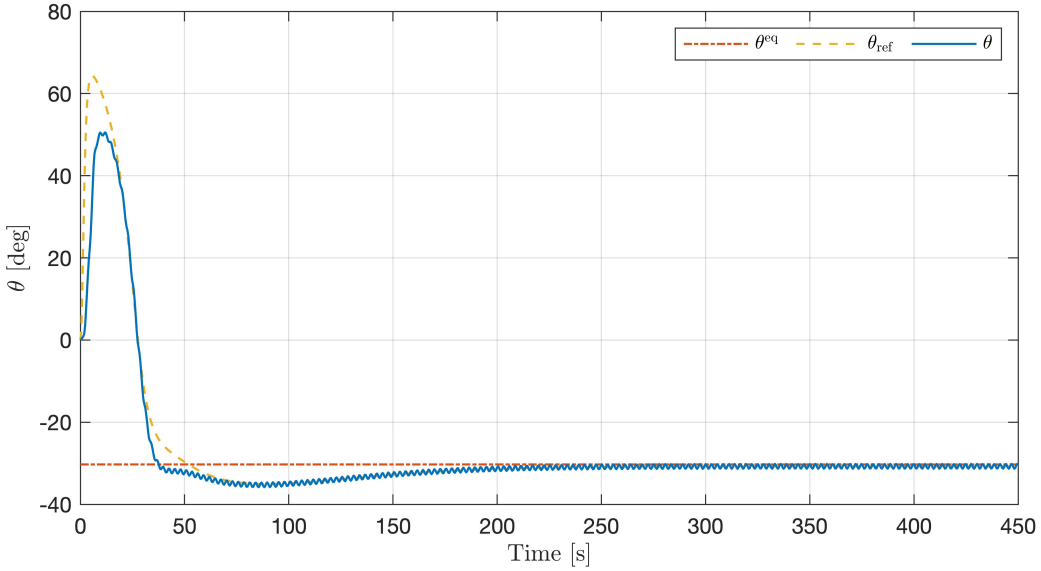

Figure 5.6: Orientation of the robot with eel-like motion

5.6.2 Simulation Analysis

In this chapter, two different scenarios were tested. Where the same ocean current was kept for both experiences.

The first one, the robot was moving with lateral undulation gait while in the second was moving with eel-like motion. The results of the simulation are visualized in figures 5.4, 5.5, 5.6, 5.1, 5.2, 5.3. In the scenario where the robot moves with the eel-like motion it can be seen that once the robot converges to the path it stays there. At first he was being dragged away by the ocean current but turns and converges nicely to the straight line path that was defined as $y^{path}_{tofollow} = 2$. After it's convergence, the robot stayed around the steady state of the orientation, θ^{eq} and thus, ϕ_0 remains around zero. In figure 5.3, the orientation of the robot converges to the reference orientation obtained from the integral line-of-sight guidance law, θ_{ref} which in latter will converge to the steady state angle θ^{eq}, that was calculated a posteriori from equation presented in 5.4. This will allow the robot to compensate for the sideways component of the current as the robot side-slips along the path.

For last, as anticipated, the relative normal velocity, $\bar{v}_{n,rel}$ converges to $0\ m/s$ when the robot is progressing along the path. From the equation (4.12) and applying the change of coordinates from (5.2c), the oscillation around the peak can be explained. This oscillation originates when the robot changes direction, i.e. its orientation, from moving south to north to north to south. The biggest peak happens when $\theta_{ref} = 0$ and joint offset is maximum, and is when the ocean currents have the biggest influence over the robot. As he turns and the gait is not enough to make him completely overcome the ocean currents there are a fluctuation in the relative normal velocity. However as soon as he starts to converge to the path after the transition of direction, the relative normal velocity starts to decrease until $\bar{v}_{n,rel} = 0$, the moment when the $\bar{v}_n$ cancels the influence of the current.

For the scenario where the robot moves with eel-like motion the same results are observed. The robot converges fast after being dragged away from the path by the ocean current. The control input, ϕ_0 stabilizes to zero once the underwater snake robot stays around the steady state of the orientation. The orientation of the robot tracks the reference orientation that is provided by the ILOS guidance law fast, that converges to θ^{eq}. The normal velocity is zero as soon as the robot is progressing along the path. It is possible to see the oscillations presented in the orientation, the control input ϕ_0, which induce turning motion, and the normal relative velocity. Those oscillations are seen as a consequence of the amplitude increase from head to tail on the eel-like movement.

On a side by side comparison, is seen that the lateral undulation doesn't show the same oscillations around the convergence points in any of the results, mostly due to the fact that the amplitude oscillations form head to tail in the snake remain constant through the body. When using the control oriented model and in the presence of ocean currents that overpasses 0.04 m/s in x and y directions, the eel-like motion can not generate enough propulsion from it's gait. Even though the gait parameters such as α can be

increased in order to compensate to that matter, from Assumption 4 they must remain lower so that the approximations remain valid. Another option would be to increase the frequency of oscillations, however an high increase in this parameter, might cause physical damages in the links of the robot, in a real case scenario. The parameters are thus kept in the following intervals: $0.07cm \leq \alpha \leq 0.09cm$ and $110^\circ/s \leq \omega \leq 130^\circ/s$. The lateral undulation, on the other hand, can handle constant and irrotational ocean currents up to 0.1. m/s in each direction, with the gait parameters being inside the aforementioned safe intervals.

The results validate the ILOS path following controller in the presence of irrotational and constant ocean currents. All the control objectives from 5.4 are met for both gaits. It is safe to assume that for the eel-like motion the objectives are still met as it oscillates around the expected values. In a real world scenario due to this oscillations, a better a safest choice would be the use of the lateral undulation gait as the oscillations around the expected values are barely existent.

6

Maneuvering Control in Straight-line Paths using Virtual Holonomic Constraints Under Ocean Currents

Contents

In the previous chapter a solution was presented for the path following problem under the influence of ocean currents. The approach taken did not considered the achievement of a desired relative forward velocity, $v_{t,rel} = v_d$, once it converges to the path. This chapter investigates the planar maneuvering problem for the USR, studied first for marine vessels in [3] and after for terrestrial snake robots [71]. In addition of the previous control objectives, a new control objective will be introduce that addresses the reference velocity constraint.

Due to the fact that making the robot move accordingly to (5.9), an approach different from the one in chapter 5 is needed since the parameters presented in (5.9), being them α, ω, δ, constant and defined a priori, directly affect the forward velocity of the robot. As a result it is not possible to guarantee that the forward velocity will reach the desired velocity once it converges. To solve this complication the proposed feedback control strategy enforces Virtual Holonomic Constraintss (VHCs). For the purposes of this thesis, VHC will encode the gaits studied previously on the USR configuration, where, parameterized by states of dynamic compensator, they will control both orientation and forward velocity. The maneuvering problem is divided into two fundamental tasks. First, a geometric task, solved in the previous chapter without VHCs, and in addition a dynamic task which is responsible to keep the forward velocity steady. The proposed control algorithm will then be tested and verified by means of simulation for different gaits under the influence of constant and irrotational ocean currents.

Contributions of this chapter

The following chapter is one the most important contribution of the thesis as it makes the bridge needed, from the Maneuvering Problem using Virtual Holonomic Constraints to the Underwater Snake Robot Formation. Here the Maneuvering Problem using Virtual Holonomic Constraints that was developed for terrestrial snake robots in [6] is extended to the Maneuvering Problem using VHC for Underwater Snake Robots. The orientation controller designed based on [4] takes into consideration the existence of ocean disturbances, unlike the approaches for terrestrial snake robots [6, 22]. Another contribution for this is the stability proof, that despite following along the same line of thought as in [6, 7], they now take into consideration the ocean disturbances and is proved that the Maneuvering Problem using VHC for Underwater Snake Robots is asymptotically exponential stable based on those and therefore all the control objectives are met. This extension of the framework is then evaluated through simulation analysis using the two most common gaits, lateral undulation and eel-like motion.

6.1 Virtual Holonomic Constraints

The method of virtual holonomic constraints is a method used frequently to solve locomotion control problems. It was first used for Snake Robots in [45], leaving aside the velocity control. The method is also used for motion control of mechanical systems [67, 72]. Moreover, VHCs are a useful concept for the control of oscillations. While performing gait pattern lateral undulation, which consists of fixed periodic body motion, all the solutions of the snake robot dynamics have inherited oscillatory behaviours, thus it can be analytically and constructively controlled based on Virtual Holonomic Constraints.

With this approach the state evolution of the mechanical system is confined to an invariant constraint manifold. Those constraints are virtual because they arise from the action of a feedback controller rather than a physical connection between two variables [67].

The time dependency presented in (5.9) will be removed guaranteeing that the time-evolution of the state variables are confined to state-dependent constraint functions [45] and will be addressed in section 6.3. On a kinematic level the system acts similar to one that holds the same physical constraints when enforcing VHC over the configuration variables. There is an extra power needed to inject by the controller into the closed-loop system in order to maintain the invariant relations [67]. As a result, the dynamic behaviour of these systems is different.

6.2 Control System Design

In this section, motivated by the work done for Snake Robots in [71], a solution for the maneuvering problem making use of the control-oriented model for the underwater snake robot, and the method of virtual holonomic constraints is presented.

The control system design for terrestrial robots from [71], which the approach for underwater robots is based on, is reviewed. In the second part a control system for manoeuvring control of underwater snake robots is proposed, where the stability proof for VHC-based manoeuvring control of terrestrial snake robots in [71] is analogous for the case of Underwater Snake Robots.

The control system for the underwater snake robot can be divided into 3 main stages, first a body shape controller, second, a velocity controller and for last the path following controller. The control approach can be seen as an hierarchical design in a sense that has three main stages, each one with prioritized control specifications. A bridge will be made between the stages for snake robots and underwater snake robots, where the redefinition of the control objectives is made in comparison with chapter 5.4.

6.2.1 Control Objectives

The control objectives needed to solve the maneuvering problem are presented next. The solution for this problem is the starting point to solve the cooperative path following. The maneuvering problem, once again can be divided into two main tasks [3].

- Geometric task: The objective is to make the robot converge to and follow a desired path
- Dynamic task: Consists in satisfying dynamical constraints, where in this case is to satisfy a desired relative forward velocity along the desired path

The first control objective is to asymptotically stabilize the desired gait pattern that produces forward propulsion given by ϕ_{ref}, such that

$$\lim_{t\to\infty} \phi(t) - \phi_{ref}(t) = 0 \tag{6.1}$$

For the second control objective we look for asymptotically stabilize $\theta \to \theta_{ref}$:

$$\lim_{t\to\infty} \theta(t) - \theta_{ref}(t) = 0 \tag{6.2}$$

Thirdly is required that the robot's position converges to the path. We can define a straight line path as $P \triangleq \{(x, y) \in \mathbb{R}^2 : y = 0\}$. As a consequence, we consider that the global x-axis is aligned with the desired straight path as motioned in remark 2.

For the robot to converge we want that the cross-track error, $\bar{p}_y$ goes to zero, $\bar{p}_y \to 0$. However it might be required that the robot, instead follows a path in a position different than zero. That way this control objective can be generalized in a way that the desired straight line path can be re-written as $P \triangleq \{(x, y) \in \mathbb{R}^2 : y = y^{path}_{tofollow}\}$, where $y^{path}_{tofollow} \in \mathbb{R}$ is the path that the robot should follow away from the origin of the global coordinate frame. The convergence is still achieved when the the cross track error converge to zero. To make sure that $\bar{p}_y \to 0$, a change in equation 5.2b is made, taking into consideration $y^{path}_{tofollow}$. Thus, the cross-track error, $\tilde{\bar{p}}_y$, is defined as:

$$\tilde{\bar{p}}_y = p_y + \epsilon \sin\theta - y^{path}_{tofollow} \tag{6.3}$$

and the third control objective defined as follow:

$$\lim_{t\to\infty} \tilde{\bar{p}}_y(t) = 0 \tag{6.4}$$

***Theorem* 1.** The control objective 6.4 is only achieved, under ocean currents, requiring that the desired reference forward velocity, v_d lies within $[V_{max}, V_{min}]$, $v_d \geq v_{t,rel} \geq V_{max} > V_{min} > 0$

For the last control objective, after it's convergence the robot must regulate the forward velocity along

the path for a desired forward velocity profile, $v_{t,ref} > 0$. A reference position along the desired path is defined as $p_{t,ref} = \int_0^t v_{t,ref}(\tau)d\tau$. The last control objective is then defined as:

$$\lim_{t\to\infty} p_t(t) - p_{t,ref}(t) = 0 \tag{6.5}$$

As soon as the objective 4 is asymptotically stabilized, the robot moves accordingly to $v_{t,rel} = v_{t,ref}$.

***Assumption* 10.** For the following sections, it is considered that $v_{t,rel}$ has no finite-escape time.

For a better understanding of the following sections bare in mind the following theorem. The theorem states that the maneuvering controller to be defined next solves the maneuvering problem based on all the stability results under the constraint manifolds defined.

***Theorem* 2.** The constraint manifolds in this chapter are defined such that $\Gamma_1 \subset \Gamma_2 \subset \Gamma_3 \subset \Gamma_4 \subset \mathcal{Q}$, where $\mathcal{Q}$ stands for the configuration space. The constraint manifold Γ_1 is a compact set as all variables used to define it in (6.54) are bounded. Furthermore, the constraint manifold Γ_i is asymptotically stable with respect to the constraint manifold $\Gamma_{i+1}, i = 1, ..., 3$. From here and according to Proposition 14 presented in [73], the constraint manifold Γ_1 is asymptotically stable for the controlled system. As a consequence of this, all the solution of the controlled system remain uniformly bounded and the four control objectives defined in 6.2.1 are all achieved.

6.3 Forward propulsion VHC and Body Shape Controller

Virtual Holonomic Constraints will encode the sinusoidal gaits, studied earlier (5.9), which allow the robot to propel forward, as it has been used in [71] for snake robots. This new formula comes by augmenting the state valued function. Motivated by the notion of dynamic VHC [74] the state vector is augmented and those new variables are used as constraint variables. In other words, dynamic VHC means that VHC depend on the solution of the dynamic compensator. For the new states ϕ_0 and $\dot{\phi}_0$, the second order time-derivative in the form of compensator will be used to control the orientation of the robot in accordance to the reference orientation (6.19). The state vector is augmented with a new state, λ, such that $\lambda(0) = 0$ and $\dot{\lambda} = \frac{2\pi}{T}$, where T denotes the period of the gait pattern. This addition allows the explicit time dependency from the reference joints (5.9) to be removed.

From section 5.1, with regards to snake robots, and using the aforementioned new states, the new reference signal is defined as follows [71]:

$$\phi_{i,ref}(\lambda, \phi_0) = \alpha g(i) \sin(\lambda + (i-1)\delta) + \phi_0, \tag{6.6}$$

where the scaling factor $g(i)$ is added for the solely purpose to achieve a more generalized class of gaits

in swimming snake robots. Equation 6.6 is the proposed VHC, for the body shape variables of the USR, where, λ and ϕ_0 represents the solutions of the compensators that are defined next:

$$\ddot{\lambda} = u_{\lambda} \tag{6.7}$$

$$\ddot{\phi_0} = u_{\phi_0} \tag{6.8}$$

u_{λ} is used as a controller to regulate the relative forward velocity of the robot while u_{ϕ_0} is used as a controller to regulate the heading of the snake. This VHC will be enforced in the robot through the control input $\bar{\boldsymbol{u}}$ in $\dot{v_{\phi}} = \bar{\boldsymbol{u}}$.

Associated with the constraint function $\phi(\lambda, \phi_0)$ is the following constraint-manifold [6].

$$\Gamma_4 = \{(x, \dot{x}, \phi_0, \dot{\phi_0}, \lambda, \dot{\lambda}) \in \mathbb{R}^{2N+8} : \phi_i = \phi_{i,ref}(\lambda, \phi_0), \dot{\phi} = \dot{\lambda}\frac{\partial \phi_{ref}}{\partial \lambda} + \dot{\phi_0}\frac{\partial \phi_{ref}}{\partial \phi_0}\} \tag{6.9}$$

To globally exponentially stabilize the solutions of joint coordinates dynamics on the constraint manifold 6.9 a linearizing feedback controller law, $\bar{\boldsymbol{u}}$ is defined motivated by [5] as :

$$\bar{\boldsymbol{u}} = \ddot{\phi}_{ref} - k_{v_{\phi}}(\dot{\phi} - \dot{\phi}_{ref}) - k_{\phi}(\phi - \phi_{ref}), i \in \{1, \ldots, N-1\}, \tag{6.10}$$

where $k_{v_{\phi}}, k_{\phi} > 0$ are constant controller gains. Defining the following joint error vector:

$$\tilde{\phi} = [\phi_i - \phi_{ref}, \ldots, \phi_N - \phi_{N,ref}] \in R^{N-1} \tag{6.11}$$

we can rewrite 6.10 as:

$$\bar{\boldsymbol{u}} = \ddot{\phi}_{ref} - k_{v_{\phi}}\dot{\tilde{\phi}} - k_{\phi}\tilde{\phi}, \tag{6.12}$$

Substituting 6.12 in $\dot{v_{\phi}} = \bar{\boldsymbol{u}}$ the tracking error dynamics of the joint angles is written as:

$$\ddot{\tilde{\boldsymbol{\phi}}} + k_{v_{\phi}}\dot{\tilde{\boldsymbol{\phi}}} + k_{\phi}\tilde{\boldsymbol{\phi}} = 0 \tag{6.13}$$

which has a globally exponentially stable equilibrium at the origin $\left(\phi - \phi_{ref}, \dot{\phi} - \dot{\phi}_{ref}\right) = (0_{N-1}, 0_{N-1})$. As a consequence, this will stabilize a lateral undulatory gait, and induce forward propulsion and thus, the control objective 6.1 is met.

6.4 Velocity Controller

The stage two unfolds into two sub-stages, the orientation controller and the speed controller, that together are responsible for the velocity controller. The speed controller is inserted in the dynamic task of the maneuvering problem while the orientation controller belongs to the geometric task.

6.4.1 Basic notation for the velocity controller

To the derivation of the controllers that constitute the control system design, the following matrices and expressions are vastly used. This expressions are modified from [6] so that they take into consideration the relative velocities, the constant and irrotational ocean currents, and the hydrodynamics of the underwater snake robot:

$$C = [\alpha \cos(\lambda), \ldots, \alpha \cos(\lambda + (i-1)\delta)]^T \in \mathbb{R}^{N-1} \tag{6.14}$$

$$\Phi_{ref} = [\phi_{1,ref}, \ldots, \phi_{N-1,ref}]^T \in \mathbb{R}^{N-1} \tag{6.15}$$

$$\eta = -\frac{c_p}{Nm}\Phi_{ref}^T A\bar{D} \in \mathbb{R}^{N-1} \tag{6.16}$$

As we use the frequency of the joint angle oscillation as an additional control term to make the relative forward velocity to follow a reference we define:

The tangential position error, $\tilde{p}_t$ and the velocity error, $\tilde{v}_{trel}$as:

$$\tilde{p}_t = p_t - p_{t,ref} \tag{6.17a}$$

$$\tilde{v}_{t,rel} = v_{t,rel} - v_{t,ref} \tag{6.17b}$$

The position error and velocity error dynamics for the Underwater snake robot evaluated in (6.9) are the following:

$$\dot{\tilde{p}}_t = \tilde{v}_{trel} \tag{6.18a}$$

$$\dot{\tilde{v}}_{trel} = -X_t v_{t,rel} + Y_t(\bar{v}_{n,rel} - Z_t) - \frac{c_p}{m}\boldsymbol{\phi}^T A\bar{D}v_\theta - \dot{v}_{tref} \tag{6.18b}$$

with $X_t, Y_t$and Z_t defined in section 5.3.1

6.4.2 Orientation Controller

In section 5 a LOS guidance law that considers an integral action to circumvent the influence of ocean disturbances was derived. Following that analysis, the same guidance law can be applied here and the

reference orientation for the robot, as a function of the cross-track error 6.3 is given by:

$$\theta_{ref} = -\arctan\left(\frac{\tilde{\bar{p}}_y + \sigma y_{int}}{\Delta}\right), \tag{6.19}$$

$$\dot{y}_{int} = \frac{\Delta\tilde{\bar{p}}_y}{\left(\tilde{\bar{p}}_y + \sigma y_{int}\right)^2 + \Delta^2}. \tag{6.20}$$

In (6.20) $\Delta > 0$ denote the look-ahead-distance and it is a fundamental parameter used to tune the rate of convergence of the snake. It is safe to say that a value of Δ that is larger than twice the length of the vehicle [1] will provide a well-damped transient motion and a good convergence time. However the reduction of this value may induce large overshoots, or even poor or unstable performance.

The control of the orientation to the reference orientation, θ_{ref} is made by using $\ddot{\phi}_0$ as an additional control term through a static compensator on the constraint manifold that we want to exponentially globally stabilize. This constraint manifold is described as follows [6]:

$$\Gamma_3 = \left\{(\theta, \dot{\theta}, \phi_0, \dot{\phi}_0, v_{t,rel}, \lambda) \in \Gamma_4 : (\tilde{\theta}, \dot{\tilde{\theta}}) = (0,0), \left\|\left[\phi_0, \dot{\phi}_0\right]\right\| \leq \epsilon_{\phi_0}\right\} \tag{6.21}$$

To stabilize Γ_3 relative to Γ_4 it requires that the orientation error, $\tilde{\theta} = \theta - \theta_{ref}$, converges exponentially to zero on the constraint manifold (6.21). Once this is verified the control objective (6.2) is achieved.

Therefore, the orientation error dynamics can be derived from $\dot{\theta} = v_\theta$ and (5.5b) and evaluated in the constraint manifold Γ_3 as follows:

$$\ddot{\theta} = -\lambda_1\dot{\theta} + \frac{\lambda_2}{N-1} v_{t,rel}\bar{\boldsymbol{e}}^T\boldsymbol{\phi} \tag{6.22}$$

substituting the orientation error, $\tilde{\theta} = \theta - \theta_{ref}$, and it's derivatives in (6.22), it's straightforward to obtain:

$$\dddot{\tilde{\theta}} = -\lambda_1\ddot{\tilde{\theta}} - \lambda_1\ddot{\theta}_{ref} + \frac{\lambda_2}{N-1} v_{t,rel}\bar{\boldsymbol{e}}^T\boldsymbol{S} + \lambda_2 v_{t,rel}\phi_0 - \dddot{\theta}_{ref} \tag{6.23}$$

To stabilize the origin $(\tilde{\theta}, \dot{\tilde{\theta}}) = (0,0)$ of (6.23) an additional control input,ϕ_0, is defined as:

$$\phi_0 = -\frac{1}{\lambda_2 v_{t,rel}}\left(\frac{\lambda_2}{N-1} v_{t,rel}\bar{\boldsymbol{e}}^T\boldsymbol{S} - \lambda_1\ddot{\theta}_{ref} - \dddot{\theta}_{ref} + K_\theta\ddot{\tilde{\theta}}\right) \tag{6.24}$$

Inserting ϕ_0 into (6.23), the orientation error dynamics of the robot (6.24) evaluated on the constraint manifold is written as:

$$\dddot{\tilde{\theta}} + \lambda_1\ddot{\tilde{\theta}} + K_\theta\dot{\tilde{\theta}} = 0, \tag{6.25}$$

which has a globally exponentially stable equilibrium point at the origin $(\tilde{\theta}, \dot{\tilde{\theta}}) = (0,0)$. This implies that the orientation errors converges exponentially to zero, i.e, the constraint manifold is globally exponen-

tially stable manifold under the joint control law (6.12) and the static compensator (6.24).

As a consequence of this the orientation of the robot will follow the reference orientation through the static compensator (responsible to steering the robot) and thus, the objective 6.2 is achieved.

The derivatives of $\dot{\phi}_0, \ddot{\phi}_0, \dot{\theta}_{ref}, \ddot{\theta}_{ref}$ are required for the gait controller and orientation controller respectively. In [6] the analytical expressions for $\dot{\phi}_0, \ddot{\phi}_0, \dot{\theta}_{ref}, \ddot{\theta}_{ref}$ are omitted. Motivated by the approach taken in [22], the time derivatives are obtained using a 3rd order low pass filter reference model that satisfies $\lim_{t\to\infty} x_{ref} = reference$, through motion control actions, with commanded state reference $reference \in \mathbb{R}$. The reason for using this approach is that the time-derivatives of ϕ_0 and θ_{ref} are complex functions of time whose analytical expressions can be quite hard to find. The method that uses the low pass filter shows some advantages from a practical point of view. Their use will make sure that the signals are smooth enough to be sent to the controller. The unknown ocean currents are part of the analytical expressions for $\dot{\theta}_{ref}$ [75]. To get around this problem the low pass filter reference model can be used to substitute the use of analytical expressions for the implementation of $\dot{\phi}_0, \ddot{\phi}_0, \dot{\theta}_{ref}, \ddot{\theta}_{ref}$. From [22] the low pass filter reference model can be written as:

$$\begin{bmatrix} \dot{x}_{ref} \\ \ddot{x}_{ref} \\ \dddot{x}_{ref} \end{bmatrix} = \begin{bmatrix} 0 & 1 & 0 \\ 0 & 0 & 1 \\ -\omega^3 & -(2\zeta+1)\omega^2 & -(2\zeta+1)\omega \end{bmatrix} \begin{bmatrix} x_{ref} \\ \dot{x}_{ref} \\ \ddot{x}_{ref} \end{bmatrix} + \begin{bmatrix} 0 \\ 0 \\ \omega^3 \end{bmatrix} reference, \tag{6.26}$$

where $\omega, \zeta > 0$, being respectively the natural frequency and the relative damping ratio. $reference$ is the commanded state reference.

6.4.3 Speed Controller (Dynamic task)

In the previous sections the compensator $\ddot{\phi}_0 = u_{\phi_0}$ is obtained by a low-pass filter reference model and used as a controller to regulate the heading of the snake. The proposed VHC (6.6) still has another compensator, λ, which is responsible for controlling the velocity, through the control input u_λ, which will make the forward and normal velocity converge to a desired reference relative forward velocity, $v_{t,ref}$, and to a small neighbourhood around the origin, respectively. The velocity changes varying the frequency of the joint angles oscillations, induced by the dynamic compensator [76].

A new constraint manifold that will exponentially stabilize relative to (6.9) is defined as following:

$$\Gamma_2 = \Big\{ (\theta, \dot{\theta}, p_t, v_{t,rel}, \bar{v}_{n,rel}, \phi_0, \dot{\phi}_0, \lambda, \dot{\lambda}) \in \Gamma_4 : \left(\tilde{\theta}, \dot{\tilde{\theta}}\right) = (0,0), (\tilde{p}_t, \tilde{v}_{t,rel}) = (0,0), \\ \|\bar{v}_{n,rel}\| \leq \epsilon_n, \left\| \left[\phi_0, \dot{\phi}_0\right] \right\| \leq \epsilon_{\phi_0}, \left\| \left[\lambda, \dot{\lambda}\right] \right\| \leq \epsilon_\lambda \Big\} \tag{6.27}$$

where $\epsilon_n, \epsilon_{\phi_0}$ and $\epsilon_\lambda > 0$ are constants.

The control input $u_\lambda = \ddot{\lambda}$ is used to stabilize both velocity and position at the origin $(\tilde{p}_t, \tilde{v}_{t,rel}) = (0,0)$

of $\dot{\tilde{v}}_{t,rel}$.

In order to derive the control input (6.7), using the techniques of back-stepping in [77] and following the analysis in [6], with the respective changes for the USR model, the Control-Lyapunov Functions (CLFs) are iteratively introduced, starting with a CLF for the position $\tilde{p}_t$.

$$V_1 = \frac{1}{2}\tilde{p}_t^2 \tag{6.28}$$

Taking the derivative in order of time,

$$\dot{V}_1 = \tilde{p}_t\dot{\tilde{p}}_t \tag{6.29}$$

and substituting the derivative of $\tilde{p}_t$ and $\tilde{v}_{t,rel}$, $\dot{V}_1$ can be written as :

$$\dot{V}_1 = \tilde{p}_t\left(v_{t,rel} - v_{t,ref}\right) \tag{6.30}$$

$v_{t,rel}$ can be taken as a virtual control input which can be used to make the Lyapunov function negative. Thus it can be defined as:

$$v_{t,rel} = v_{t,ref} - k_{z_0}\tilde{p}_t, \tag{6.31}$$

with $k_{z_0} > 0$ being a constant gain. The error variable and the error dynamics of the error variable, to perform the backstepping are defined as:

$$z_1 = v_{t,rel} - v_{t,ref} + k_{z_0}\tilde{p}_t \tag{6.32}$$

$$\dot{z}_1 = \dot{\tilde{v}}_{t,rel} + k_{z_0}\dot{\tilde{p}}_t \tag{6.33}$$

Nonetheless the expression of $\dot{V}_1$ can be rewritten inserting (6.32) in (6.30) as:

$$\dot{V}_1 = -k_{z_0}\tilde{p}_t^2 + z_1\tilde{p}_t. \tag{6.34}$$

Extending a new, augmented CLF, V_2 can be presented as:

$$V_2 = V_1 + \frac{1}{2}z_1^2 \tag{6.35}$$

Taking the time derivative of V_2 we get:

$$\dot{V}_2 = \dot{V}_1 + z_1 \dot{z}_1 \tag{6.36a}$$

$$= -k_{z_0} \tilde{p}_t^2 + z_1 \left(\tilde{p}_t + \dot{\tilde{v}}_{t,rel} + k_{z_0} \dot{\tilde{p}}_t \right) \tag{6.36b}$$

$$= -k_{z_0} \tilde{p}_t^2 + z_1 \left(\tilde{p}_t - \frac{c_t}{m} v_{t,rel} + Y_t \bar{v}_{n,rel} - Z_t v_\theta + \eta \dot{\lambda} C + \eta \bar{\boldsymbol{e}} \dot{\phi}_0 - \dot{v}_{t,ref} + k_{z_0} \dot{\tilde{p}}_t \right) \tag{6.36c}$$

$$= -k_{z_0} \tilde{p}_t^2 + z_1 \left(\tilde{p}_t - \frac{c_t}{m} v_{t,ref} - \frac{c_t}{m} z_1 + \frac{c_t}{m} k_{z_0} \tilde{p}_t + Y_t \bar{v}_{n,rel} - Z_t v_\theta + \eta \dot{\lambda} C + \eta \bar{\boldsymbol{e}} \dot{\phi}_0 - \dot{v}_{t,ref} + k_{z_0} \dot{\tilde{p}}_t \right) \tag{6.36d}$$

To make $\dot{V}_2$ negative, we define:

$$\delta_1 \left(\phi_0, \lambda \right) = \eta C \tag{6.37}$$

That can be numerically verified that is uniformly bounded away from the origin due to the phase shift in (6.6)

Solving $\dot{V}_2$, $\dot{\lambda}$ can be presented as:

$$\begin{aligned} \dot{\lambda} = \frac{1}{\delta_1} \left(-\tilde{p}_t + \frac{c_t}{m} v_{t,ref} - \frac{c_t}{m} k_{z_0} \tilde{p}_t - \frac{2 c_p}{N m} \bar{v}_{n,rel} \bar{\boldsymbol{e}} \boldsymbol{\phi}_{ref} - \eta \bar{\boldsymbol{e}} \dot{\phi}_0 + \dot{v}_{t,ref} + Z_t v_\theta - k_{z_0} \dot{\tilde{p}}_t - k_{z_1} z_1 \right) \\ = \delta_2 \left(\phi_0, \dot{phi}_0, \dot{\lambda}, p_t, v_{t,rel} \right), \end{aligned} \tag{6.38}$$

with $k_{z_1} > 0$ is a constant gain. Defining the second error variable and the dynamics error to use in the backstepping controller:

$$z_2 = \dot{\lambda} - \delta_2 \tag{6.39}$$

$$\begin{aligned} \dot{z}_2 &= \ddot{\lambda} - \dot{\delta}_2 \\ &= u_\lambda - \dot{\delta}_2 \end{aligned} \tag{6.40}$$

Inserting (6.40) in (6.36), $\dot{V}_2$ can be written as:

$$\dot{V}_2 = -k_{z_0} \tilde{p}_t^2 - \left(\frac{c_t}{m} + k_{z_1} \right) z_1^2 + z_1 z_2 \delta_1 \tag{6.41}$$

For last, a new augmented Lyapunov Function and it's derivative are defined along the solution of $\dot{\tilde{v}}_{t,rel}$ as

$$V_3 = V_2 + \frac{1}{2} z_2^2 \tag{6.42}$$

$$\dot{V}_3 = \dot{V}_2 + z_2 \dot{z}_2 \tag{6.43}$$

$\dot{V}_3$ can be written substituting $\dot{V}_2$ and $\dot{z}_2$ in V_3 yields:

$$\dot{V}_3 = -k_{z_0}\tilde{p}_t^2 - \left(\frac{c_t}{m} + k_{z_1}\right) z_1^2 + z_2\left(z_1\delta_1 + u_\lambda - \dot{\delta}_2\right) \tag{6.44}$$

$$u_\lambda = -z_1\delta_1 + \dot{\delta}_2 - k_{z_2}z_2 \tag{6.45}$$

with $k_{z_2} > 0$ is a constant gain. Inserting (6.45) in (6.44) we get the closed-form for $\dot{V}_3$:

$$\dot{V}_3 = -k_{z_0}\tilde{p}_t^2 - \left(\frac{c_t}{m} + k_{z_1}\right) z_1^2 - k_{z_2}z_2^2 \tag{6.46}$$

From this last step of backstepping it can be shown that $(\tilde{p}_t, \tilde{v}_{t,rel}) = (0,0)$ is exponentially stable. This implies that both relative forward velocity and tangential position will converge asymptotically to their references and the control objective (6.5) is met as it can be shown that $\dot{V}_3 \leq -\beta_3 V_3$, $\beta_3 > 0$ is a constant [6].

Before proceeding to the geometric task, the highest level of hierarchy of the control system, a few remarks must be made regarding the velocity control manifold. The constraint manifold $\Gamma_3 \subset \Gamma_2$. That way stabilizing Γ_2 relative to the constraint manifold Γ_4 implies not only that the robot will follow the reference heading but also the reference velocity.

The solution of the compensator λ, u_λ, will remain bounded, where in order to be bounded, both $\bar{v}_{n,rel}$ and $v_{t,rel}$ must be bounded, which they are proved to be in [6], without any environment disturbance. Following the same line as thought, it can be proved that both $\bar{v}_{n,rel}$ and the relative forward velocity are bounded. In that case and considering that the robot is under the influence of ocean currents, the proof goes as follows :

Defining the Lyapunov function candidate and taking it's derivative,

$$V = \frac{1}{2}\bar{v}_{n,rel}^2 \tag{6.47}$$

$$\dot{V} = \bar{v}_{n,rel}\dot{\bar{v}}_{n,rel} \tag{6.48}$$

with $\dot{\bar{v}}_{n,rel}$ given by the equation (5.5d). With the following change of variable $X' = \epsilon\left(\frac{c_n}{m} - \lambda_1\right) + V_x\cos\theta + V_y\sin\theta$, $\dot{V}$ can be written as:

$$\dot{V} = X' v_\theta \bar{v}_{n,rel} - Y\bar{v}_{n,rel}^2, \tag{6.49}$$

with $Y = \frac{c_n}{m}$.

From Young's inequality [78] we have that:

$$ab \leq \frac{\gamma a^2}{2} + \frac{b^2}{2\gamma} \tag{6.50}$$

Using the inequality in 6.49 we obtain the following:

$$\dot{V} \leq \left(-Y + \frac{\gamma|X'|}{2}\bar{v}_{n,rel}^2\right) + \frac{|X'|v_\theta^2}{2\gamma}, \tag{6.51}$$

$\gamma > 0$ and constant. Taking into consideration the assumption 10 and the previous stability results,

$$\frac{|X'|v_\theta^2}{2\gamma} \leq \beta_1,$$

$\beta_1 > 0$ and constant. For a small value of γ, it is possible to write that [6],

$$\dot{V} \leq -\beta_2 V + \beta_1 \tag{6.52}$$

As in [6], relying on Comparison Lemma [77] is trivial to show $\|\bar{v}_{n,rel}\| \leq \epsilon_n$. Furthermore, the bounding of the forward velocity is proved using $\dot{\lambda} = z_2 + \delta_2$ since z_2 converges to zero and δ_2 is uniformly bounded, hence $\dot{\lambda}$ remains also uniformly bounded. Based on these it is straightforward to show that the dynamic compensator u_λ is bounded. The proof in [6] can as well be applied for the case that it considers ocean currents and uses an USR model. By denoting a new and augmented state vector given by:

$$x = \left[p_t, v_{t,rel}, p_n, \bar{v}_{n,rel}, \phi_0, \dot{\phi}_0, \lambda, \dot{\lambda}\right] \in \mathbb{R}^2,$$

Considering for this matter the controllers defined so far (6.12), (6.45) and (6.24) the closed-loop dynamics can be presented as

$$\dot{x} = f(x)$$

It can be shown that:

$$\|f(x)\| \leq K\left(1 + \|x\|\right),$$

with $K \in \mathbb{R}_{>0}$, since all closed-loop functions proved to be bounded. Moreover, the velocity control manifold Γ_2 is asymptotically stable relative to Γ_4 when using (6.12), (6.24) and (6.45).

6.4.4 Path following controller (Geometric task)

The last step of the control system, and also the highest level of the hierarchy is the path following control, where we aim to stabilize $\bar{p}_y \to y_{tofollow}^{path}$, or in other words $\tilde{\bar{p}}_y \to 0$. Making use of the aforementioned stability results it is straightforward to prove that $\bar{p}_y$ converges to the desired path. Due to the oscillating nature of the robot, it will converge to a sufficient small neighbourhood around the desired path and the

cross track error to a small neighbourhood close to zero. To stabilize $\bar{p}_y \rightarrow y^{path}_{tofollow}$ we use the definition made in 6.3 and in addition we define the normal velocity cross track error as:

$$\tilde{\bar{v}}_{n,rel} = \bar{v}_n - v_{n,ref}, \tag{6.53}$$

where $v_{n,ref} = 0$. The manifold on which the path following problem (geometric task) is acheieved is defined as:

$$\Gamma_1 = \left\{ (\theta, \dot{\theta}, p_t, v_{t,rel}, \tilde{\bar{p}}_y, \bar{v}_{n,rel}, \phi_0, \dot{\phi}_0, \lambda, \dot{\lambda}) \in \Gamma_2 : \tilde{\bar{p}}_y \leq \epsilon_p \right\} \tag{6.54}$$

Considering the dynamics of the position $\dot{\bar{p}}_y$ (5.5c), the error coordinates for the position can be written as:

$$\dot{\tilde{\bar{p}}} = (\tilde{v}_{rel} + v_{t,ref}) \sin\left(\tilde{\theta} + \theta_{ref}\right) + \tilde{\bar{v}}_{n,rel} \cos\left(\tilde{\theta} + \theta_{ref}\right) \tag{6.55}$$

The equation (6.55) evaluated on the exponentially stable manifold Γ_2 can be written as follows:

$$\dot{\tilde{\bar{p}}}_y = (\tilde{v}_{rel} + v_{t,ref}) \sin\left(\theta_{ref}\right) + \tilde{\bar{v}}_{n,rel} \cos\left(\theta_{ref}\right) \tag{6.56}$$

substituting the reference orientation (6.19) in (6.56) we can rewrite it as :

$$\dot{\tilde{\bar{p}}}_y = -\frac{v_{t,ref}\left(\tilde{\bar{p}}_y + \sigma y_{int}\right)}{\sqrt{\left(\tilde{\bar{p}}_y + \sigma y_{int}\right)^2 + \Delta^2}} + \frac{\tilde{\bar{v}}_{n,rel}\Delta}{\sqrt{\left(\tilde{\bar{p}}_y + \sigma y_{int}\right)^2 + \Delta^2}} \tag{6.57}$$

Using the following Lyapunov Function:

$$V = \frac{1}{2}\tilde{\bar{p}}_y^2 \tag{6.58}$$

and taking the derivative of (6.58), the derivative is given as follows

$$\dot{V} = \tilde{\bar{p}}_y \dot{\tilde{\bar{p}}}_y \tag{6.59}$$

Substituting (6.57) in (6.59) we get and applying the Young's inequality :

$$\dot{V} \leqslant -\left(\frac{v_{min}\tilde{\bar{p}}_y^2}{\sqrt{\left(\tilde{\bar{p}}_y + \sigma y_{int}\right)^2 + \Delta^2}}\right) + \epsilon_n \left(\frac{\gamma \tilde{\bar{p}}_y^2}{2} + \frac{1}{2\gamma}\right) \tag{6.60}$$

We need to make the derivative smaller or equal to zero so that the V(t) is asymptotically exponentially stable and $\tilde{p}$ converges to 0. Equation (6.60) can be written as:

$$\dot{V} \leqslant -\beta V + \eta \tag{6.61}$$

where is assumed that exists a sufficient small positive constant $\beta \in \mathbb{R}_{>0}$. Using the Comparison Lemma, the following can be written:

$$V(t) \leqslant V(0)e^{-\beta t} + \frac{\eta}{\beta} \tag{6.62}$$

This implies that V converges to a ball of radius $\frac{\eta}{\beta}$ and therefore because of (6.58) that $\tilde{\bar{p}}$ converges to a ball of radius $\sqrt{\frac{2\eta}{\beta}}$, meaning that $\dot{\tilde{\bar{p}}}$ is stable at the origin.

6.5 Simulation results

In this section, the control oriented model defined in Chapter 5 is used. Here we present the simulation results for the proposed maneuvering problem using Virtual Holonomic Constraints under the influence of constant and irrotational ocean currents.The path-following and speed controller, (6.24) and (6.45), respectively, so as the control oriented model were implemented in Matlab R2019b. The dynamics of the system were computed using the **ode45** solver, with absolute tolerance and relative tolerance equals to 10^{-6}.

Two different experiences were performed one using the lateral undulation motion and other using the eel-like motion, both under the influence of ocean currents.

The Underwater Snake Robot parameters are the same ones defined in Table 5.1 and once again follow the same values as the physical robot Mamba [70]. The frequency of joint oscillations of the robot is now a dynamic compensator that changes accordingly, independent of time. The gait parameters resume to only α and δ.

The value of ϵ is the same as in section 5.6 and equal to $\epsilon = -34.3\ cm$. The gains of the joint controller in 6.10 are set to $k_\phi = 20$ and $k_{v_\phi} = 5$.

Lateral Undulation	Value	Eel-like	Value	Controller Gains	Value
$g(i)$	1	$g(i)$	$\frac{N-i}{N+1}$	k_{theta}	0.6
α	$0.08\ cm$	α	$0.09\ cm$	k_{z_0}	0.1
δ	$40°/s$	δ	$40°/s$	k_{z_1}	1.2
$\boldsymbol{v}_c\ m/s$	$[-0.1, 0.1]\ m/s$	$\boldsymbol{v}_c$	$[-0.04, 0.04]\ m/s$	k_{z_2}	0.1
$v_{t,ref}$	$0.4\ m/s$	$v_{t,ref}$	$0.4\ m/s$		
Guidance system parameters					
Look ahead distance, Δ	$2 \cdot N \cdot l\ m$	Look ahead distance, Δ	$2 \cdot N \cdot l\ m$		
Integral gain, σ	$0.1\ cm/s$	Integral gain, σ	$0.1\ cm/s$		

Table 6.1: Table with parameters for Straight Line Path Following

The guidance law parameters, integral gain, σ, and look-ahead-distance, Δ were defined in table 6.1. And so as the gain of the orientation controller, k_θ, the speed controller gains k_{z_0}, k_{z_1}, k_{z_2}. Moreover, the constant and irrotational ocean current chosen for the experiences are as well defined in Table 6.1.

The initial conditions of the simulations were such that $\bar{p}_x = 0$ and $\bar{p}_y = 2$. The joint coordinates

were set to zero, $\phi = 0$ and the straight line path following to follow is $y_{tofollow}^{path} = 0$. The initial relative tangential velocity, $v_{t,rel}$, is set such that complies with the Assumption 9, and so, $v_{t,rel}(0) = 0,1\ m/s$ in both experiences . Nonetheless the reference relative forward velocity, which is the velocity to maintain once the robot converges to the path, must also be chosen based on Assumption 9 and it is defined in Table 6.1. The position reference was defined as $p_{t,ref} = \int_0^t v_{t,ref}(\tau)d\tau$. All the rest of the variables and states are initially set to zero.

6.5.1 Straight-line path using Lateral Undulation enforcing VHC

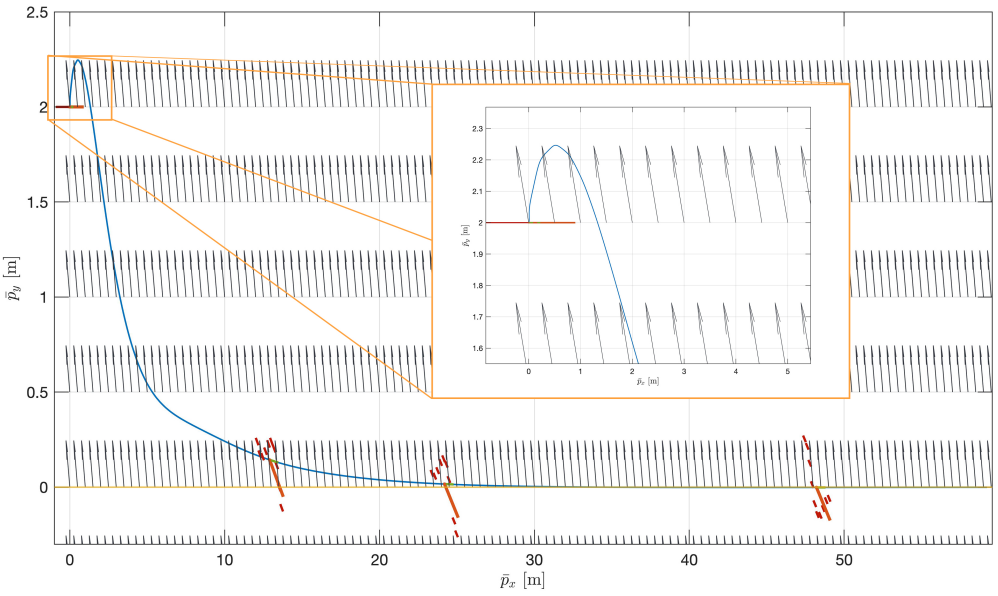

Figure 6.1: Path of the robot to $y = 0$ with lateral undulation motion

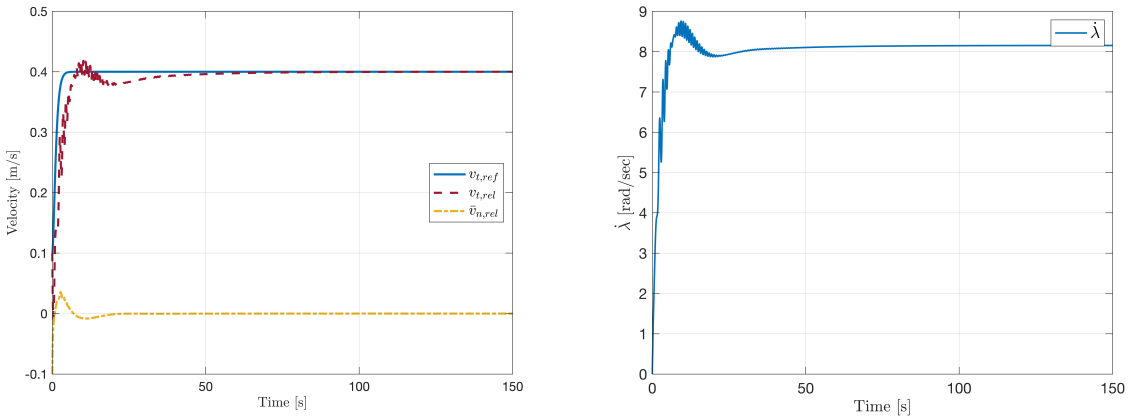

(a) Forward, Sideways and Reference Velocities

(b) Joint Oscillation Frequency $\dot{\lambda}$

Figure 6.2: System Velocities, $v_{t,rel}$, $\bar{v}_{n,rel}$, $v_{t,ref}$ and Joint Oscillation Frequency, $\dot{\lambda}$

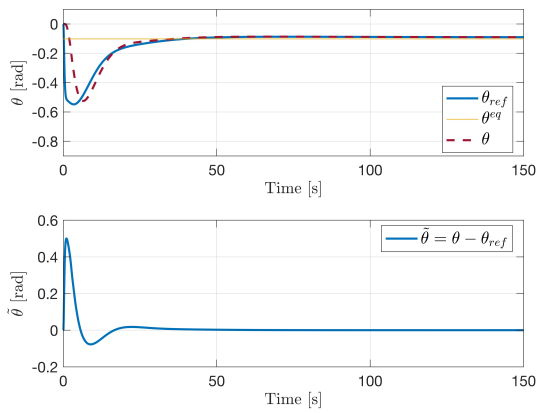

(a) Orientation reference tracking and error

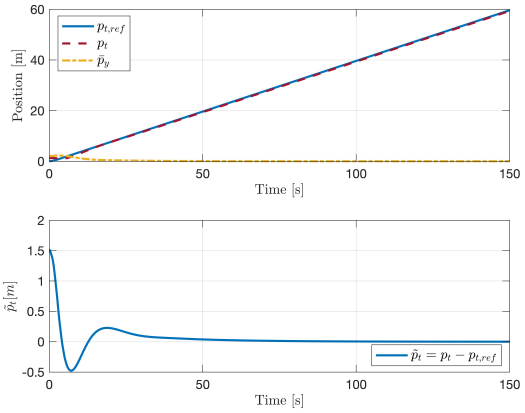

(b) Position reference tracking and error

Figure 6.3: Orientation and position reference and error, θ_{ref}, $\tilde{\theta}$, $p_{t,ref}$, $\tilde{p}_t$

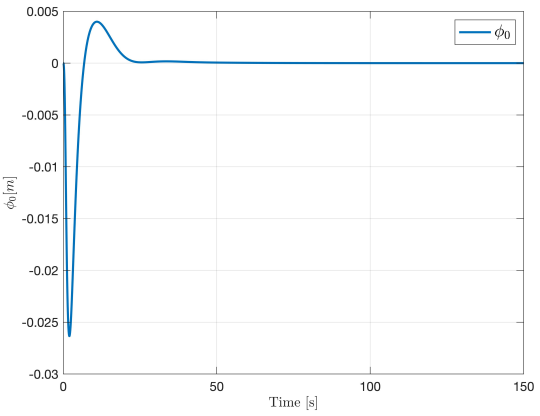

(a) Reference Joint Offset, ϕ_0

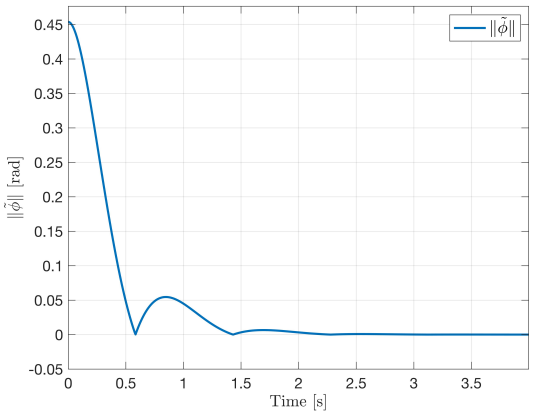

(b) Exponential stability of the joints

Figure 6.4: Joint Offset and Exponential stability

6.5.2 Straight-line path using Eel-like enforcing VHC

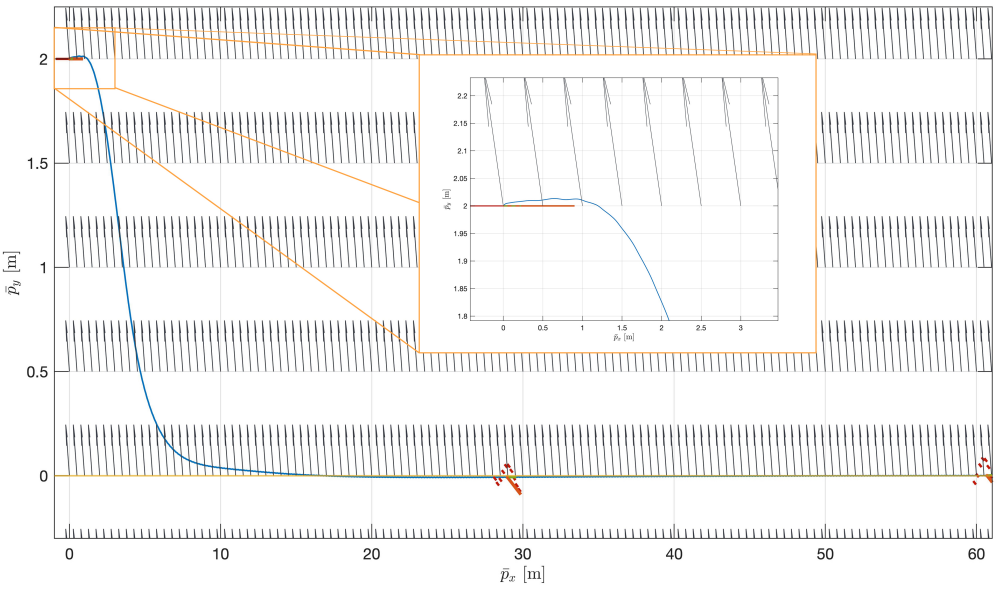

Figure 6.5: Path of the robot to $y = 0$ with eel-like motion

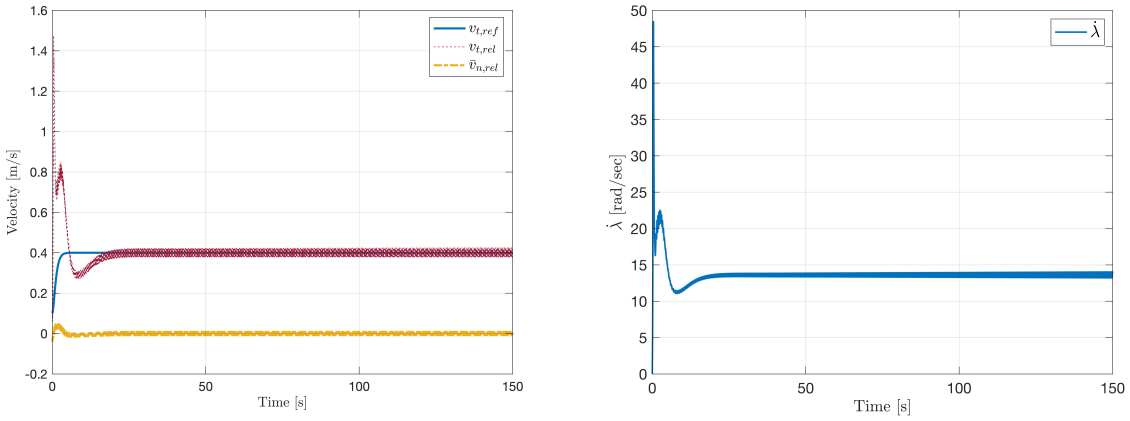

(a) Forward, Sideways and Reference Velocities

(b) Joint Oscillation Frequency $\dot{\lambda}$

Figure 6.6: System Velocities, $v_{t,rel}$, $\bar{v}_{n,rel}$, $v_{t,ref}$ and Joint Oscillation Frequency, $\dot{\lambda}$

6.5.3 Simulation analysis Straight-Line Path

The simulation results for both Lateral Undulation and Eel-Like motion are depicted in figures 6.1, 6.5, 6.2,6.6, 6.3,6.7 and 6.4, 6.8.

For the control system presented in this chapter, the underwater snake robot converges to the reference path and moves along it (figures 6.1 and 6.5) with the relative forward velocity, $v_{t,rel}$ converging to the desired reference velocity, $v_{t,ref}$, that was defined in Table 6.1. This is the first difference between

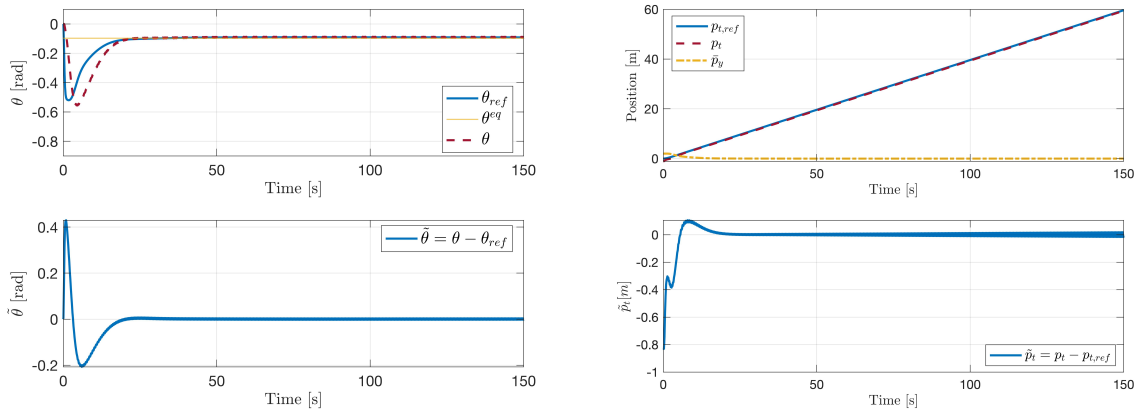

(a) Orientation reference tracking and error

(b) Position reference tracking and error

Figure 6.7: Orientation and position reference and error, θ_{ref}, $\tilde{\theta}$, $p_{t,ref}$, $\tilde{p}_t$

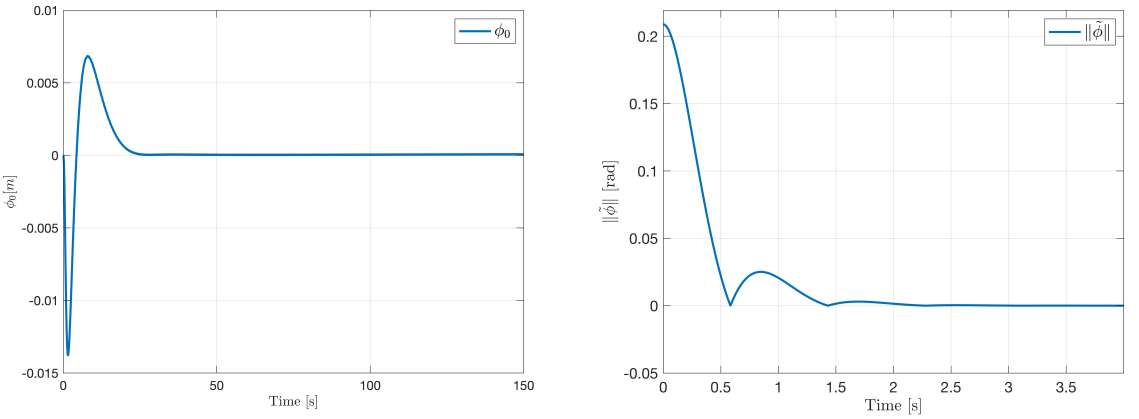

(a) Reference Joint Offset, ϕ_0

(b) Exponential stability of the joints

Figure 6.8: Joint Offset and Exponential stability

the control system presented in Chapter 5 and this control system. In Chapter 5 the frequency of oscillation, ω was dependent time dependent in a way that, aside the fact that would converge to the path and progress along it, it would never achieve the desired speed as ω, which is responsible to make the robot move faster or slower is a fixed parameter. The introduction of the compensator λ, and being a time-independent parameter, can be used to control the forward velocity, reducing or increasing the frequency of oscillation, and therefore its velocity, accordingly. In both experiences the underwater snake robot achieved the desired reference speed once it has converged to the path (6.2, 6.6). An important thing to bare in mind is the time of convergence to the path, taking into consideration the joint oscillation

frequency.

The eel-like motion, as the wave propagates through the slender body with increasing amplitude, will generate less forward speed for the same joint oscillation frequency when compared with the lateral undulation.

Both experiences were defined with the same reference velocity, but even though the ocean current, $\boldsymbol{v}_c$, is different, what was said still applies and can be seen in figures 6.2 and 6.6, where despite the fact that $\boldsymbol{v}_c$ is smaller for the eel-like, it always requires a bigger joint oscillation frequency to keep $v_{t,rel} = v_{t,ref}$, as opposite to the lateral undulation (6.2 and 6.6).

Another interesting point is how eel-like motion can turn its body to converge to the path faster than the lateral undulation. This arises from the fact that the biggest oscillation amplitudes are close to the tail of the snake which is also close to the point where the underwater snake robot can generate a pure rotational motion and no sideways force, and thus ϕ_0 is smaller in this case (fig. 6.4, 6.8). Different other experiments were performed and different controller gains were tested and tuned so that the overshoot when converging to the path was as minimal as possible or even nonexistence. This tuning comes with a set-back, that either compromises the velocity or the smoothness of convergence. They were chosen to favour the smoothness, as the velocity would originate overshoots which from a physical robot standpoint could mean a bigger stress in the robot joints.

From figure 6.1 and 6.5, can be noticed that at the beginning the robot is ”washed” away by the ocean current but compensates for the disturbance fast showing that the controller defined by equations (6.19), (6.20) and (6.24) allow to compensate for the ocean current while converging to the path. The orientation of the robots over time, θ_{ref} and the orientation error, $\tilde{\theta}$ can be visualized in figures 6.3 and 6.6. In both experiences the robot converge fast towards θ_{ref} that is from the guidance law in equation (6.19). Afterwards it goes to the orientation equilibrium θ^{eq} defined in Chapter 5.

With regard to the velocities, both achieved $v_{t,rel} = v_{t,ref}$ and the relative velocity in the normal direction goes to zero, $\bar{v}_{n,rel} = 0$.

With respect to the position reference both movements follow the position reference $p_{t,ref}$ and can be shown from fig.6.4 and 6.8 that the joint tracking errors are both exponential stable going accordingly to the theoretical stability proofs. Despite the fact that the results validate the Maneuvering Problem controllers and solves the Maneuvering Problem itself in the presence of ocean current, there are things to consider:

The use of the control oriented model requires that some parameters stay in well defined intervals in order for the approximations and simplifications still hold. With this, we must pay attention to the joint oscillations frequency of the eel-like motion, which for the same reference velocity, has almost the double of the frequency of the lateral undulation. This will place the oscillation frequency outside of the interval defined in section 5.6.2 and therefore a jitter on the relative forward velocity in figure 6.6 arises.

7

Cooperative Path Following in Underwater Snake Robots

Contents

This chapter addresses the problem of cooperative path following for underactuated underwater snake robots governed by the transformed control oriented model redefined in Chapter 5 and the additional changes introduced in chapter 6. To make it congruent with the past chapters, straight line paths are considered and is taken into account that the robot is being affected by ocean currents. In addition and in order to expand results, a simulation with respect to a sinusoidal path is also presented for last.

The cooperative path following have been studied for fully actuated marine vessels in [79, 80] and in [81, 82] for underactuated marine vessels. In spite of significant progress in the area a solution was never proposed for a fully-submerged snake robot. These references and also [6] will be highly used because of the similarities with the underwater snake robot in terms of underactuation and the dynamics of the system.

Many difficulties may aride when working with vehicles with complex vehicle dynamics, specially the underactuated ones, whose dynamics cannot simply be ignored or drastically simplified for control design purposes. However, for the special case of underwater snake robots, a simplified model used for control purposes exists, and has been the one we will continue to rely further on.

When dealing with underactuated vehicles, the cooperative path following must be considered only at a level of individual and whole group systems [7].

This problem can be formulated as a problem where given a straight line path, a pattern formation and a desired forward velocity, the robots aim to achieve the desired formation which then moves along the desired path with such desired forward velocity.

Contributions of this chapter

The main contribution of this chapter is the derivation of a control method for coordination control of multiple underwater snake robots. This control method is an extension of the control method for coordination control of terrestrial snake robots of [6] and the work done in [7] for underactuated surface vessels. Here are considered relative forward velocities due to the ocean currents in opposition of the work in [6] where environment disturbances were not considered. The works of [6, 7] lack on diversity of formations and number of robots working to achieve a desired formation. As a result, a simulation analysis focusing in increasing the number of robots and the type of formations is presented in latter.

7.1 Control Objectives

The cooperative path following problem unfolds into two important problems. A **path following problem** and a **formation control problem**.

The key idea explored here is the same as in [81], where a vehicle is elected to be the leader and the formation of the other vehicles (followers) is build around him.

With decentralized laws for each snake, the desired path for each robot in the formation is a straight line, which is achieved through the fulfillment of the geometric task in 6.4.4. For each snake on the path, the velocity is controlled using the speed controller defined in chapter 6, equation 6.38. By adjusting the speed of each snake along the straight line, or sinusoidal trajectory using the desired speed as synchronization control term, we can ensure that the desired formation pattern is achieved.

Since the problem requires multiple underwater snake robots, a way to identifying them is needed, so the superscript j is used to denote the snakes number. We define $j = \{1, \ldots, n\}$, where n indicates the total number of snakes.

For completeness, the objectives related to the path following problem will once again be defined, and, in addition the objectives that concerns the formation control problem will be introduced. However one is referred to chapter 6 for the derivation of the controllers and respective stability proofs, since the focus of this chapter will be the achievement of the formation control objectives.

- Objective I - Concerns the desired gait pattern of the snake and aims to asymptotically stabilize $\phi \to \phi_{ref}$.
- Objective II - Concerns the orientation of the snake and aims to asymptotically stabilize $\theta \to \theta_{ref}$.
- Objective III - Concerns the convergence to the path and aims to asymptotically stabilize $\tilde{p}_y \to 0$.
- Objective IV- Concerns the regulation of the forward velocity of the robot along the path to a desired velocity profile, $v_{t,ref}$. So, given a desired velocity $v_{t,ref}$ and position $p_{t,ref}(t) = \int_0^t v_{t,ref}(\tau)d\tau$, we aim to stabilize $p_t \to p_{t,ref}$ and $v_{t,rel} \to v_{t,ref}$

The aforementioned control objectives concern the geometric and dynamic task of the path following problem presented in Chapter 6.

For the formation control we want to make sure that all the followers follow a certain formation based on the x-axis distances between the leader and them. This can be enclosed in a matrix form, which can be called Formation Matrix, d_{ij}. This matrix can be designed in two different ways.

1. The first one is considering the distance relations between all the snake robots, where for all $i = j$ (the distance from one robot to the same), must always be 0, and the elements with the subscript $i \neq j$ must be chosen such that only considers the distance from the leader to the followers and vice-versa.

2. The second one is considering only the relations between the leader and it's followers, and in that case all the entrances such that $i \neq leader \wedge j \neq leader$ must be equal to 0 and so as when $i = j$.

Considering 3 snake robots seeking a formation, the Formation Matrix can be written as follows:

$$d_{ji} = \begin{bmatrix} 0 & d_{12} & d_{13} \\ d_{21} & 0 & d_{23} \\ d_{31} & d_{32} & 0 \end{bmatrix} \tag{7.1}$$

where $d_{ji} = -d_{ij} \in \mathbb{R}$ for all $j \neq i$ with $i, j \in \{1, \ldots, Snakes\}$ such that $d_{j,i} = D_{x_j} - D_{x_i}$. The parameter $d_{j,i}$ represents the desired x-axis distances between the j-th and the i-th robot in the formation.

Furthermore the position of each robot is given by $p_x^j(t)$, and the control **Objective V**, that concerns the achievement of the desired formation is defined as:

$$\lim_{t\to\infty} \left[\sum_{j=1}^{n} \sum_{i=1}^{n} \left(p_x^j - p_x^i - d_{ji} \right) \right] = 0 \tag{7.2}$$

If it is chosen to take into consideration only the relations between the leader and the followers, a constraint over the argument of the summation, $p_x^j - p_x^i - d_{j,i}$, must be defined in order to get rid of the relation between the followers. This constraint goes as follows:

$$p_x^j - p_x^i - d_{j,i} = \begin{cases} 0, & \text{if} \quad j \neq leader \wedge i \neq leader \\ p_x^j - p_x^i - d_{j,i}, & \text{if} \quad otherwise \end{cases} \tag{7.3}$$

This constraint must be applied whenever the argument $p_x^j - p_x^i - d_{ji}$ is presented and if the Formation matrix is defined accordingly to 2 Despite this being the ultimate goal of the cooperative path following, some changes are needed when deriving the controller 6.45 in order to achieve this last objective. The next section will address those changes and provide a solution.

7.2 Coordination control of multiple underwater snake robots

In previous chapters controllers were designed (6.12, 6.24, 6.45) that guarantees that each underwater snake robot converges to the desired straight line path and progresses along with a desired velocity profile. The commanded velocity provided to the robot would, after convergence, be equal to the desired velocity profile, $v_{t,ref} = v_d$. As we seek to achieve a desired formation, a control law for the commanded velocity, $v_{t,rel}^j, j = 1, \ldots, n$, must be design, satisfying the theorem 1 as well as that all the snakes achieve 7.2. Thus, the commanded velocity will be modified to adjust the relative forward speed based on the desired velocity profile, as before, but also highly influenced by the different distance to the formation. That way, once the objective 7.2 is achieved, they all can tune their velocity to match the desired velocity profile v_d. From [7] and considering the theorem 1, we can assume that the desired speed profile lies within the interval $[V_{min}, V_{max}]$, i.e, there exists an $a > 0$ so that $v_d \in [V_{min} + a, V_{max} - a]$.

The change of velocity of each snake is made under the velocity controller defined in 6.45, to which the velocity dynamics of each j-th robot is given by:

$$v_{t,rel}^{j} = v_{t,ref}^{j} - k_{z_0}\tilde{p}_t^j \tag{7.4}$$

From the results in [7], the control law for the commanded velocity is tuned through the reference velocity for each snake [6]:

$$v_{t,ref}^{j} = v_d - g\left(\sum_{i=1}^{n}\gamma_{ji}\left(p_x^j - p_x^i - d_{j,i}\right)\right), \tag{7.5}$$

where d_{ji} was defined above and linkage parameters γ_{ji} are nonnegative and satisfy $\gamma_{ji} = \gamma_{ij}$, $\gamma_{ji} = 0$ for $i = j$.

The function g, makes one underwater snake robot move slower or faster than the others to compensate for their different distance to the formation through adding or decreasing the speed of each USR in the formation. It is a continuously differentiable non-decreasing function with bounded derivative satisfying $g'(0) > 0, g(0) = 0$ and $g(x) \in (-a, a)$ with a being the parameter defined above. By choosing the function $g(x)$ equal to $g(x) = \frac{2a}{\pi}\arctan(x)$ it is certainly bounded and for the problem in question converges to zero as soon as the desired formation is achieved, i.e, for all snake robots, $p_{x_i} - p_{x_j} - d_{ji}$ will be zero. Afterwards, the snakes will move according to the desired velocity profile v_d.

Substituting 7.5 in 7.4 the velocity dynamics is presented as follows:

$$v_{t,rel}^{j} = v_d - g\left(\sum_{i=1}^{n}\gamma_{ji}\left(p_x^j - p_x^i - d_{j,i}\right)\right) - k_{z_0}\tilde{p}_t^j \tag{7.6}$$

From the following change of coordinates $\hat{p}_x^j = p_x^j - D_{x_j} - \int_0^t v_d(\tau)d\tau$:

$$\dot{\hat{p}}_x^j = -g\left(\sum_{i=1}^{n}\gamma_{ji}\left(\hat{p}_x^j - \hat{p}_x^i\right)\right) - k_{z_0}\tilde{p}_t^j \tag{7.7}$$

With the following notations $\hat{p}_x = \left[\hat{p}_x^1, \dots \hat{p}_x^n\right]^T$, $g(\hat{p}_x) = \left[g(\hat{p}_x^1), \dots g(\hat{p}_x^n)\right]^T$, and $\tilde{p}_t = \left[\tilde{p}_t^1, \dots, \tilde{p}_t^n\right]^T$, we have that:

$$\dot{\hat{p}}_x = -g(\Gamma\hat{p}_x) - k_{z_0}\tilde{p}_t \tag{7.8}$$

where the matrix Γ is given by [7]:

$$\Gamma = \begin{bmatrix} \sum_{j=1}^{n}\gamma_{1j} & -\gamma_{12} & \cdots & -\gamma_{1n} \\ -\gamma_{21} & \sum_{j=1}^{n}\gamma_{2j} & \cdots & -\gamma_{2n} \\ \vdots & \vdots & \ddots & \vdots \\ -\gamma_{n1} & -\gamma_{n2} & \cdots & \sum_{j=1}^{n}\gamma_{nj} \end{bmatrix} \tag{7.9}$$

The matrix Γ holds the property $\Gamma v_1 = 0$, where $v_1 = [1, \dots, 1]^T$. This property implies that Γ has a zero eigenvalue, where v_1 express the corresponding eigenvector [7]. Therefore the formation control goal for the system 7.8 is equivalent to:

$$\lim_{t\to\infty} \hat{p}_x(t) - cv_1 = 0, \tag{7.10}$$

where c denotes a positive constant. The system 7.8 coupled with the error dynamics of every snake robot through the term $k_{z_0}\tilde{p}_t^j$, assuming that the zero eigenvalue of matrix Γ has multiplicity one and that Theorem 2 holds for every snake in the formation, 7.10 will be achieved exponentially. The above statement can be proved based on cascade systems theory and reader is referred to [7] where a similar proof is presented.

7.3 Simulation Results

In this section results regarding the Formation control using the control system enforcing VHC from Chapter 6 are presented for underwater snake robots under the influence of ocean currents. It is once again used the control oriented model defined in Chapter 5. The dynamics of the system were computed and implemented using Matlab R2019b and **ode45** solver, with absolute and relative tolerance equals to 10^{-6}.

An experience for lateral undulation motion under the influence of the ocean currents. For the guidance system parameters, so as for the values of the controller gains and as well for the gait parameters, ocean current and desired reference forward velocity the reader is referred to section 6.5 more specifically to Table 6.1. Since this chapter requires more than one robot, a table with the initial positions and the path to follow is defined next, with an highlight for the leader as the formation defined with respect to him. The remaining initial conditions are identical to the ones defined in section 6.5.

	Initial positions		Path to follow
Underwater Snake Robots	$\bar{p}_x$	$\bar{p}_y$	$y^{path}_{tofollow}$
$snake\ 1$	3	2	1
$snake\ 2$	0	0	0
$snake\ 3$	2	0	-1
$snake\ 4$	0	4	0
$snake\ 5$	6	0	-0.5

Table 7.1: Initial conditions Formation Control, and desired path for each robot. At yellow is highlighted the leader of the formation.

The Formation matrix parameters are defined as: $d_{1,2} = -3$, $d_{3,2} = -5$, $d_{4,2} = -10$, $d_{5,2} = -20$. Be aware that the Formation Matrix in this case was defined only by the relations between the leader and the followers as it was referred in section 7.1.

7.3.1 Cooperative Path-Following for 5 USRs on a straight-line trajectory

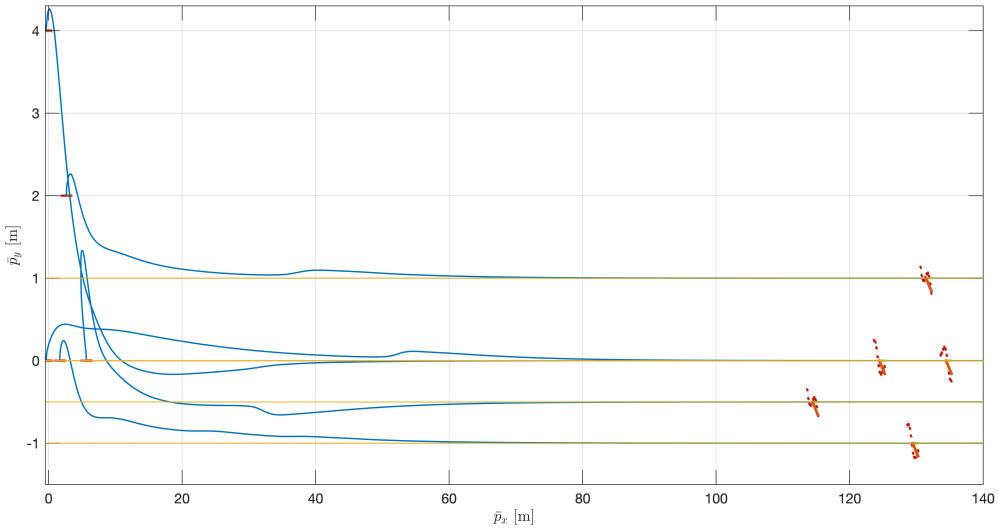

Figure 7.1: Underwater Snake robots in the desired formation

The simulation results of the Cooperative path following are presented in this section figures. They enclose the results for every one of the five robots when it's appropriated and will be analyzed as a whole, instead of analysing the results of each robot individually. In the previous Chapter was shown that the snake robots, individually converge to the path and progress along with the desired reference velocity. However, aside the fact that we want the system to work in a similar way, in addition it's wanted that all robots maintain a desired geometric formation. From figure 7.5, all five underwater snake robots converge to the path, but is not possible to attest if the desired formation was indeed met while also maintaining the desired velocity, $v_{t,ref}$. The velocity of all robots is showcased in figure 7.2 as well as the joint oscillation frequency, which is intrinsically linked to the increase or decrease of the velocity of the robots.

All the velocities converge to the desired reference velocity of the formation after compensating the formation error. Before they converge, they change over time, in order to compensate and adjust to the desired formation. On the other hand we have the oscillation frequency, which changes almost in the same way as the velocity, converging to a positive constant. This constant is the same in all robots and is the frequency of oscillation that makes all the robots move with velocity $v_{t,rel} = 0.4\ m/s$ while overcoming to the ocean currents.

The most important part is still the achievement of the control objective 7.2. The synchronization error describes the difference between the distance from each robot to the leader ($p_x^i - p_x^2, i \in \{1, 3, 4, 5\}$) and the desired distance that is sought between them ($d_{i,2}, i \in \{1, 3, 4, 5\}$). The cross track error re-

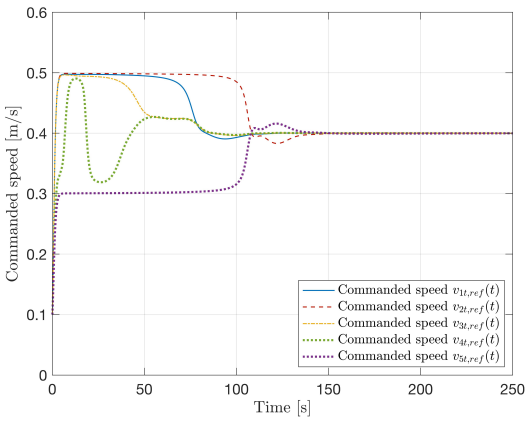

(a) Reference velocities

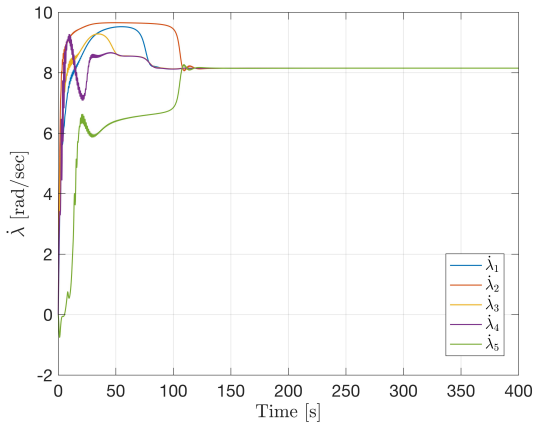

(b) Joint Oscillation Frequency, $\dot{\lambda}$

Figure 7.2: Reference velocities and Joint Oscillation Frequency for each snake

spects the distance between the position of each robot and the actual position of the path ($D_{y,i}$). The achievement of the control objective 7.2 requires then, that the synchronization error converges to zero, which can be attested from figure 7.3, where the synchronization error for all the robots, indeed converge to zero and therefore the desired formation is achieved. Is important to refer that all robots converged to their respective paths as well (in compliance with the achievement of the path following problem) in the presence of ocean currents as the cross track errors goes to zero, meaning that the Orientation controller still compensates for it when the formation is sought. With regards to the position reference all the robots follow it (fig. 7.4).

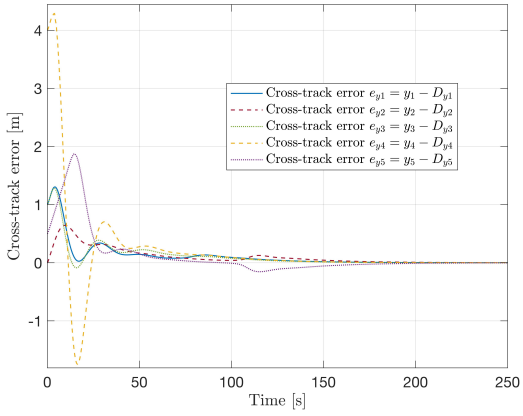

(a) Cross-track errors

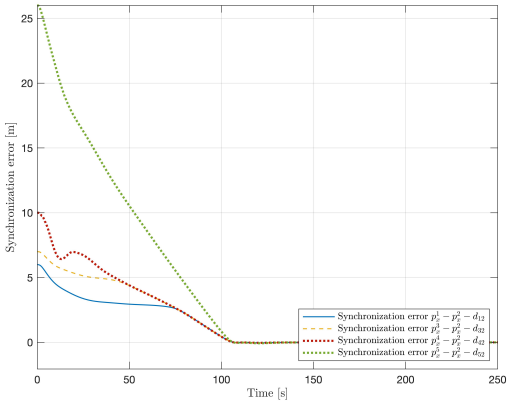

(b) Synchronization errors

Figure 7.3: Cross track error and synchronization error for each snake

About the orientation, θ, all the robots converge fast towards the reference orientation θ_{ref}. Once this happens it happens also that the cross track error is zero for all the robots (around 200s). This doesn't come as a surprise as once the robot is on the path it should maintain the same orientation reference that makes it not only stay in the path but also to overcome the effect of the constant and irrotational ocean currents.

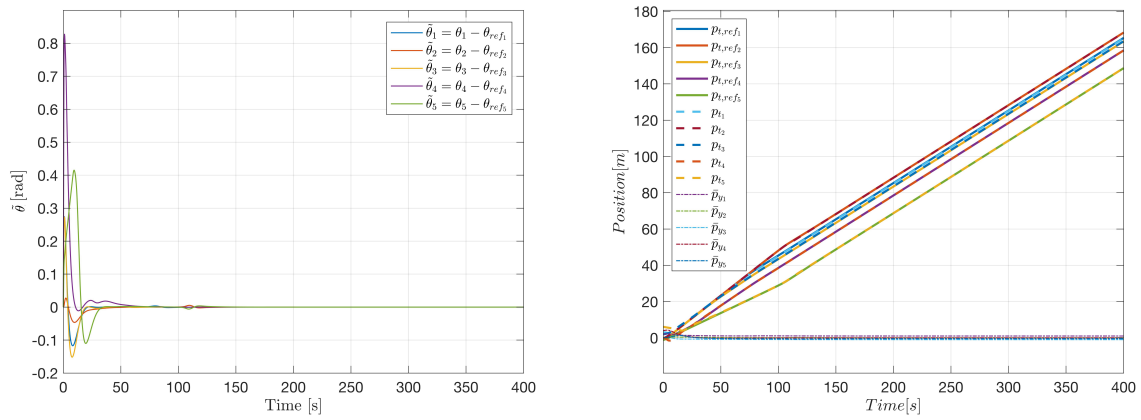

(a) Orientation error

(b) Position references

Figure 7.4: Orientation error, $\tilde{\theta}$ and Position references, $p_{t,ref}$

A representation of the underwater snake robots moving in the desired geometric formation can be seen in figure 7.5. Based on all this results we can state that the control method for coordination control of multiple underwater snake robots meets all control objectives from 7 and therefore the desired formation is achieved with all the robots moving on their paths with the desired velocity defined a posterior.

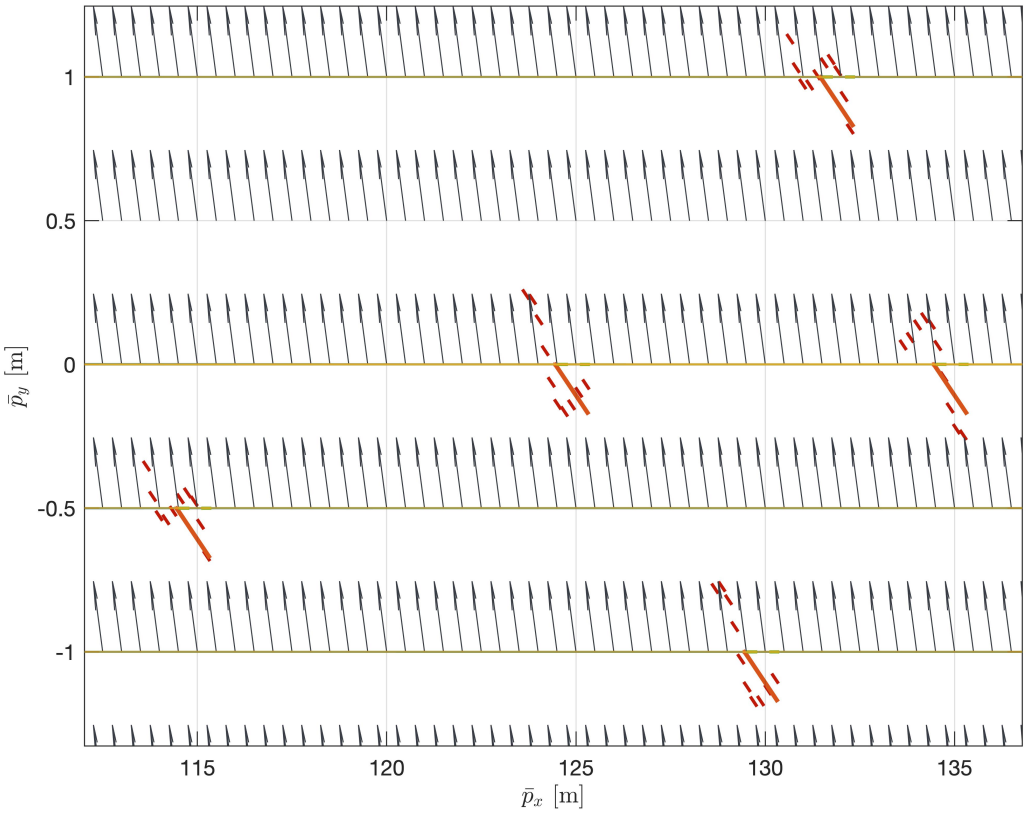

Figure 7.5: Desired underwater snake robot formation

7.3.2 Cooperative Path-Following for 3 USRs on a sinusoidal trajectory

The results presented for a sinusoidal path come as a way to enrich the work with more simulations and also to show that the approach considered for the problem of cooperative path following and inherently the maneuvering problem can be extended for a different trajectories. The achievement of the control objectives is then supported by the analysis of the new simulations presented above.

Each robot must now follow a path that is described by $\sin(2\pi p_{x,i}/40) \in \{1, \ldots, n_{snakes}\}$ and the Formation Matrix parameters are now defined as $d_{1,2} = -3$ $d_{3,2} = -5$.

The figure 7.6 shows the trajectory taken by the robot while performing the Cooperative-Path-Following problem.

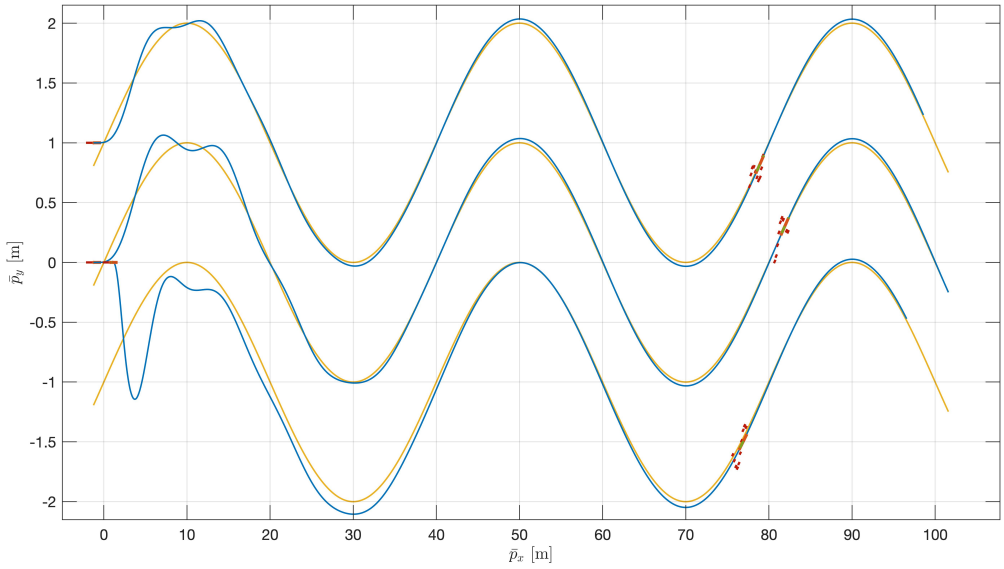

Figure 7.6: Underwater Snake robots in the desired formation

On the sinusoidal path the robots were able to achieve the desired formation and follow the desired sinusoidal path. This is corroborated by the convergence of the synchronization errors to zero, while at the same time the convergence of the cross track error to zero (figures 7.7.b, and 7.7.a, respectively).

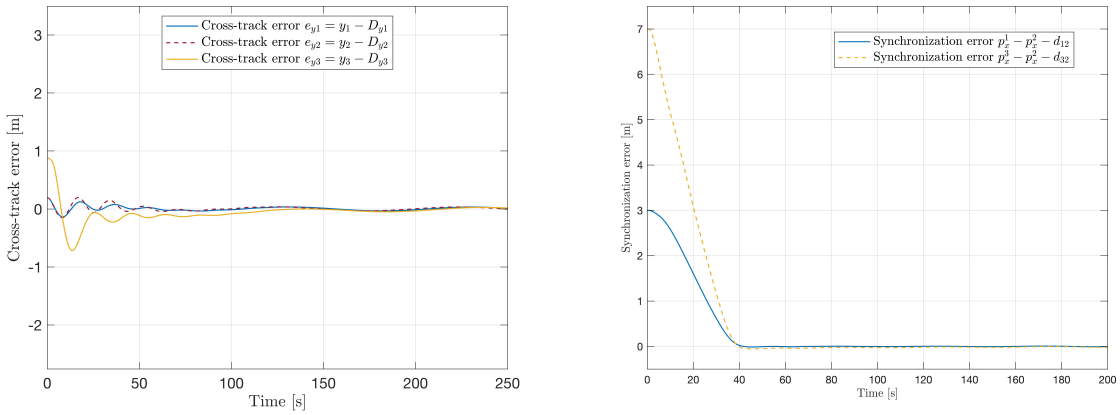

(a) Cross-track errors

(b) Synchronization errors

Figure 7.7: Cross track error and synchronization error for each snake

With regard to the velocity, the same behaviour happens when compared with the straight-line path. Both reference velocities(figure 7.8.a) and Joint Oscillation frequency (figure 7.8.b) evolve in the same exact way, as they are intrinsically linked, and as expected, once the robots are moving on the path, the

velocity converges to the desired velocity v_d and therefore the joint oscillation keeps a positive constant value. In fact the values do not converge exactly to zero or a constant value but instead they oscillate around the origin (cross- track error and synchronization) and around a positive value very close to the desired one (reference velocities and joint oscillation frequency).

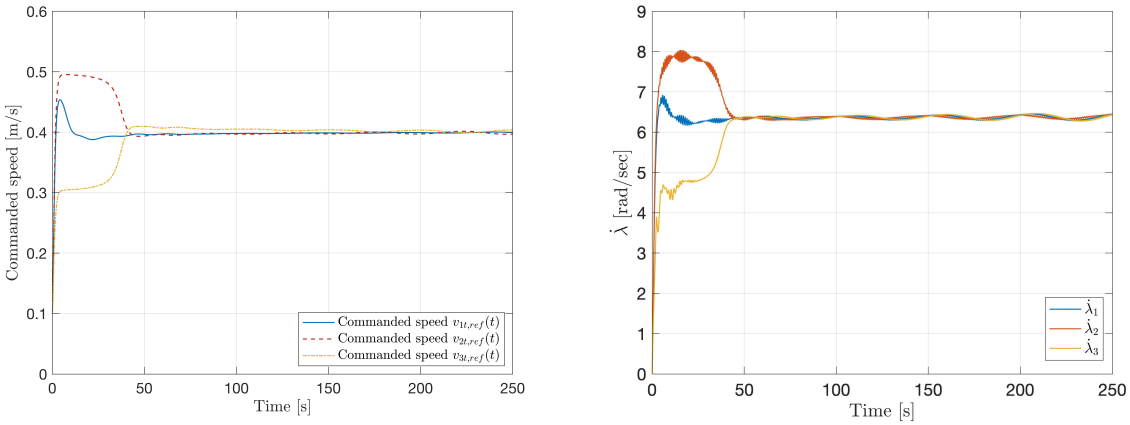

(a) Reference velocities

(b) Joint Oscillation Frequency, $\dot{\lambda}$

Figure 7.8: Reference velocities and Joint Oscillation Frequency for each snake

This behavior can be easily explained by the frequency with which the path changes. A way to reduce the amplitude of oscillations, is reducing the frequency of the path.However the oscillations will always exist due to the oscillatory nature of the path. Regardless the oscillation is minimal and doesn't affect the performance required.

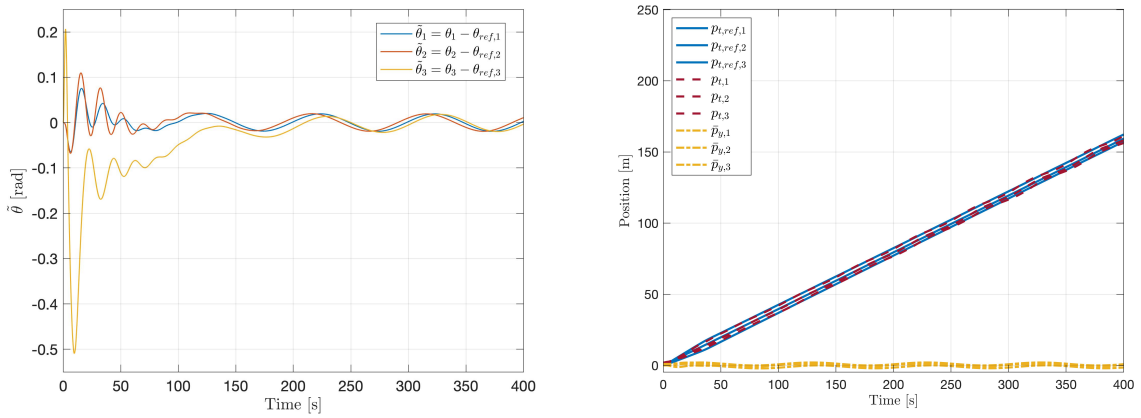

(a) Orientation error

(b) Position references

Figure 7.9: Orientation error, $\tilde{\theta}$ and Position references, $p_{t,ref}$

These oscillations are also present, when it comes to the error orientation (figure 7.9.a) where it never convergence to the origin but oscillates around it. And as expected the position references are followed as they were in the straight-line CPF.

Based on this results we can state that the control method used can be extended for different paths and still work as required (meeting all the control objectives from 7) and therefore the desired formation is achieved with all the robots moving on their paths with the desired velocity.

8

Conclusion and Future Work

This thesis considers an underwater snake robot that moves on a 2D horizontal plane with a biologically inspired sinusoidal gait. Two models are presented, where the main focus is on the Control-Oriented model, a derivation from the Complex model, based on the model for the terrestrial snake robots. Both models rely on the assumption that the ocean currents are constant and irrotational, and that the robot is neutrally buoyant. The guidance system developed throughout the chapters aim to reject environmental disturbances, more specifically, the rejection of ocean currents.

The first system designed in this thesis, is a two fundamental loop system similarly to the one in [22], where an inner loop is responsible to make the robot propel forward by making its links to follow a joint coordinates reference ϕ_{ref}. And an outer loop, which makes the robot steer towards the path and progress along it, is dependent on the orientation controller obtained from the integral-line-of-sight guidance law. The system used was validated through simulation analysis and allows the Path Following problem to be solved within the theoretical requirements. Although the Path-Following problem is solved, the achievement of a desired velocity isn't within reach as the proposed system relies on a gait controller dependent on time and fixed parameters, so a new approach was taken into consideration for the robot to reach a desired speed.

By using a Virtual Holonomic Constraints (VHCs) approach, a different reference joint coordinates ϕ_{ref} was defined by making use of two dynamical compensators λ and ϕ_0. A 3-stage hierarchical control design based on the work for terrestrial snake robots was proposed to solve the Maneuvering Problem, which can be defined as two fundamental tasks, a geometric task responsible to make the robot converge to the path a progress along it and a dynamic task responsible to achieve the desired speed. To meet all the control objectives and solve the Maneuvering Problem, for each control objective a defined constraint manifold must be exponentially stabilized while all the solutions of the control system remain uniformly bounded. Since ocean currents were considered, stability proofs that contemplate the presence of ocean currents were included.

The theoretical deductions were validated through simulation analysis for straight line paths in the presence of ocean currents. This simulations showed that the approach of VHCs is able to solve the Maneuvering problem for Underwater Snake Robots.

As for the Cooperative Path Following, the same 3-stage hierarchical approach was used. The difference comes with respect to the Velocity controller that must now be able to tune the robots velocity accordingly to the formation that is sought (Formation Control Problem). Once this is accomplished and the robots are following their paths, the velocity must converge to the desired velocity (Maneuvering Probelm).

The Cooperative Path Following was validated for both straight line path and sinusoidal path, showing that the Maneuvering Problem can be extended for different paths.

Future work would be related to the Cooperative Path Following. The idea of expanding the CPF

to a more generalized planar curves and introduce obstacle avoidance guidance for when the robots are moving in a formation seems reachable. In fact the problem of obstacle avoidance was already addressed for a single robot using the complex USR model. Another interesting topic would be the experimental simulations of the controllers in real USRs and the extension of the work for a 3D space.

Bibliography

[1] T. I. Fossen, *Introduction*. John Wiley & Sons, Ltd, 2011, ch. 9, pp. 227–239. [Online]. Available: https://onlinelibrary.wiley.com/doi/abs/10.1002/9781119994138.ch9

[2] P. Jousset, T. Reinsch, T. Ryberg, H. Blanck, A. Clarke, R. Aghayev, G. Hersir, J. Henninges, M. Weber, and C. Krawczyk, "Dynamic strain determination using fibre-optic cables allows imaging of seismological and structural features," *Nature Communications*, vol. 9, 12 2018.

[3] R. Skjetne, "The maneuvering problem," PhD dissertation, NTNU, 2005.

[4] E. Kelasidi, K. Pettersen, P. Liljebäck, and J. Gravdahl, "Integral line-of-sight for path following of underwater snake robots," *2014 IEEE Conference on Control Applications, CCA 2014*.

[5] K. Y. Pettersen, "Snake robots," *Annual Reviews in Control*, vol. 44, pp. 19 – 44, 2017. [Online]. Available: http://www.sciencedirect.com/science/article/pii/S1367578817301050

[6] E. Rezapour, K. Pettersen, J. Gravdahl, and A. Hofmann, "Formation control of underactuated bio-inspired snake robots," *Artificial Life and Robotics*, vol. 21, 07 2016.

[7] E. Borhaug, A. Pavlov, and K. Y. Pettersen, "Cross-track formation control of underactuated surface vessels," in *Proceedings of the 45th IEEE Conference on Decision and Control*, 2006, pp. 5955–5961.

[8] J. GRAY, "Studies in animal locomotion," *Journal of Experimental Biology*, vol. 10, no. 1, pp. 88–104, 1933. [Online]. Available: https://jeb.biologists.org/content/10/1/88

[9] J.GRAY, "The mechanism of locomotion in snakes," *Journal of Experimental Biology*, vol. 23, no. 2, pp. 101–120, 1946. [Online]. Available: https://jeb.biologists.org/content/23/2/101

[10] G. Seetharaman, A. Lakhotia, and E. Blasch, "Unmanned vehicles come of age: The darpa grand challenge," *Computer*, vol. 39, pp. 26 – 29, 01 2007.

[11] S. Hirose, P. Cave, and C. Goulden, *Biologically Inspired Robots: Serpentile Locomotors and Manipulators*. USA: Oxford University Press, Inc., 1993.

[12] S. Hirose and H. Yamada, “Snake-like robots [tutorial],” *IEEE Robotics Automation Magazine*, vol. 16, no. 1, pp. 88–98, March 2009.

[13] J. K. Hopkins, B. W. Spranklin, and S. K. Gupta, “A survey of snake-inspired robot designs,” *Bioinspiration & Biomimetics*, vol. 4, no. 2, p. 021001, jan 2009. [Online]. Available: https://doi.org/10.1088%2F1748-3182%2F4%2F2%2F021001

[14] J. C. McKenna, D. J. Anhalt, F. M. Bronson, H. B. Brown, M. Schwerin, E. Shammas, and H. Choset, “Toroidal skin drive for snake robot locomotion,” in *2008 IEEE International Conference on Robotics and Automation*, May 2008, pp. 1150–1155.

[15] S. Ma and N. Tadokoro, “Analysis of creeping locomotion of a snake-like robot on a slope,” *Auton. Robots*, vol. 20, no. 1, p. 15–23, Jan. 2006. [Online]. Available: https://doi.org/10.1007/s10514-006-5204-6

[16] S. A. Fjerdingen, P. Liljebäck, and A. A. Transeth, “A snake-like robot for internal inspection of complex pipe structures (piko),” in *2009 IEEE/RSJ International Conference on Intelligent Robots and Systems*, Oct 2009, pp. 5665–5671.

[17] C. Wright, A. Buchan, B. Brown, J. Geist, M. Schwerin, D. Rollinson, M. Tesch, and H. Choset, “Design and architecture of the unified modular snake robot,” in *2012 IEEE International Conference on Robotics and Automation*, May 2012, pp. 4347–4354.

[18] A. A. Transeth, R. I. Leine, C. Glocker, K. Y. Pettersen, and P. LiljebÄck, “Snake robot obstacle-aided locomotion: Modeling, simulations, and experiments,” *IEEE Transactions on Robotics*, vol. 24, no. 1, pp. 88–104, Feb 2008.

[19] P. Liljebäck, K. Y. Pettersen, and [U+FFFD] Stavdahl, “A snake robot with a contact force measurement system for obstacle-aided locomotion,” in *2010 IEEE International Conference on Robotics and Automation*, May 2010, pp. 683–690.

[20] H. YAMADA, “Development of amphibious snake-like robot acm-r5,” *Proc. 36th Int. Symp. on Robotics, Tokyo, 2005*, vol. 3, 2005. [Online]. Available: https://ci.nii.ac.jp/naid/10028166347/en/

[21] E. Kelasidi, K. Pettersen, J. Gravdahl, and P. Liljebäck, “Modeling of underwater snake robots,” 09 2014.

[22] P. Liljebäck, K. Y. Pettersen, O. Stavdahl, and J. T. Gravdahl, *Snake Robots: Modelling, Mechatronics, and Control*. Springer Publishing Company, Incorporated, 2012.

[23] F. Boyer, D. Chablat, P. Lemoine, and P. Wenger, “The eel-like robot,” *Proceedings of the ASME Design Engineering Technical Conference*, vol. 7, 08 2009.

[24] A. Crespi and A. Ijspeert, "Amphibot ii: An amphibious snake robot that crawls and swims using a central pattern generator," *Proceedings of the 9th International Conference on Climbing and Walking Robots (CLAWAR 2006)*, 01 2006.

[25] E. D. Tytell and G. V. Lauder, "The hydrodynamics of eel swimming," *Journal of Experimental Biology*, vol. 207, no. 11, pp. 1825–1841, 2004. [Online]. Available: https://jeb.biologists.org/content/207/11/1825

[26] I. Borazjani and F. Sotiropoulos, "On the role of form and kinematics on the hydrodynamics of self-propelled body/caudal fin swimming," *Journal of Experimental Biology*, vol. 213, no. 1, pp. 89–107, 2010. [Online]. Available: https://jeb.biologists.org/content/213/1/89

[27] J. E. Colgate and K. M. Lynch, "Mechanics and control of swimming: a review," *IEEE Journal of Oceanic Engineering*, vol. 29, no. 3, pp. 660–673, July 2004.

[28] G. I. Taylor, "Analysis of the swimming of long and narrow animals," *Proceedings of the Royal Society of London. Series A. Mathematical and Physical Sciences*, vol. 214, no. 1117, pp. 158–183, 1952. [Online]. Available: https://royalsocietypublishing.org/doi/abs/10.1098/rspa.1952.0159

[29] E. D. Tytell, "The hydrodynamics of eel swimming ii. effect of swimming speed," *Journal of Experimental Biology*, vol. 207, no. 19, pp. 3265–3279, 2004. [Online]. Available: https://jeb.biologists.org/content/207/19/3265

[30] G. Antonelli, *Underwater Robots*, 3rd ed. Springer Publishing Company, Incorporated, 2013.

[31] M. Breivik and T. I. Fossen, "Guidance laws for autonomous underwater vehicles," in *Underwater Vehicles*, A. V. Inzartsev, Ed. Rijeka: IntechOpen, 2009, ch. 4. [Online]. Available: https://doi.org/10.5772/6696

[32] S. Moe, K. Pettersen, T. Fossen, and J. Gravdahl, "Line-of-sight curved path following for underactuated usvs and auvs in the horizontal plane under the influence of ocean currents," 06 2016, pp. 38–45.

[33] A. Lekkas and T. Fossen, *Line-of-Sight Guidance for Path Following of Marine Vehicles*, 06 2013.

[34] E. Borhaug, A. Pavlov, and K. Pettersen, "Integral los control for path following of underactuated marine surface vessels in the presence of constant ocean currents," 01 2009, pp. 4984 – 4991.

[35] W. Caharija, K. Pettersen, J. Gravdahl, and A. Sørensen, "Topics on current compensation for path following applications of underactuated underwater vehicles," *IFAC Proceedings Volumes (IFAC-PapersOnline)*, vol. 3, pp. 184–191, 01 2012.

[36] P. Encarnação, A. Pascoal, and M. Arcak, "Path following for marine vehicles in the presence of unknown currents1," *IFAC Proceedings Volumes*, vol. 33, no. 27, pp. 507 – 512, 2000, 6th IFAC Symposium on Robot Control (SYROCO 2000), Vienna, Austria, 21-23 September 2000. [Online]. Available: http://www.sciencedirect.com/science/article/pii/S1474667017379806

[37] C. Paliotta and K. Y. Pettersen, "Geometric path following with ocean current estimation for asvs and auvs," in *2016 American Control Conference (ACC)*, 2016, pp. 7261–7268.

[38] M. L. Castaño and X. Tan, "Model Predictive Control-Based Path-Following for Tail-Actuated Robotic Fish," *Journal of Dynamic Systems, Measurement, and Control*, vol. 141, no. 7, 04 2019, 071012. [Online]. Available: https://doi.org/10.1115/1.4043152

[39] K. Morgansen, P. Vela, and J. Burdick, "Trajectory stabilization for a planar carangiform robot fish," vol. 1, 12 2001.

[40] J. Guo, "A waypoint-tracking controller for a biomimetic autonomous underwater vehicle," *Ocean Engineering*, vol. 33, no. 17, pp. 2369 – 2380, 2006. [Online]. Available: http://www.sciencedirect.com/science/article/pii/S0029801806000230

[41] P. A. Vela, K. A. Morgansen, and J. W. Burdick, "Underwater locomotion from oscillatory shape deformations," in *Proceedings of the 41st IEEE Conference on Decision and Control, 2002.*, vol. 2, Dec 2002, pp. 2074–2080 vol.2.

[42] K. A. Morgansen, B. I. Triplett, and D. J. Klein, "Geometric methods for modeling and control of free-swimming fin-actuated underwater vehicles," *IEEE Transactions on Robotics*, vol. 23, no. 6, pp. 1184–1199, Dec 2007.

[43] M. Kruusmaa, P. Fiorini, W. Megill, M. Vittorio, O. Akanyeti, F. Visentin, L. Chambers, H. el Daou, M.-C. Fiazza, J. Jezov, M. Listak, L. Rossi, T. Salumae, G. Toming, R. Venturelli, D. Jung, J. Brown, F. Rizzi, A. Qualtieri, and A. Liszewski, "Filose for svenning: A flow sensing bioinspired robot," *Robotics & Automation Magazine, IEEE*, vol. 21, pp. 51–62, 09 2014.

[44] T. Salumäe, I. Rañó, O. Akanyeti, and M. Kruusmaa, "Against the flow: A braitenberg controller for a fish robot," in *2012 IEEE International Conference on Robotics and Automation*, May 2012, pp. 4210–4215.

[45] E. Rezapour, K. Y. Pettersen, P. Liljebäck, and J. T. Gravdahl, "Path following control of planar snake robots using virtual holonomic constraints," in *2013 IEEE International Conference on Robotics and Biomimetics (ROBIO)*, Dec 2013, pp. 530–537.

[46] F. Vanni, A. P. Aguiar, and A. M. Pascoal, "Cooperative path-following of underactuated autonomous marine vehicles with logic-based communication," *IFAC Proceedings Volumes*, vol. 41, no. 1, pp.

107 – 112, 2008, 2nd IFAC Workshop on Navigation, Guidance and Control of Underwater Vehicles. [Online]. Available: http://www.sciencedirect.com/science/article/pii/S1474667015355105

[47] S. Moe, K. Y. Pettersen, T. I. Fossen, and J. T. Gravdahl, "Line-of-sight curved path following for underactuated usvs and auvs in the horizontal plane under the influence of ocean currents," in *2016 24th Mediterranean Conference on Control and Automation (MED)*, June 2016, pp. 38–45.

[48] E. Borhaug, A. Pavlov, and K. Y. Pettersen, "Integral los control for path following of underactuated marine surface vessels in the presence of constant ocean currents," in *2008 47th IEEE Conference on Decision and Control*, Dec 2008, pp. 4984–4991.

[49] F. Rego, N. T. Hung, and A. M. Pascoal, "Cooperative path-following of autonomous marine vehicles: theory and experiments," in *2018 IEEE/OES Autonomous Underwater Vehicle Workshop (AUV)*, 2018, pp. 1–6.

[50] Y. Zhou, Y. Zhang, F. Ni, and H. Liu, "A head control strategy of the snake robot based on segmented kinematics," *Applied Sciences*, vol. 9, p. 5104, 11 2019.

[51] G. Gillis, "Environmental effects on undulatory locomotion in the american eel anguilla rostrata: kinematics in water and on land," 1998.

[52] E. Kelasidi, P. Liljebäck, K. Y. Pettersen, and J. T. Gravdahl, "Biologically inspired swimming snake robots : Modeling , control and experimental investigation," 2016.

[53] J. E. Colgate and K. M. Lynch, "Mechanics and control of swimming: a review," *IEEE Journal of Oceanic Engineering*, vol. 29, no. 3, pp. 660–673, July 2004.

[54] P. Liljebäck, K. Pettersen, [U+FFFD] Stavdahl, and J. Gravdahl, "A simplified model of planar snake robot locomotion," 10 2010, pp. 2868–2875.

[55] E. Kelasidi, K. Y. Pettersen, and J. T. Gravdahl, "A control-oriented model of underwater snake robots," in *2014 IEEE International Conference on Robotics and Biomimetics (ROBIO 2014)*, Dec 2014, pp. 753–760.

[56] E. Kelasidi, P. Liljebäck, K. Pettersen, and J. Gravdahl, "Experimental investigation of efficient locomotion of underwater snake robots for lateral undulation and eel-like motion patterns," *Robotics and Biomimetics*, vol. 2, 12 2015.

[57] P. Liljeback, I. U. Haugstuen, and K. Y. Pettersen, "Path following control of planar snake robots using a cascaded approach," *IEEE Transactions on Control Systems Technology*, vol. 20, no. 1, pp. 111–126, Jan 2012.

[58] M. Sato, M. Fukaya, and T. Iwasaki, “Serpentine locomotion with robotic snakes,” *IEEE Control Systems Magazine*, vol. 22, no. 1, pp. 64–81, 2002.

[59] A. Wiens and M. Nahon, “Optimally efficient swimming in hyper-redundant mechanisms: Control, design, and energy recovery,” *Bioinspiration & biomimetics*, vol. 7, p. 046016, 11 2012.

[60] A. J. Ijspeert and A. Crespi, “Online trajectory generation in an amphibious snake robot using a lamprey-like central pattern generator model,” in *Proceedings 2007 IEEE International Conference on Robotics and Automation*, 2007, pp. 262–268.

[61] X. wu and S. Ma, “Cpg-based control of serpentine locomotion of a snake-like robot,” *Mechatronics*, vol. 20, pp. 326–334, 03 2010.

[62] L. Buono and M. Golubitsky, “Models of central pattern generators for quadruped locomotion i. primary gaits,” *Journal of Mathematical Biology*, vol. 42, pp. 291–326, 04 2001.

[63] A. Kuo, “The relative roles of feedforward and feedback in the control of rhythmic movements,” *Motor control*, vol. 6, pp. 129–45, 05 2002.

[64] P. Liljebäck, [U+FFFD] Stavdahl, K. Y. Pettersen, and J. T. Gravdahl, “Mamba - a waterproof snake robot with tactile sensing,” in *2014 IEEE/RSJ International Conference on Intelligent Robots and Systems*, 2014, pp. 294–301.

[65] K. A. McIsaac and J. P. Ostrowski, “Motion planning for anguilliform locomotion,” *IEEE Transactions on Robotics and Automation*, vol. 19, no. 4, pp. 637–652, 2003.

[66] K. Do and J. Pan, “Global tracking control of underactuated ships with off-diagonal terms,” vol. 2, 01 2004, pp. 1250 – 1255 Vol.2.

[67] E. Westervelt, J. Grizzle, C. Christine, J. Choi, and B. Morris, *Feedback Control of Dynamic Bipedal Robot Locomotion*, 01 2007.

[68] M. Breivik and T. I. Fossen, “Guidance-based path following for autonomous underwater vehicles,” in *Proceedings of OCEANS 2005 MTS/IEEE*, 2005, pp. 2807–2814 Vol. 3.

[69] A. Kohl, K. Pettersen, E. Kelasidi, and J. Gravdahl, “Planar path following of underwater snake robots in the presence of ocean currents,” *IEEE Robotics and Automation Letters*, vol. 1, pp. 1–1, 01 2016.

[70] E. Kelasidi, P. Liljeback, K. Y. Pettersen, and J. T. Gravdahl, “Innovation in underwater robots: Biologically inspired swimming snake robots,” *IEEE Robotics Automation Magazine*, vol. 23, no. 1, pp. 44–62, 2016.

[71] E. Rezapour, A. Hofmann, K. Y. Pettersen, A. Mohammadi, and M. Maggiore, “Virtual holonomic constraint based direction following control of planar snake robots described by a simplified model,” in *2014 IEEE Conference on Control Applications (CCA)*, 2014, pp. 1064–1071.

[72] M. Maggiore and L. Consolini, “Virtual holonomic constraints for euler–lagrange systems,” *Automatic Control, IEEE Transactions on*, vol. 58, pp. 1001–1008, 04 2013.

[73] M. El-Hawwary and M. Maggiore, “Reduction theorems for stability of closed sets with application to backstepping control design,” *Automatica*, vol. 49, p. 214–222, 01 2013.

[74] M. Maggiore and L. Consolini, “Virtual holonomic constraints for euler–lagrange systems,” *IEEE Transactions on Automatic Control*, vol. 58, no. 4, pp. 1001–1008, 2013.

[75] D. J. W. Belleter, “Control of underactuated marine vehicles in the presence of environmental disturbances,” PhD dissertation, NTNU, 2016.

[76] A. M. Kohl, E. Kelasidi, A. Mohammadi, M. Maggiore, and K. Y. Pettersen, “Planar maneuvering control of underwater snake robots using virtual holonomic constraints.” *Bioinspiration & biomimetics*, vol. 11 6, p. 065005, 2016.

[77] H. K. Khalil, *Nonlinear systems; 3rd ed.* Upper Saddle River, NJ: Prentice-Hall, 2002, the book can be consulted by contacting: PH-AID: Wallet, Lionel. [Online]. Available: https://cds.cern.ch/record/1173048

[78] V. Arnold, *Mathematical methods of classical mechanics*. Springer, 1989, vol. 60.

[79] R. Skjetne, S. Moi, and T. I. Fossen, “Nonlinear formation control of marine craft,” in *Proceedings of the 41st IEEE Conference on Decision and Control, 2002.*, vol. 2, 2002, pp. 1699–1704 vol.2.

[80] R. Ghabcheloo, D. Carvalho, A. Pascoal, and C. Silvestre, “Coordinated motion control of multiple autonomous underwater vehicles,” in *International Workshop on Underwater Robotics (IWUR). November 9-11, 2005, Genoa, Italy*, 2005, p. 10 p, contribution: organisation=iha,FACT1=1.

[81] L. Lapierre, D. Soetanto, and A. Pascoal, “Coordinated motion control of marine robots,” *IFAC Proceedings Volumes*, vol. 36, 09 2003.

[82] A. P. Aguiar, R. Ghabcheloo, A. Pascoal, C. Silvestre, J. Hespanha, and I. Kaminer, *Coordinated Path Following Control of Multiple Vehicles subject to Bidirectional Communication Constraints*, 2006, vol. 336, pp. 93–111.